TAMPERE UNIVERSITY
OF APPLIED SCIENCES

OPTIMIZATION OF THE ALUMINIUM GRAVITY CASTING TOOL PREHEATING PROCESS

Jarno Mastomäki

Bachelor's thesis
March 2018
Mechanical Engineering
Product Development

TIIVISTELMÄ

Tampereen ammattikorkeakoulu
Konetekniikan koulutus
Tuotekehitys

MASTOMÄKI, JARNO:
Valumuottien esilämmitys ja sen optimointi.

Opinnäytetyö 118 sivua, joista liitteitä 38 sivua
Maaliskuu 2018

Tämä opinnäytetyö on tehty yhteistyössä KS Kolbenschmidt GmbH:n kanssa. Yritys valmistaa valuosia autoteollisuuden tarpeisiin. Työn tarkoituksena oli selvittää alumiinin valamisessa käytetyn kokillimuotin esilämmitysprosessin optimointimahdollisuuksia. Tässä työssä on analysoitu lämmöntuonnin tehokkuutta ja sitä, mitkä ulkoiset seikat vaikuttavat lämmitysprosessiin. Opinnäytetyön mittausosuus suoritettiin Tšekin tasavallassa Ustin kaupungissa lokakuun 2017 ja tammikuun 2018 aikana.

Opinnäytteen päämääristä sovittiin yhdessä KS Kolbenschmidtin valimon johtajan kanssa. Muottien esilämmitys oli valimossa toteutettu maakaasuliekillä, joka puhalletaan suoraan muotin jakopinnoille. Muotin lämmitysprosessi oli erittäin epätaloudellinen, sillä kaasun poltossa suurin osa energiasta haihtuu ympäröivään ilmaan. Muotteja esilämmitetään, jotta niihin saavutettaisiin hyvä täytösaste ja lopputuotteen laatu pysyisi tasaisena. Valuprosessin onnistumisen kannalta tuli muotin lämpötilan olla noin 200 astetta.

Opinnäytetyö jakautui viiteen osaan, joista ensimmäisessä käsiteltiin teoriaa lämmönsiirrosta pakotetussa konvektiossa. Toisessa osassa käsiteltiin käytännön mittauksia ja niiden tuloksia. Kolmannessa osassa laskimme teoreettiset esilämmitysajat valumuotille soveltaen erilaisien poltinmallien ominaisuuksia. Laskemalla ja mittaamalla saatua tietoa sovelsimme tunnistaaksemme optimoinnille olennaiset seikat, joka on myös esitetty työn kolmannessa osassa. Opinnäytetyön neljäs osa koostui optimoinnin validoinnista, joka tehtiin käyttämällä elementtimenetelmää. Laskenta suoritettiin Ansys Fluent -ohjelmalla, jonka ratkaisua käytettiin lämmitysajan laskemiseen. Työn viimeiseen osaan olemme koonneet laskennan tulokset sekä arvioineet niitä. Olemme myös tuoneet esille vaihtoehtoisia toimintatapoja esilämmitysprosessin tehostamiselle.

Työn teoreettisena viitekehyksenä on saksalaisen fyysikon, Martin Holgerin, kehittämä teoria. Martinin tutkimus valmistui vuonna 1977 Karlsruhen yliopiston teknisen termodynamiikan laitoksella. Tutkimalla Martinin teoriaa löysimme polttoprosessista ne merkitsevät tekijät, joita muuttamalla pystyimme vaikuttamaan prosessin tehokkuuteen merkittävästi. Saavutetut tulokset validoitiin vertaamalla niitä mitattuihin arvoihin.

Asiasanat: fluent, optimointi, lämmönsiirto, termodynamiikka

ABSTRACT

Tampereen ammattikorkeakoulu
Tampere University of Applied Sciences
Mechanical Engineering
Product Development

MASTOMÄKI, JARNO:
Optimization of the Aluminium Gravity Casting Tool Preheating Process

Bachelor's thesis 118 pages, appendices 38 pages
March 2018

This thesis work was assigned by KS Kolbenschmidt GmbH. Company produces casted parts for car industry. The purpose of this study was to investigate the possibilities to optimize the preheating process of an aluminum casting tool. This thesis analyses the characteristics of the preheating process of aluminum casting moulds. Furthermore, this work shows what actions are needed when considering the optimization of preheating process. The empirical part of this study was conducted at Usti nad Labem in The Czech Republic and was carried out during October 2017 and January 2018.

The goals of this thesis were settled in liaison with KS Kolbenschmidt Czech Republic. Preheating was performed by nozzle injected natural gas combustion flame direct to the solid surface of the casting tool. The preheating process was, at the time of this thesis work, quite energy inefficient because of the huge energy losses in the burning. Before the casting process can start, the mould needs to be preheated to temperature of 200 Celsius. This is done to ensure that the molten aluminum fills the whole cavity of the steel mould.

This work divided into five main sections. The first part encases the theory of physics which is applied in this case. The second part covers the practical measurements conducted in the foundry in Czech Republic and how the measured information is applied in this work. In third part the theory of impinging jet flow is applied to this case and the theoretical heating times for each burner are calculated. By using this knowledge, the characteristics for optimization process was identified. The fourth section discusses the validation of calculations and the optimization process through the use of computer aided modelling. In the final part of this work the achieved results are compared and evaluated. Furthermore, the alternative options for improving the mould heating are also discussed.

In this work the heating process is studied by applying the correlations made for the impinging jet applications. The correlations were suggested by a German physicist Martin Holger in 1977 at University of Karlsruhe in faculty of Technical Thermodynamics. Studying the process by using these theories, approximate directions for the optimization process could be pointed out. For getting more accurate results, computer aided modelling was used for calculating the heat transfer in the process. The program used for validation was Ansys Fluent and Ansys Transient Thermal. The computations, made by the program, were validated by measured results done on-site at the foundry.

Key words: impinging jet, heat transfer, fluent, optimization, burning

CONTENTS

ABBREVIATIONS AND TERMS

TAMK	Tampere University of Applied Sciences
SRN	Single round nozzle
ARN	Array of round nozzles
ARO	Array of round orifices
LNG	Liquified Natural Gas
CAD	Computer Aided Design
FEM	Finite Element Method
FVM	Finite Volume Method
DM	Design Modeller

1 INTRODUCTION

Purpose of this thesis was to improve the aluminum gravity casting tool preheating process. This work was done for the use of KS Kolbenschmidt foundry Usti nad Labem in The Czech Republic. Thesis work was proceeded with close co-operation with foundry technical staff. The foundry manager, ing. František Brož told about the urgent need to do improvements for the casting tools preheating process because of the huge consumption of natural gas and long preheating times. The conversation was held after practical seminar work which was completed during summer 2017.

Main targets of this thesis are to improve the preheating time and fuel efficiency of preheating burner used in the automatized casting machine. The casting tool is divided in several sections. The main body of the mold is in two parts and these parts have direct surface touch with the molten aluminum. Both of these parts need to reach certain temperature before the casting process can be started. After preheating the liquid aluminum keeps mould in operating temperature while high rises are cooled down with automatized water circulation.

Mold heating is done by flame combustion of natural gas via jet nozzles. To study the physics of this application the theory of heat and mass transfer in impinging gas jet flows was used. For simplification the gas flow was considered as an incompressible ideal gas flow. By using the correlation suggested for the similar case approximate directions was able to reach for process optimizing. For more accurate results computer aided calculations was applied. The goals of our work were reached by using the finite volume method and comparing the results to the correlations. The calculations were validated by comparing them to known values.

We want to thank following individuals for making this possible,

Thesis Director, M.Sc. Jari Puranen,

Foundry Manager, ing. František Brož,

Foundry Specialist, ing. Petr Šifalda,

EDR Medeso, CFD Specialist, Jarmo Korpijärvi

and all the staff of

Tampere University of Applied Sciences and KS Kolbenschmidt CZ

2 THEORY OF IMPINGING JET FLOW

In this chapter, we show the theoretical knowledge behind the physical phenomenon of this thesis case. A lot of these theories are based to the classical physics and many of those require enormous simplifications in modelling. This need to be taken under consideration, because the physical phenomenon, covered in this work, is highly complex.

2.1 Newtons law of cooling

Newtons law of cooling was developed by Sir Isaac Newton (1642 – 1726) (Massoud 2005, 518). By noticing that when body with higher temperature is brought to the atmosphere of lower temperature there will be heat transfer from body to atmosphere. The heat transfer rate between body and its surroundings is proportional to the temperature difference between body and surrounding atmosphere and is represented by heat transfer coefficient *h*. The heat flux is expressed in the following form

$$\dot{q}'' = h\left(T_{body} - T_f\right), \tag{1}$$

where *T* is temperature. Sir Isaac Newton suggested this in 1701, according to Massoud (2005, 518).

2.2 Reynolds number

Reynolds number is named after its developer, physicist and engineer, Osborne Reynolds (1842-1912) (Daintith & Martin 715, 2010). This dimensionless number describes the nature of fluid flow. Flow can be described as laminar or turbulent, depending on the forces affecting the fluid particle. Reynolds number can be calculated by using following expression

$$Re = \frac{v_s L \rho}{\mu_d}, \tag{2}$$

where v_s is speed of flow, L is length, ρ is density of fluid and μ_d is the dynamic viscosity of the fluid. Reynolds number is interpreted as follow. When *Re* in internal pipe flow is under 2300 the flow is laminar. When the number reaches the level of 4000 the flow can be read to be turbulent. Between these two phases the form of flow is difficult to define. Correlations are based on experimental measures of Mr. Reynolds and they were presented in year 1880, says Puranen (2015, 32).

2.3 Sherwood number

Sherwood number is dimensionless number named in honour after American physicist Thomas Kilgore Sherwood (1903 – 1976) (Hottel 1994, 505). The Sherwood number is defined as following

$$Sh = \frac{K}{D/L}, \tag{3}$$

where K is convective mass transfer rate, D is mass diffusivity and L is length. Sherwood number is used to depict the ratio of convective mass and the diffusive mass transport (Subramarian N/A, 1).

2.4 Nusselt number

Nusselt number is dimensionless number which is used to describe the heat transfer as a ratio of the convective and conductive heat transfer. Nusselt number is named in honour after a German engineer Ernst Kraft Wilhelm Nusselt (1882 – 1957) (Massoud 2005, 250). Nusselt number is basically a convective heat transfer coefficient without dimension. Nusselt number is defined as following

$$Nu = \frac{\dot{q}''_{convection}}{\dot{q}''_{conduction}} = \frac{h}{k/L}, \tag{4}$$

where h is the convective heat transfer coefficient, L is characteristic dimension and k is thermal conductivity of the fluid (Puranen 2015, 51). Nusselt number equal to 1 means

that the conductive and convective heat transfer rates are equal. Larger value of *Nu* means that the convection dominates the heat transfer.

2.5 Prandtl number

Prandtl number is named after its developer Ludwig Prandtl (1875 – 1953) (Massoud 2005, 250). Prandtl number is a ratio between kinematic viscosity and diffusion of heat in fluid (Puranen 2015, 52). Prandtl number can be calculated by following formula

$$Pr = \frac{v}{\alpha} = \frac{\mu_d c_p}{k}, \tag{5}$$

where μ_d is dynamic viscosity, c_p is specific heat and k is thermal conductivity (Puranen 2015, 52). Prandtl number is developed to descript the ratio between the speed of convective and diffusive heat transfer. Following table (1) show the known Prandtl number for various common fluids.

TABLE (1) Prandtl number for various common fluids in industry. All materials are considered as fluids (Massoud 2005, 520).

Fluid	Metals	Gases	Water	Organic	Oil	Glycerine
Pr number	0,003 - 0,05	0,7 - 1	1 - 13	5 - 50	50 - 10000	2000 - 8500

2.6 Schmidt number

Schmidt number is named after its developer, German engineer Ernst Heinrich Wilhelm Schmidt (1892 – 1975) (Daintith etc. 2010, 87). Schmidt number has a similar role in mass transfer as Prandtl number has in heat transfer. It was developed to describe the correlation between the ability of fluid's momentum transportation by molecular level to ability of that same fluid to transport small entities by molecular means. (Subramarian. N/A, 2) Schmid number is calculated by following formula

$$Sc = \frac{v}{D} = \frac{\mu}{\rho D}, \tag{6}$$

where v represents kinematic viscosity, D is mass diffusivity, μ is dynamic viscosity and ρ is density of fluid. When fluid is in liquid form the molecules are packed tight on one to another and diffusion appears slow. In this case the momentum is transmitted highly efficient through molecules by using their interaction. When compared to gases the efficiency of the gases capability for transport small entities by molecular means is weak. Schmidt number for gases are normally three times smaller than for liquids, according to Subramarian (N/A, 2).

2.7 Hydrodynamics of Impinging Flow

In the case of this thesis the gas jet is discharged into ambient temperature of the factory hall. The axisymmetric nozzles or orifices in the preheater forms jets, with burning natural gas compound. The jet blow stagnates to the wall of the casting mould, which is oriented normal to jet direction. This is known as impinging jet flow.

The hydrodynamics of impinging flow are studied mainly by picturing the flow region as a laminar and fully developed all the way from the nozzle exit to the impinging zone and to the wall jet region. The velocity profiles at nozzle exit are assumed to be nearly rectangular and further down taking the form of gaussian normal distribution as we ca see in the figure (1). According to Martin (1977, 3) the approximation of the flow profile can be described by following function

$$\frac{w(x,\acute{z})}{w(0,\acute{z})} = exp\{-(x/C\acute{z})^2\}\,, \tag{7}$$

where C is constant 0,1, w is speed as a function of flow directions. The value of the constant depends slightly on the Reynold's number of the flow at the nozzle exit. For simplification, we can say that the flow speed reaches its maximum in the flow symmetry axis and is reduced by 95 % near the edge of the flow profile. Considering realistic flow conditions, the presumption of laminar flow is more than over optimistic. In many, nearly all, cases the flow developing from nozzle exit to the end of the free jet zone is more or less turbulent (Martin 1977, 2). An illustration of impinging jet flow can be seen in the figure (1).

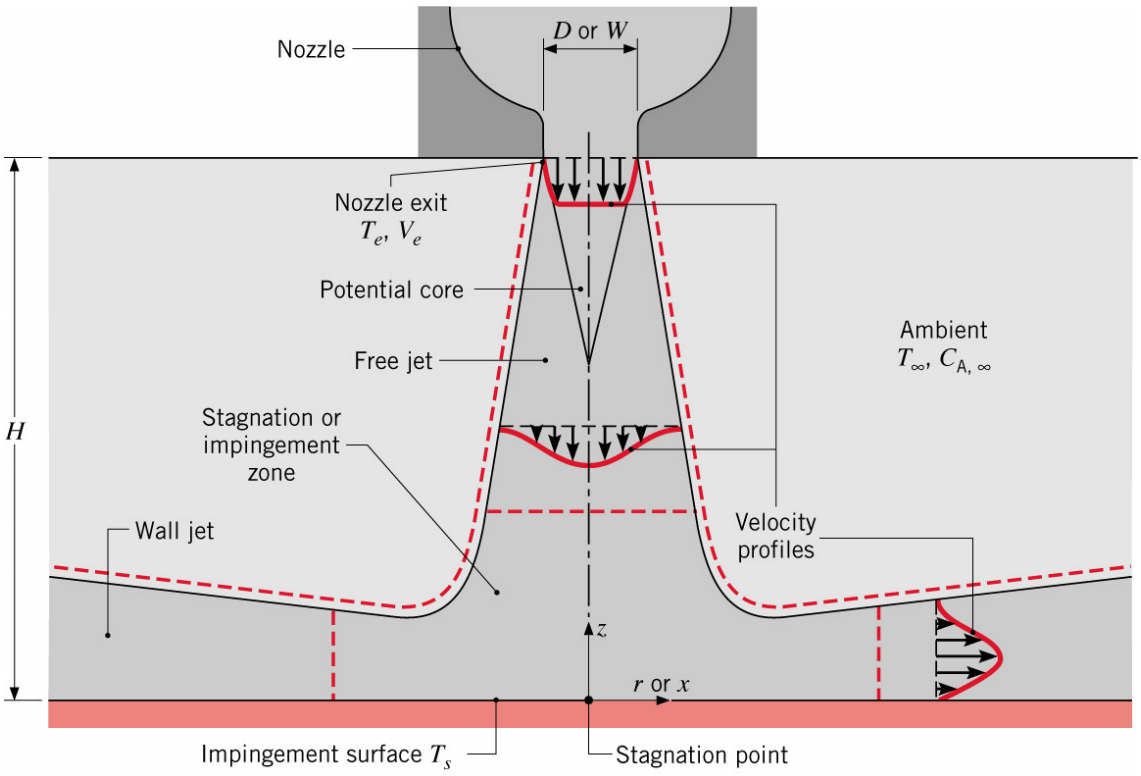

FIGURE 1. Schematic view of the velocity field of impinging jet (Incropera).

The speed of the flow will decrease over the growing distance from jet exit in the direction of z, which is shown in the figure (1). The speed is also accelerated and decelerated by influence of the impinging surface in directions x and r. This is caused by jet flow penetration in to zero momentum ambient fluid which is slowing the flow down. By these means the impinging jet is divided in three main sections called free jet region, impinging zone and wall jet region (or lateral flow area). (Incropera 2002, 403)

Decelerating stagnation flow is found to form relatively close to the impinging wall. According to Martin (1977, 4) the turning point between free jet zone and stagnation zone is located approximately 1,2 times the nozzle or orifice maximum diameter away from the impinging surface. The vertical velocity component of the flow (in the lateral area) is known to be restricted by the thin layer boundary flow, near the solid surface, where influence of shear is restricting the flow significantly. Another boundary is the zero-momentum ambient air where lateral flow is spread.

2.8 Geometric considerations

In theory of impinging jet flow in heat and mass transfer the biggest effects to the end result can be settled by changing the few main geometric values. These are the nozzle or orifice diameter, the geometry of stagnation of multiple gas outlets and distance between gas exit and the impingement surface (Incopera 2002, 403.) Nozzle design is simplified in axisymmetric form and does not consider any other complex forms than nozzle or orifice. Nozzle means a convergent outlet for fluid flow and while orifice is just described as a simple hole in the plate with no significant thickness. The differences between these two types of gas outlets can be seen in the figure (2).

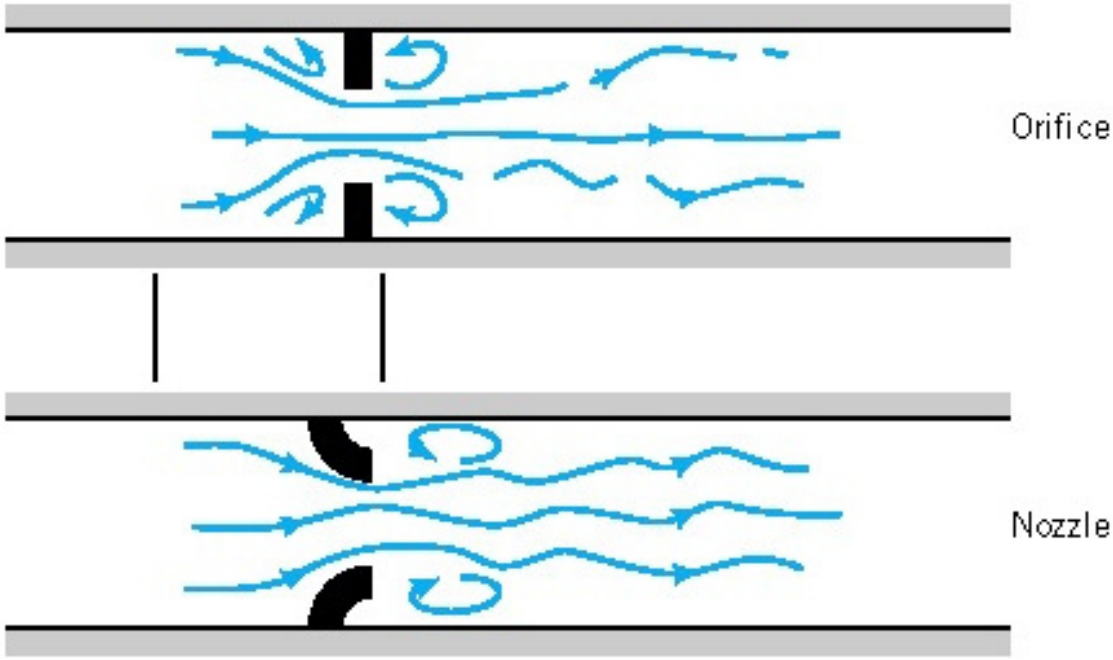

FIGURE 2. Flow through nozzle and orifice. (C.Samaras, modified)

According to Samaras the empirical discharge coefficient between these two different ways to discharge the gas flow is approximately 0,60-0,65 for orifice and 0,98 for nozzle. These differences are formed by energy losses caused by friction and turbulence.

2.8.1 Single round nozzle

One of the pertinent geometrical considerations in the impinging jet flow is the effective area of the jet nozzle or orifice. In the figure (3) below we can see various jet nozzles staggered in different forms. The single round nozzle, further SNR, and its correlation for affective area can be seen first from the left in figure (3a).

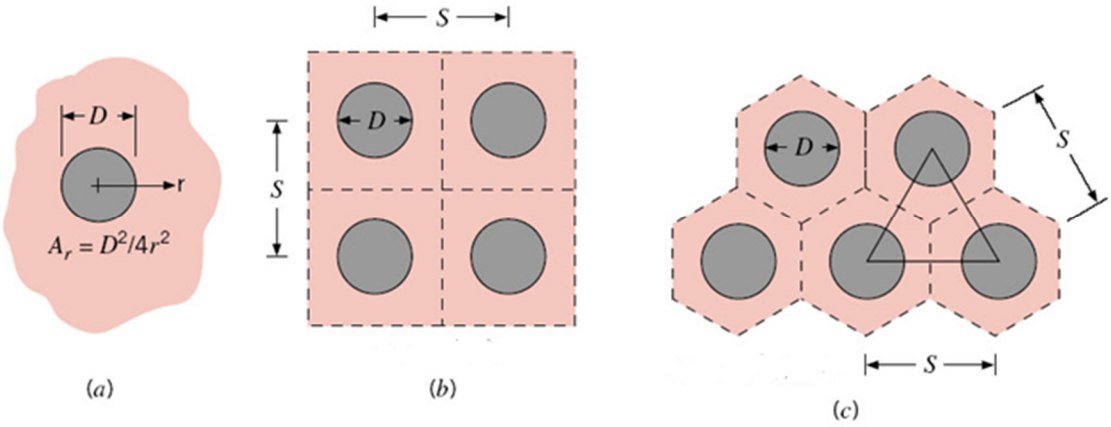

FIGURE 3. Different ways to stagger the nozzle jets. (Incropera, modified)

Various expressions for the relative total nozzle area for single and regularly arranged jet nozzles and orifices are given in table (2). In the table, *A* represents the total relative nozzle area (Martin 1977, 15).

TABLE 2. Expressions for total relative area for jet nozzles.

	SRN	$ARN_{hexagon}$	ARN_{square}
A	$\frac{1}{4}\left(\frac{D}{r}\right)^2$	$\frac{\pi}{2\sqrt{3}}\left(\frac{D}{S}\right)^2$	$\frac{\pi}{4}\left(\frac{D}{S}\right)^2$

2.8.2 In- line array of round nozzles

In-line array of round jet nozzles, further $ARN_{square,}$ and its effective area is illustrated in the figure (3b). Square array of nozzles or orifices can be seen second from the left (b). The form of arrangement of the nozzles can be defined as the way of effective area shape around of the nozzle exit. If the space between the nozzles can be divided in square sections and the dimension of the centre point of the nozzle to another is same in horizontal and vertical direction, we can call it as in -line array.

2.8.3 Staggered array of round nozzles

Staggered array of round jet nozzles, further $ARN_{hexagon}$, and their affective area is illustrated in the figure (3c). Staggered array of nozzles or orifices can be seen third from the left (c). The form of arrangement of the nozzles can be defined as the way of effective area is around the nozzles. If we can divide the nozzles in triangular form, we can call it as hexagonal staggered form.

2.9 Nusselt and Reynolds number in impinging jet application

The theory for impinging jet heat transfer is derived through Nusselt number because of the high role of convection in the heat transfer system. For forming an average Nusselt number from characteristic dimensions of the jet nozzle, we need to know few things first. Incropera (2002, 404) talks about hydraulic diameter of the nozzle. This is nozzle diameter multiplied by four and divided the product by wetted perimeter of the nozzle. In this thesis, we can simplify the case by assuming that the hydraulic diameter is equal to the nozzle diameter (Incropera 2002, 404).

For distribution of the local Nusselt number the theory can be divided in two sections. First one considers the Nusselt theory behaviour in small pacing between the nozzle exit and stagnation surface. Second one considers the large spacing between these two boundaries. In following figure (4), Incropera (2002, 405) has illustrated the distribution for local Nusselt number in function of distance between nozzle exit and impinging surface.

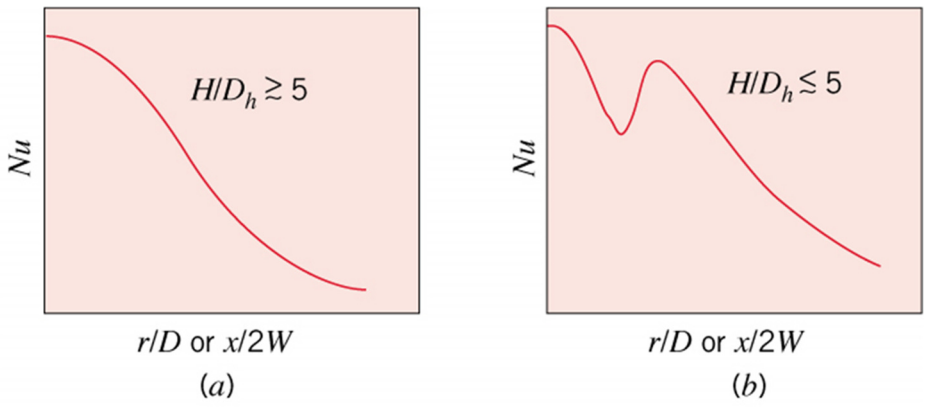

FIGURE 4. Local Nusselt number distribution as a function of distance. (Incropera)

Incropera (2002, 403) explicates the peak in the figure (4b) by the turbulent behaviour of flow, loosely associated with the length of the potential core. This can be seen in the previous figure (1). According to Martin (1977, 5) peak also indicates a secondary stagnation point. This point forms in the interaction between two wall jets in the application of multiple jet nozzles. We can define the average Nusselt number by following formula

$$\overline{Nu} \equiv \frac{\bar{h}D}{k}, \tag{8}$$

where $\bar{h}$ is average convective heat transfer coefficient and k is thermal conductivity of the fluid. Reynolds number can be calculated by following formula

$$Re = \frac{V_e D}{\mu}, \tag{9}$$

where V_e represents flow speed at the nozzle exit and μ is for kinematic viscosity of the fluid.

2.10 Equations and correlations for SRN

According to both Martin (1977, 15) and Incropera (2002, 405) the heat and mass transfer could be correlated to SRN by following function

$$\left(\frac{\overline{Sh}_1}{Sc^{0,42}}\right)_{SRN} = \left(\frac{\overline{Nu}}{Pr^{0,42}}\right)_{SRN} = G\left(\frac{r}{D}, \frac{H}{D}\right) F(Re), \tag{10}$$

where $\overline{Sh}$ is average Sherwood number, *Sc* is Schmidt number, *Pr* is Prandtl number, $\overline{Nu}$ is average Nusselt number. Function *F(Re)* can be written in form (Incropera 2002, 406)

$$F = 2Re^{0,5}(1 + 0{,}005Re^{0,55})^{0,5}, \tag{11}$$

where *Re* represents the Reynolds number. Martin (1977, 15) recommends following correlation for the G

$$G = 2A^{0,5}\frac{1 - 2,2A^{0,5}}{1 + 0,2(H/D - 6)A^{0,5}}, \quad (12)$$

where *A* represents the relative nozzle area, calculated by table (2) formulas. Because these correlations are based for the measured data and they are highly complex, the range of validity is restricted to following boundaries listed in the table (3) says Martin (1977, 16).

TABLE 3. Ranges of validity for SRN correlations.

Min value		Max value
2000	*Re*	400000
2	*H/D*	12
0,004	*A*	0,04

2.11 Equations and correlations for ARN

According to both Martin (1977, 15) and Incropera (2002, 406) the heat and mass transfer could be correlated to ARN by following function

$$\left(\frac{\overline{Sh}_1}{Sc^{0,42}}\right)_{ARN} = \left(\frac{\overline{Nu}}{Pr^{0,42}}\right)_{ARN} = K\left(A, \frac{H}{D}\right) G\left(A, \frac{H}{D}\right) F(Re), \quad (13)$$

where $\overline{Sh}$ is average Sherwood number, *Sc* is Schmidt number, *Pr* is Prandtl number, $\overline{Nu}$ is average Nusselt number. Function *F(Re)* can be written in form (Incropera 2002, 406)

$$F = 0,5Re^{2/3}, \quad (14)$$

where *Re* represents the Reynolds number. For function G, Martin (1977, 15) recommends same correlation as used in the SRN -case. This can be seen in the previous section. The *K* in formula (13) is suggested to be written as following function (Incropera 2002, 406)

$$K = \left[1 + \left(\frac{H/D}{0{,}6/A^{0{,}5}}\right)^6\right]^{-0{,}05}. \quad (15)$$

Because these correlations are based for the measured data and they are highly complex, the range of validity is restricted, according to Martin (1977, 22), to following boundaries listed in the table (4).

TABLE 4. Ranges of validity for ARN correlations.

Min value		Max value
2000	*Re*	100000
2	*H/D*	12
0,004	*A*	0,04

2.12 Equations and correlations for ARO

Nozzle can also mean just a plain orifice. These are more or less sharp-edged holes. According to Martin (1977, 22.) this kind of case can be covered by using a multiplier in all geometric values. An example is given in ARN correlation (Martin 1977, 22). In following equations

$$\left(\frac{\overline{Sh}_1\sqrt{\epsilon}}{Sc^{0{,}42}}\right)_{ARN} = \left(\frac{\overline{Nu}\sqrt{\epsilon}}{Pr^{0{,}42}}\right)_{ARN} = K\left(A, \frac{H}{D}\right) G\left(A, \frac{H}{D}\right) F(Re), \quad (16)$$

$$F = 0{,}5\left(\frac{Re}{\sqrt{\epsilon}}\right)^{2/3}, \quad (17)$$

$$G = 2\epsilon A^{0{,}5}\,\frac{1 - 2{,}2\epsilon A^{0{,}5}}{1 + 0{,}2(H/D/\sqrt{\epsilon} - 6)\epsilon A^{0{,}5}}, \quad (18)$$

$$K = \left[1 + \left(\frac{H/D/\sqrt{\epsilon}}{0{,}6/\epsilon A^{0{,}5}}\right)^6\right]^{-0{,}05}, \quad (19)$$

where multiplier ϵ is a ratio between the orifice minimum diameter and geometrical diameter.

3 PRACTICAL MEASUREMENTS

The prime purpose of this thesis was to examine the ways to improve the heating process of the casting mould. For those reasons we first had to measure the inception point of our studies. In this section, we discuss about the measurements needed to proceed for completing and validating the computer aided calculations and the results of the theoretical examination.

3.1 Measuring circumstances

The casting tool is a complex assembly of multiple steel parts. It is usually installed in the casting machine which has all the operative apparatus included. These are the parts of cooling system, mechanics for mould moving and possibility to use automatized casting system. The mould assembly itself is quite massive and heavy to move. Because these reasons the mould preheating was occasionally done on-site on the machine. Picture (1) of the mould assembled in the casting machine can be seen below.

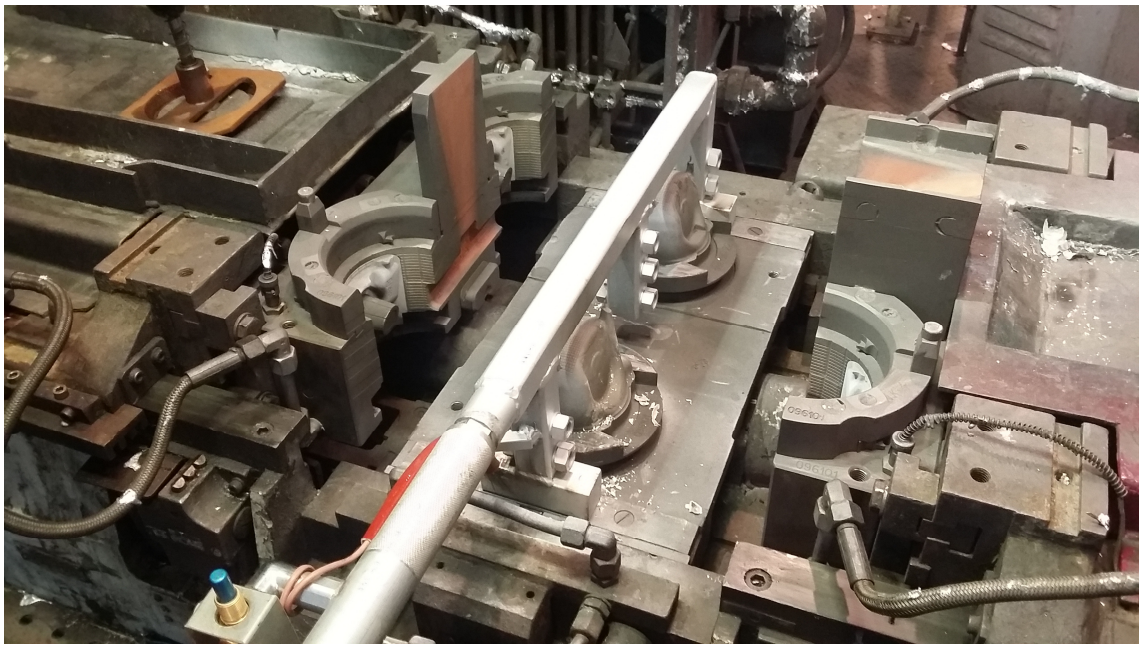

PICTURE 1. Mould assembled in machine bed with burner mounted in place (silver object in the middle).

The preheating itself was done by burning natural gas, further LNG. Burners was tailored just for this purpose and the foundry uses three different models in production. One of

those burners were premixing model, one was a nozzle mixing and third was operating with pressurized air and gas inlets. All models can be seen in the picture (2).

PICTURE 2. Measured burner types

We needed to replicate the circumstances of the atmosphere in the foundry, for the measurements. We could not have done the measurements in the actual casting machine, because that would have required an interception of production. We decided to take one of the moulds, which were on repairing phase of the circulation, and do the measurements at the side of the production. For that reason, we had a movable platform for the mould, including non-flammable insulator underneath. We moved the platform and the mould near a casting machine, so we could reach the beginning temperature of the mould and atmosphere. After the mould had stand in the foundry temperature long enough and we were sure that the beginning conditions were reached, we were able to begin the measurements. For each and every measurement we took a time so the tool could set the beginning temperature in steady state. The mould had a great amount of capacity to storage heat energy, so the time required to reach low and steady temperature was so long that we decided to let the mould cool down over night. In the picture (3) we can see the platform and the mould pieces used in measurements.

PICTURE 3. Measured mould and platform.

3.1.1 Surface emissivity specification

One of the critical points of the surface temperature measurements, by optic manners, was the surface emissivity. This is a dimensionless value which describes the surface capability to emit and absorb radiation. The value is given between 1 and 0. Ideal “black” object reaches value 1. This means that its good source of heat radiation. Object coated with black paint reaches approximated value of 0,95 (Puranen 2015, 44-45). We specified the mould outer surface value for emissivity by doing a comparison between two different measuring devices, while the temperature in measuring circumstances where known.

First, we coated the outer surface of the mould with ceramic slurry. After this we measured the outer temperature with thermocouple. We ensured that the mould was on the ambient temperature overnight and got enough time to become in steady state from outer influences. After this we used the Fluke Thermal camera to find the same temperature, by adjusting the emissivity, as the thermocouple showed. After couple of rounds for researching the right emissivity, we ended up using 0,92.

3.2 Measurement arrangements

For measuring the temperature, we had multiple different ways to operate. In production, the casting operators determine the optimal beginning temperature by measuring the mould inner temperature with two thermocouples. These sensors are located in both ends of the mould halves. Placement of the thermocouple sensors can be seen in the picture (4). The mould is considered to be at an optimal temperature when the value reaches 200 ºC in those points seen in the picture.

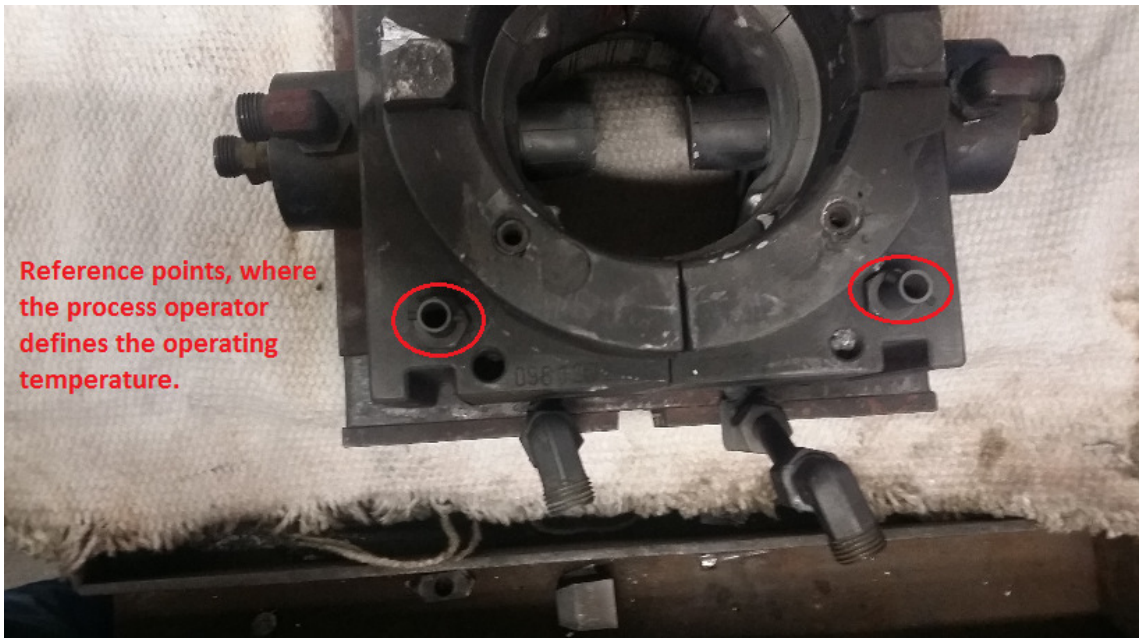

PICTURE 4. Positioning of original thermocouple sensors.

We used the 200 ºC as a reference temperature for our measurements. First, we took initial values up from the measuring site conditions. Those were the ambient temperature of the casting machine area and the temperature of the solid mould. This was done with thermocouple sensors (K-type, Inconell insulated and Omega HH12B) and with infrared thermometer (Benetech GM700). These devices can be seen in the picture (5). The full data sheet of measuring devices can be found in appendices (1, 2 and 3)

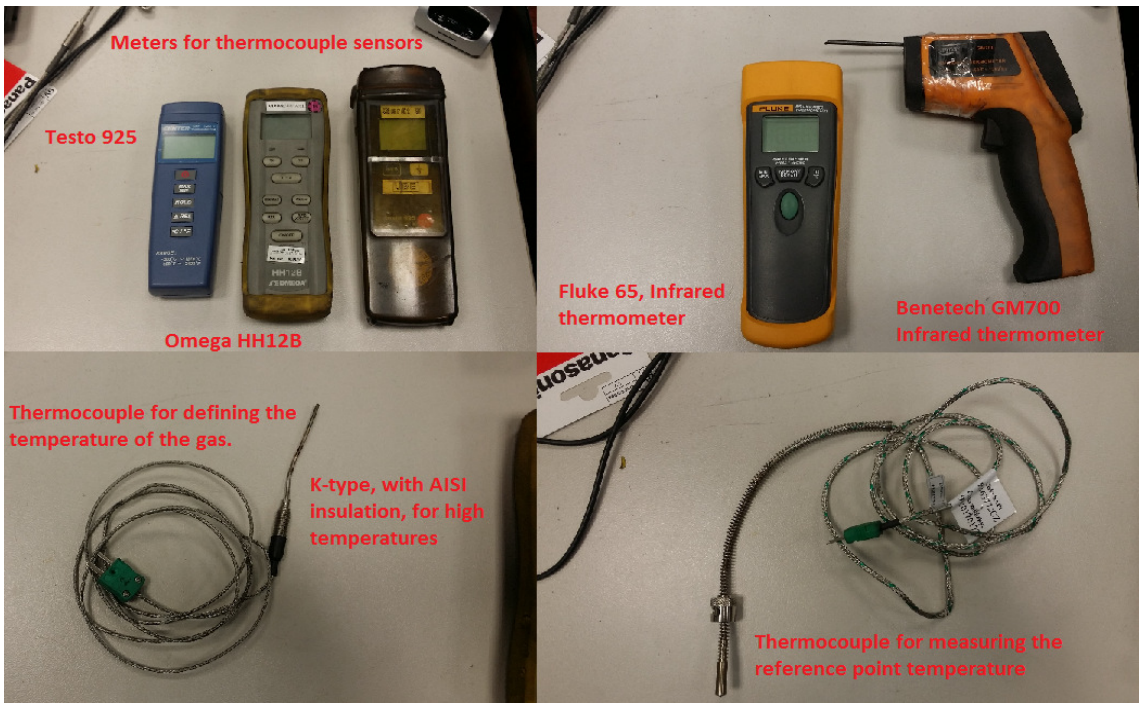

PICTURE 5. Measuring devices used, named in the picture.

We used the temporary platform and non-flammable insulation as a workbench. On that surface, we assembled the mould, which was formed in three separated parts. The first part was underplate with bushings for the product core. The rest of mould bodywork, which was divided into two almost identical parts, were assembled on that underplate. Distance between the mould halves was determined by the width of burner T-junction part. The experimental arrangements can be seen in the picture (6).

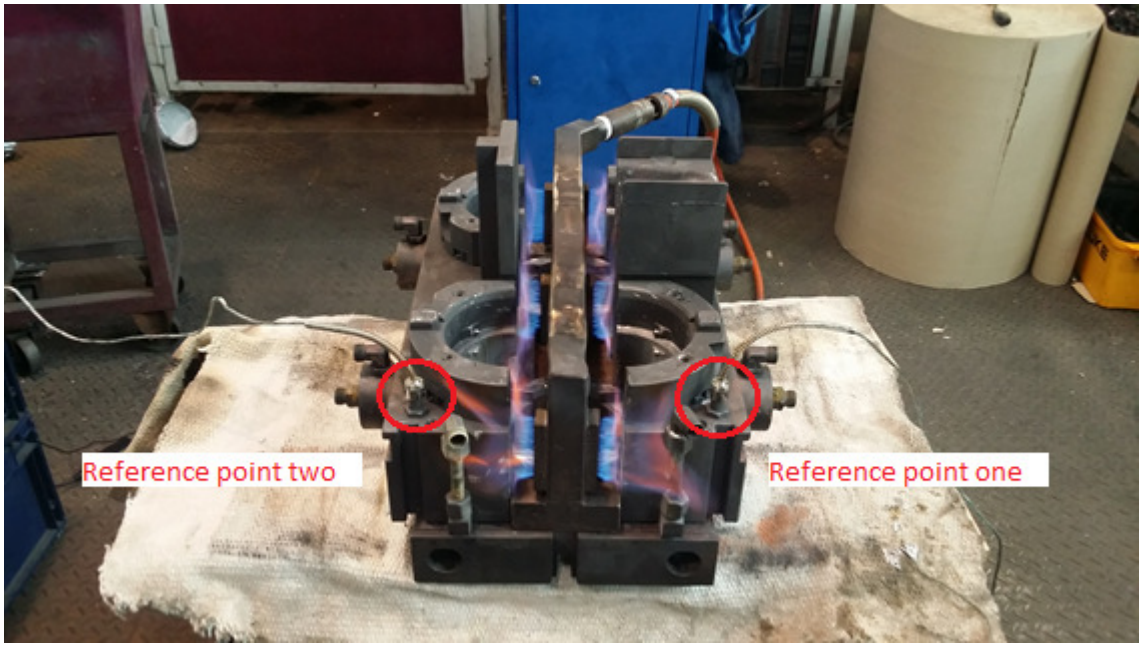

PICTURE 6. Measuring arrangements.

After setting everything up, we began the measurements. We measured each of the burners to figure out how long it would take to reach the operating temperature of the mould. Furthermore, we wanted to know what the surface temperature was during and after this process. We got help for the measurements from the local University, which staff was on site to operate a professional thermal camera. By having two independent temperature measuring instrument, we were able to confirm the process objectivity. The measurements were taken by 20 ºC interwall from beginning temperature up to 200 ºC according to the first reference point. The reference point was monitored in the same manner as it is done in the production conditions. This means a thermocouple sensor installed in the predrilled hole located in the place seen in the picture (6).

We measured the time it takes for the mould to reach the operating temperature from atmospheric conditions. We also measured the surface temperatures from six different points with infrared thermometer (Benetech GM 700). This was done and recorded with every 20 ºC increase of reference point one temperature. This way we were able to form a picture of heat distribution in the mould during the preheating process. These measurements were double checked from the data from the thermal camera. Example of the thermal camera data can be seen in the picture (7). In this following picture we can see Italian type heater in the last stage of heating time measurement. The burner is equipped with an inline array of round jet nozzles. In every main nozzle, there is five small round nozzles inside. This picture is taken in the moment when the reference point one is indicating an optimal operating temperature.

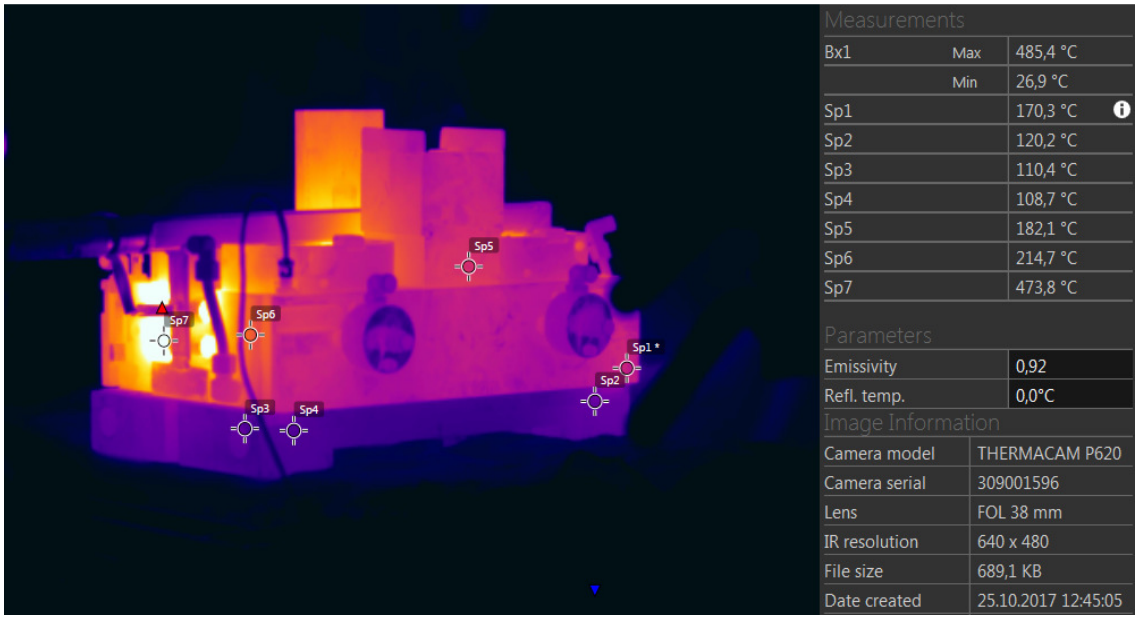

PICTURE 7. Mould preheated in the operating temperature.

Same measuring procedure was used with every three types of burner. All the data were recorded in Excel sheet for further analysis. The temperature was measured from eight different points of the mould. Two of those were measured from pre-drilled holes by using thermocouples and six other points were measured from the opposite sides of the mould, three in both halves of mould. This was done directly on the same point where the stagnation area is in the burner side. Results can be seen in the table (5). Complete measuring data can be found in appendices (4).

3.3 Measured data

TABLE 5. Measured time data from preheating.

Subject	Value	Unit
Italian model		
Average temperature, nozzle	1178	°C
Time	34 min 37 s	
Reference. Point. 1	200	°C
Reference. Point. 2	235	°C
German model		
Average temperature, nozzle	986	°C
Time	34 min 47 s	
Reference point. 1	200	°C
Reference point. 2	240	°C
Czech model		
Average temperature, nozzle	1200	°C
Time	36 min 36 s	
Reference point. 1	200	°C
Reference point. 2	204	°C

Mould heating up is figured in figures (5, 6 & 7) below as a function of time. Each measuring point is coloured separately.

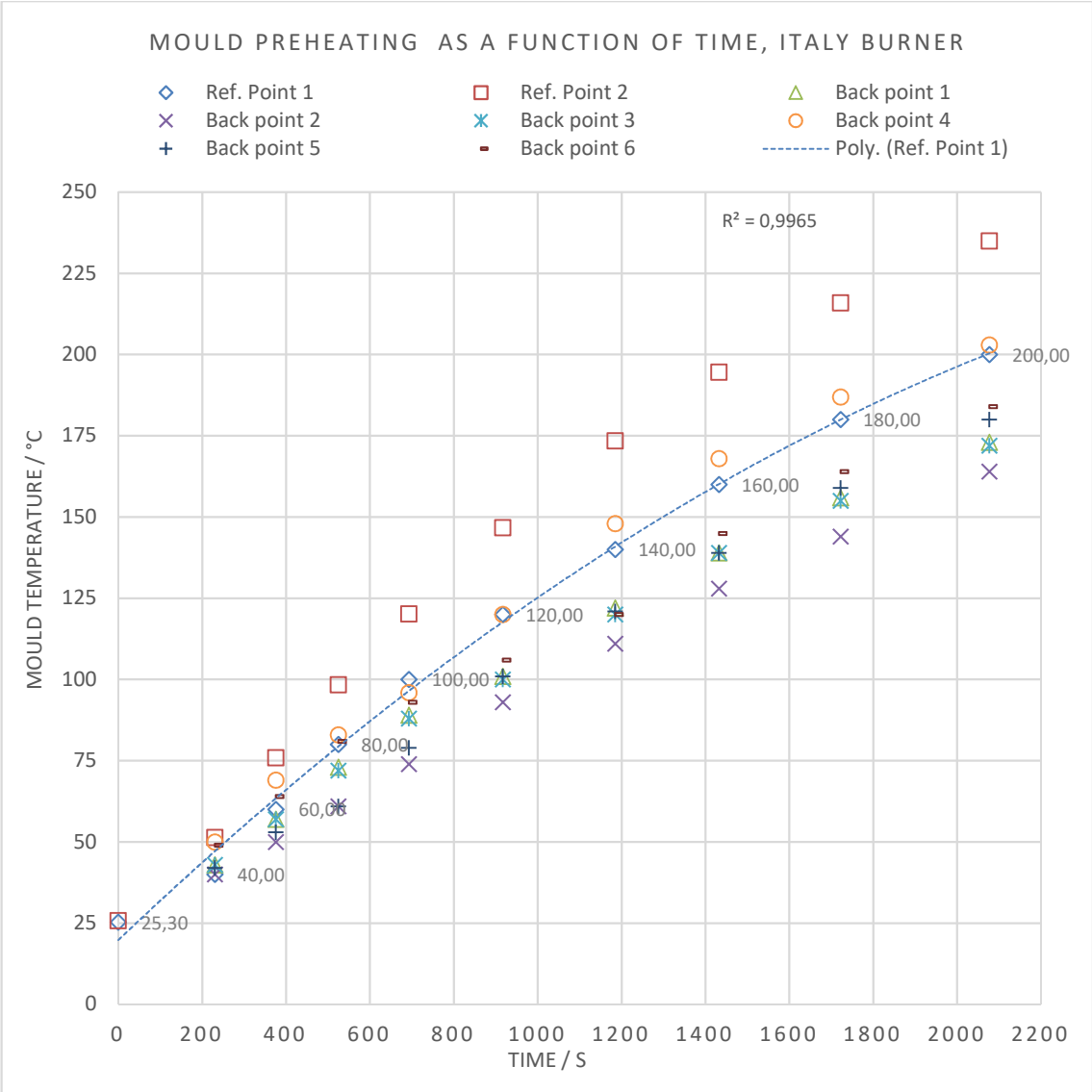

FIGURE 5. Mould preheating as a function of time, Italian burner used.

In the figure (5) the regression is taken from the points, indicating first reference point temperature rise. From those two measuring points used in the production, the first reference point is the last one which reaches the value of wanted limit in temperature. This observation we found to be logical because the mould halves are not complete symmetrical. Where the reference point one is located is slightly more mass than the second mould half. This is caused by the downgate, which is located in the same mould half where the first reference point is. This observation can be seen across the whole preheating process including the two other burner types. Only deviant is the Czech burner. In that model, both of the reference points, reached the wanted temperature, nearly in same period of time. This can be seen in the figure (6).

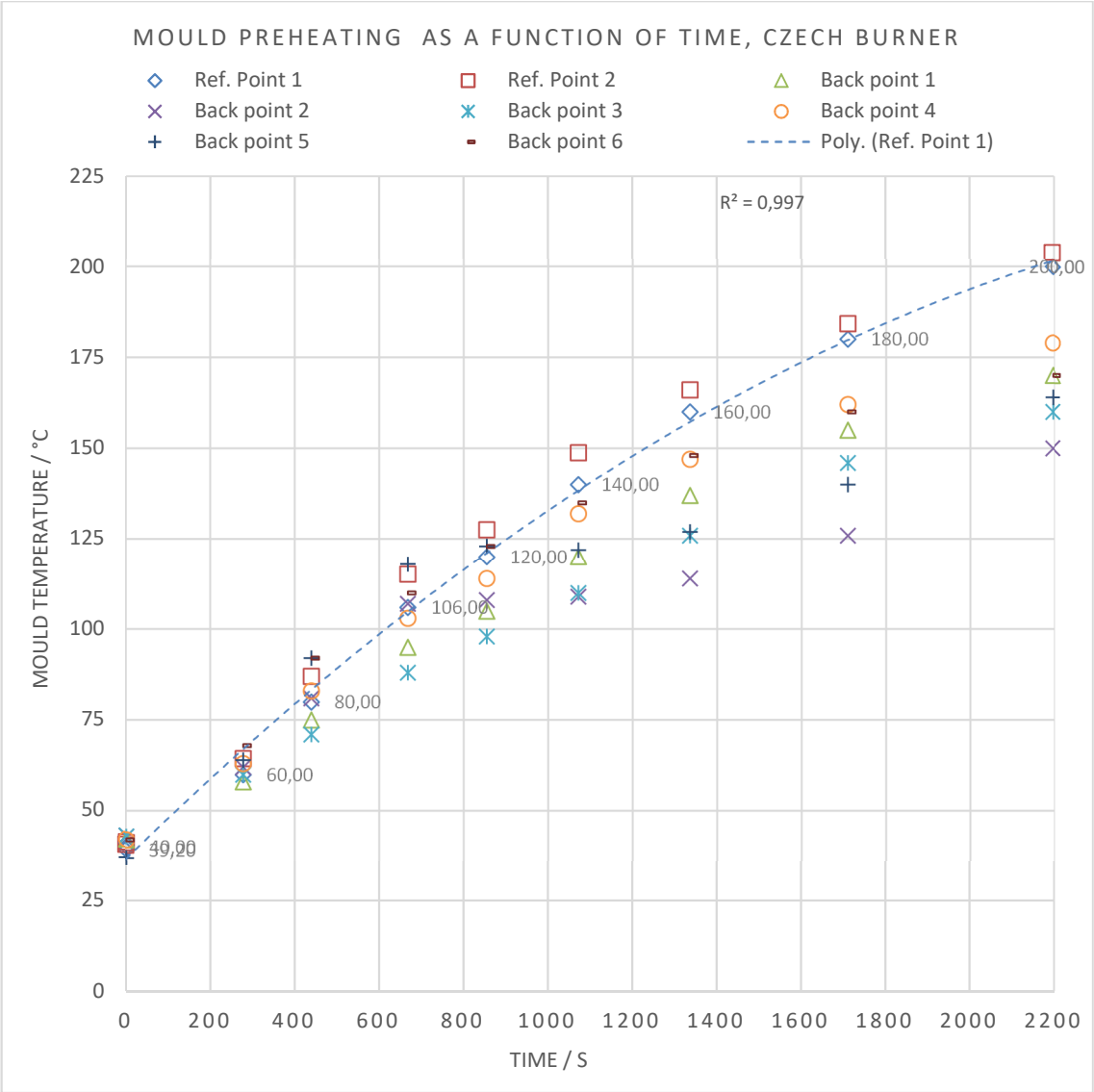

FIGURE 6. Mould preheating as a function of time, Czech burner used.

Like we can see in all the figures (5, 6 & 7) the second-degree regression descripts accurately the dependence between time and temperature. In our case this means accurate prediction for heating time and energy consumption.

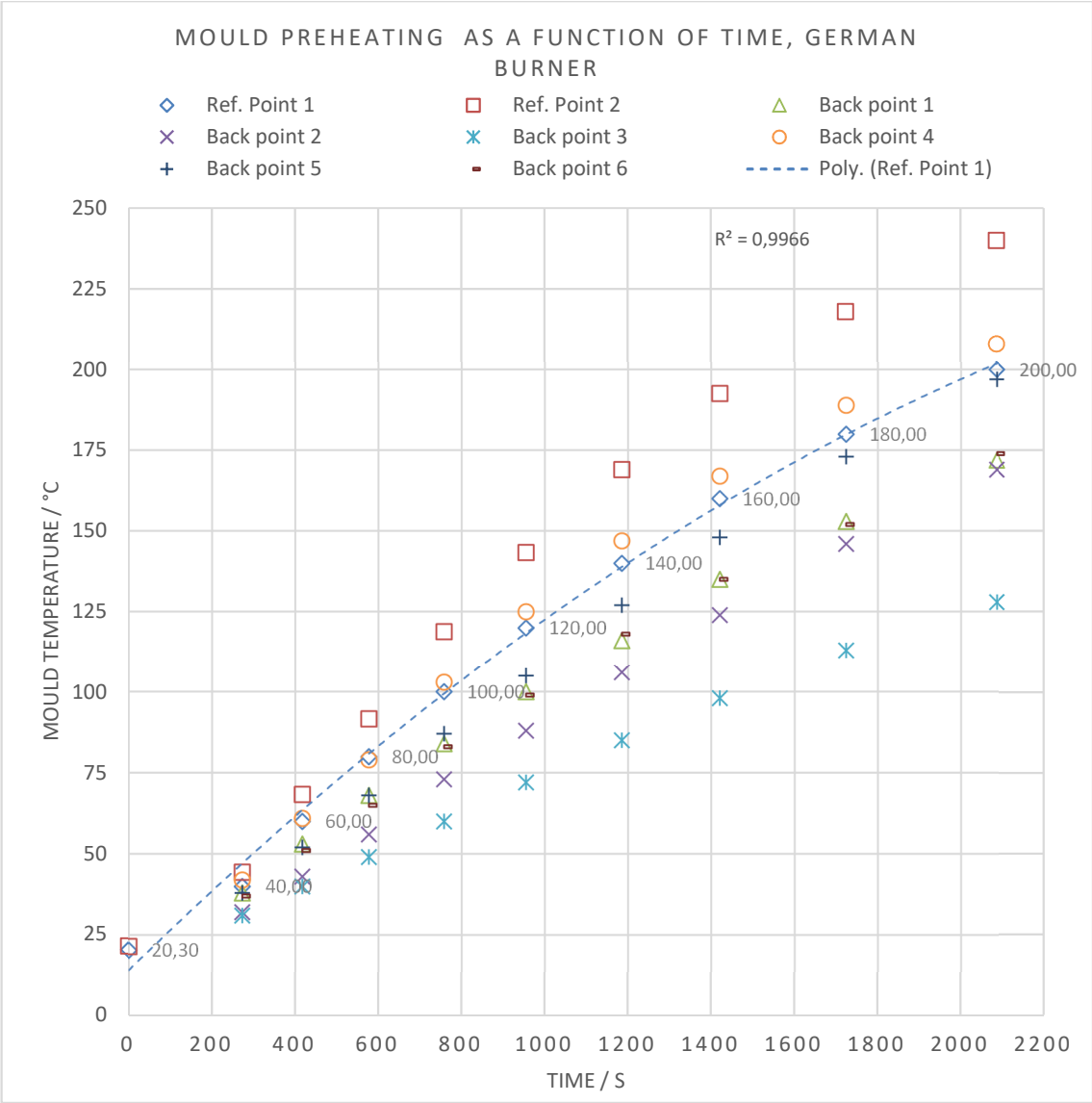

FIGURE 7. Mould preheating as a function of time, Czech burner used.

3.4 Gas mass flow measurements

The gas flow measurements were executed by using double instrument method. First, we monitored the gas line with rotameter and second point was measured on the burner frame between the second and third duct. In this point we assume that the flow speed had it natural mean value. By using the optimal air-fuel ratio for LNG, we could calculate the flow speed by using the known pressure and volumetric flow of natural gas. Because the air-fuel mixing procedure was a bit different in each burner, we had to determine the total gas consumption by different means. All those are suggested in the following chapter.

3.4.1 Measuring equipments

To ensure the reliability of measurement we ended up using double instruments. We used a rotameter (Kytölä instruments) which was installed directly on the gas line and a mass flow meter with hot wire sensor (Testo 432) installed in the burner body. These instruments can be seen in the picture (8).

PICTURE 8. Measuring instruments used in gas flow measurements.

3.4.2 Measuring arrangements

Flow speed was measured from the line by specially made rotameter and also with commercial mass flow meter. In both measurements required us to do modifications for the preheating system. The rotameter was installed to the pressurised gas line. For mass flow meter, we drilled a hole in each burner body. The hole diameter was measured in a way that the measuring device would barely fit in to it. The assembly was sealed with tape

around the measuring device head. The anemometer was inserted in to the burner body in flow direction. Measuring arrangements can be seen in the picture (9).

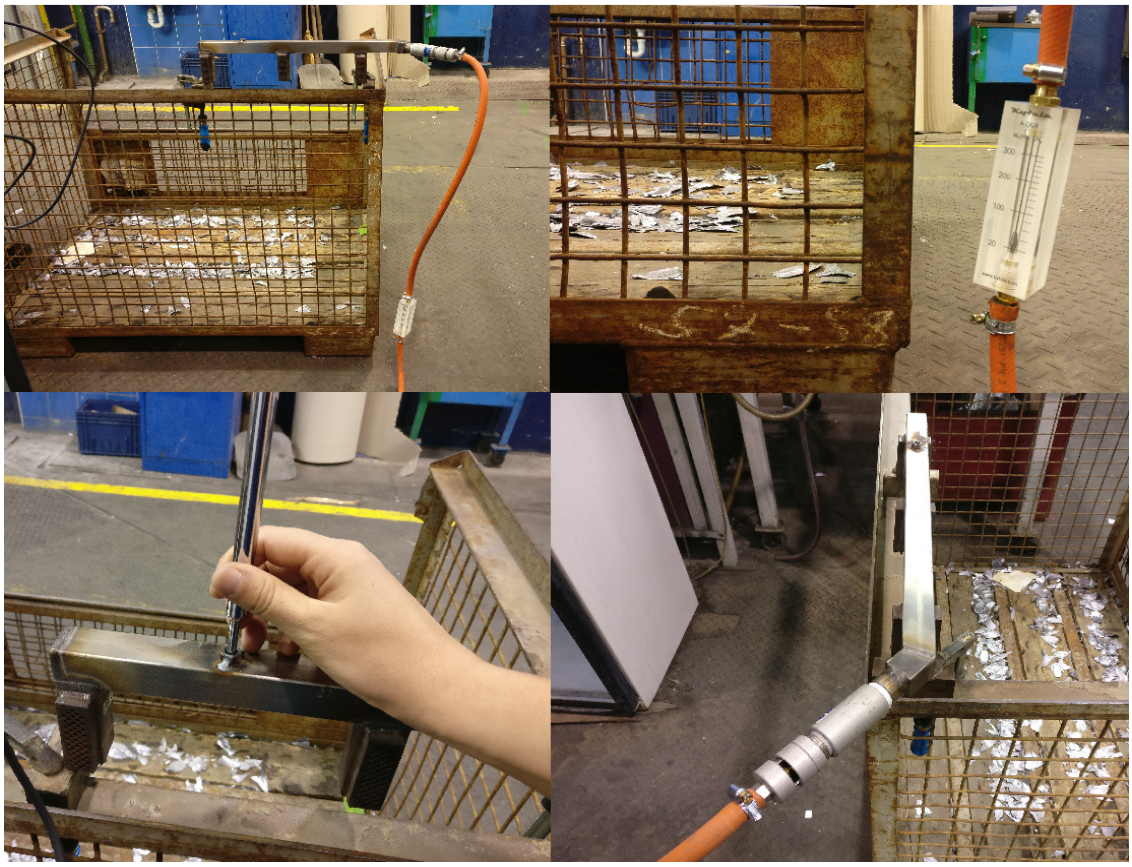

PICTURE 9. Gas flow measuring arrangements.

3.4.3 Natural gas compound and properties

As s fluid properties we have used methane values, which was the main part (98,39 %) of natural gas compound used in the process. From the figure (9) we can see all the contents in the natural gas compound. The contents are from the supplier's data.

FIGURE 9. Gas compound used in preheating process.

From the figure (10) we can see the density change of specific gas compound used in preheating as a function of pressure.

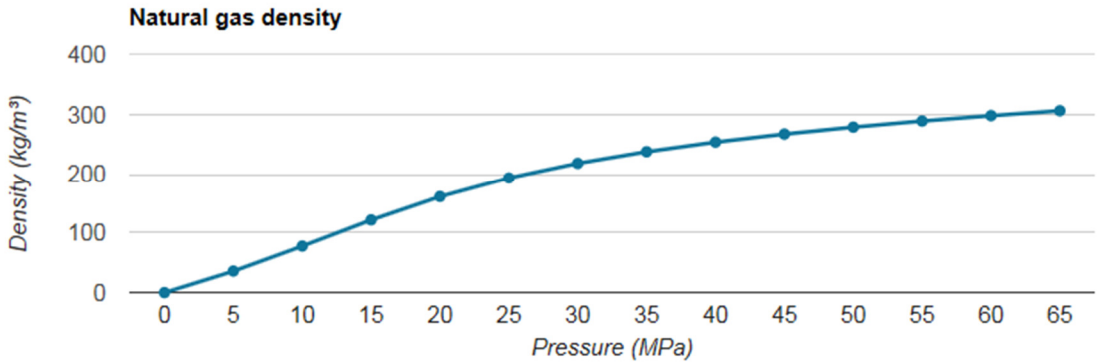

FIGURE 10. Gas compound density as a function of pressure. (Unitrove calculator 2018)

The gas compound and the properties can be seen in the table (7) below. Information is gathered from various sources.

TABLE 7. Gas properties.

Methane	Value	Unit	Sign
Dynamic viscosity	10,995	10^{-6}·(Pa·s)	μ
Kinematic viscosity	16,451	10^{-6}·m^2/s	μ_k
Density of methane	0,659	kg/m^3	$\rho_{methane}$
Compressibility factor	0,998	-	C_f
Specific Heat	2220	J/kg·K	c_p
Thermal Conductivity	0,035	W/m·K	k_f
Speed of sound	445	m/s	c
Density of air	1,20	kg/m^3	ρ_{air}
Density of gas mixture	1,149	kg/m^3	ρ_{mix}
Air-Fuel ratio	9,53/1	-	-

Gas properties is calculated via peace software online tool by using the atmospheric pressure and 20 ℃ for gas temperature (Peace Software, website). Value for thermal conductivity is gain from Engineering Toolbox online service (The Engineering ToolBox website). For density we have used a tabular value from Technical Formulas -book (Mäkelä, M., Soininen, L., Tuomola, S. & Öistämö, J. 2013, 179)

3.4.4 Measured data

All the measured data was collected to table for further analysis. Because some of the measured values were not directly in the usable form we had to perform some calculations so that we had all the needed values for the nozzle exit speed calculations. For the simplification we had to assume few things for the measurements. First we assumed that the gas flow from nozzles was in constant temperature. Second assumption was that the burning process ran with ideal air-fuel ratio. By following these assumptions we calculated the real flow of the gas through the burner. All the data from the flow measurements can be seen in the table (6). Complete measuring proceedings can be found in appendices (5). In figure (8) we can read the estimated values for gas consumption based on the flow measurements. For calculations we needed to have a specific density of gas mixture used in burning process. For simplification we assumed that the natural gas is pure methane

and mixture includes ideal amount of each compound for perfect air-fuel ratio for combustion. Density of the gas mixture was calculated by following formula

$$\rho_{mix} = \frac{(\rho_{methane} \cdot v_{methane} + \rho_{air} \cdot v_{air})}{(v_{methane} + v_{air})}, \quad (20)$$

where v is for part of volume for ideal air-fuel ratio for combustion. Substituting the variables by values from tabular data we end up having a density for air fuel mixture.

$$\rho_{mix} = 1{,}149 \ \frac{kg}{m^3}$$

Full calculations can be found in appendices (6)

TABLE 6. Measured flow values in every burner type.

Subject	Value	Unit
Italian model		
Rotameter (Gas)	19	L/min
MAF	23,3	m^3/h
Real flow calc. rotameter	319	L/min
Real flow calc. MAF	389	L/min
Discharge speed	107	m/s
German model		
Rotameter (Total)	203	L/min
MAF	32,8	m^3/h
Real flow calc. rotameter	325	L/min
Real flow calc. MAF	548	L/min
Discharge speed	19	m/s
Czech model		
Rotameter (Gas)	20	L/min
MAF	14,8	m^3/h
Real flow calc. rotameter	1375	L/min
Real flow calc. MAF	248	L/min
Discharge speed	12	m/s

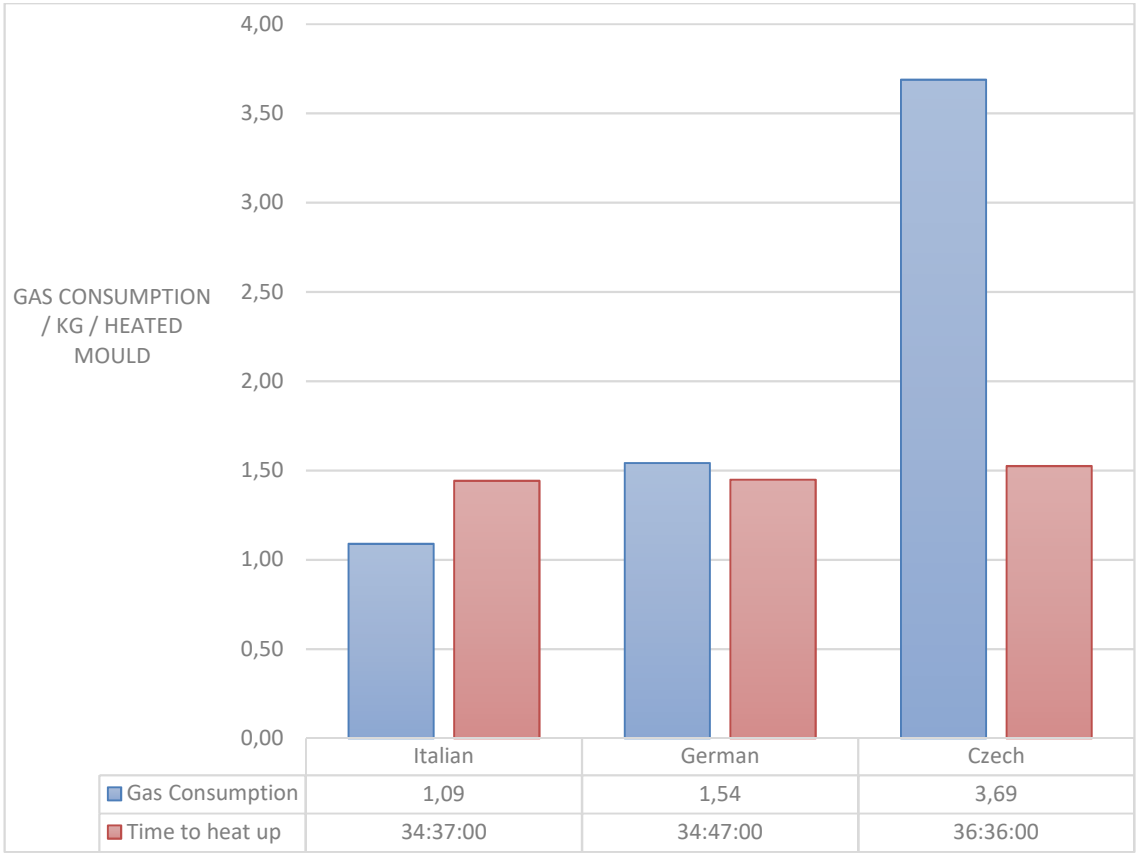

FIGURE 8. Estimated gas consumption based on the flow measurements.

4 ANALYTICAL SCRUTINY

In this chapter we will go through the analytical calculations for heat transfer by forced convection in the impinging jet application. For clarity the calculation process is divided in several sections.

4.1 Boundary conditions

In this thesis work we were forced to do a lot of assumptions. Mainly these assumptions were made in the field of boundary conditions. Because of the complicated form of burners and fairly heterogeneous types of nozzles we had an urgent need to do some simplifications. First, we decided to speak about nozzles. We didn't have chance to have a closer examination about the burners gas discharging holes. We determined the form by using rough estimation based on CAD drawings and we decided to consider all the discharging holes as nozzles. This assumption requires that the flow through the discharging hole is much less disrupted than it would be with orifices, but with orifices there would have been more than 29 % increase in discharge coefficient (Samaras 2012).

Second big assumption is also related to the nozzles. We had to assume that the nozzles were uniform and have a similar flow pattern to each other. We also needed to assume that the nozzle exit velocity is distributed even between every nozzle. Lastly we assumed that the flow rate was equal. Third one was considering about the equal flow rate in every part of burner. Because the burner bodies and gas channels didn't have any compensation for decreasing flow speed we knew that the flow speed is different in each duct in burner body.

For calculations we had to crop a certain stagnation area. This was done by observing the heating process and defining the area by slicing the CAD model face and measuring the area. Example of this can be seen in the picture (10).

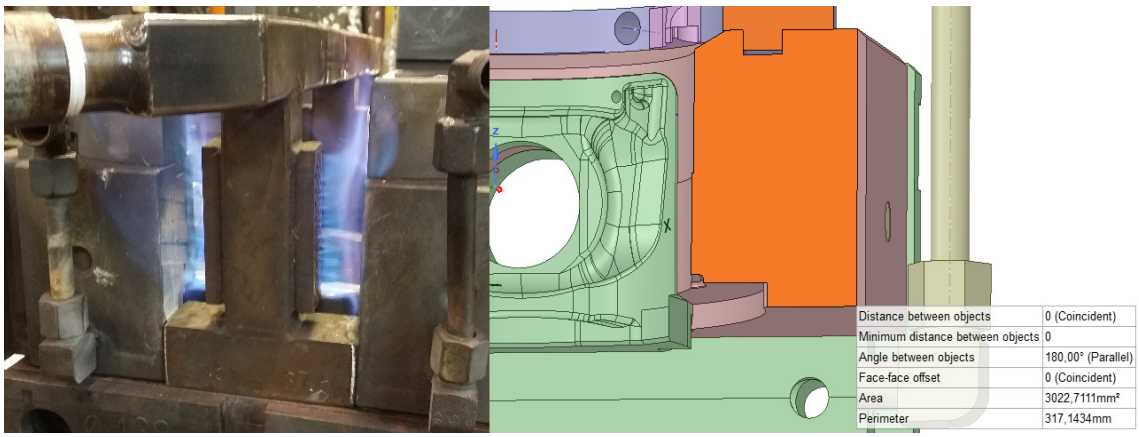

PICTURE 10. Restricting the stagnation area by slicing the body in SpaceClaim.

4.2 ARN, Italian burner

For each burner we used the ARN correlations. In Italian burner is case we had five nozzles staggered in one main “nozzle”. In the nozzle can be seen that there is actually four orifices and one nozzle. This means that the flow is more laminar from the discharging hole in the middle than from the holes on the edge of the pattern. Probably for that reason the flow is forced to go around the plate in the middle of the pattern. As we monitored the burning process while measuring the preheating, the burning process seemed to be quite laminar in this model. Illustrative picture (11) of the nozzle construction can be seen below.

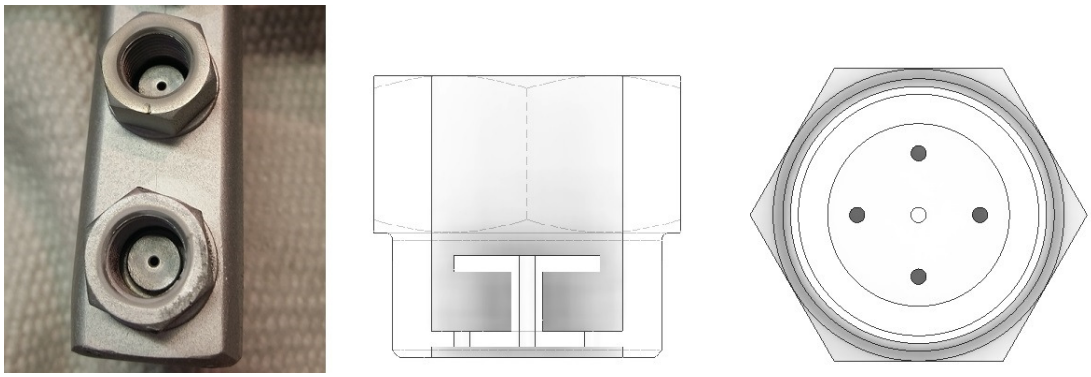

PICTURE 11. Italian burner nozzle and the cross-section of the junction from 3D-model.

For ARN problem we used the correlation (22), which can be seen below

$$\left(\frac{\overline{Nu}}{Pr^{0,42}}\right)_{ARN} = K\left(A,\frac{H}{D}\right)G\left(A,\frac{H}{D}\right)F(Re), \tag{21}$$

this correlation is formed directly from equation (13) shown in chapter (2.11). Because array correlation is difficult to define, we ended up using the same conclusion that M. Attalla (2015, 143) has done in his paper, where he studied a stagnation region in heat transfer for circular jets impinging. In Attalla's paper he considered that the dimensions of in line –array region can be defined through the middle axis of five nozzle arrange. Illustrative picture can be seen in the figure (11) below.

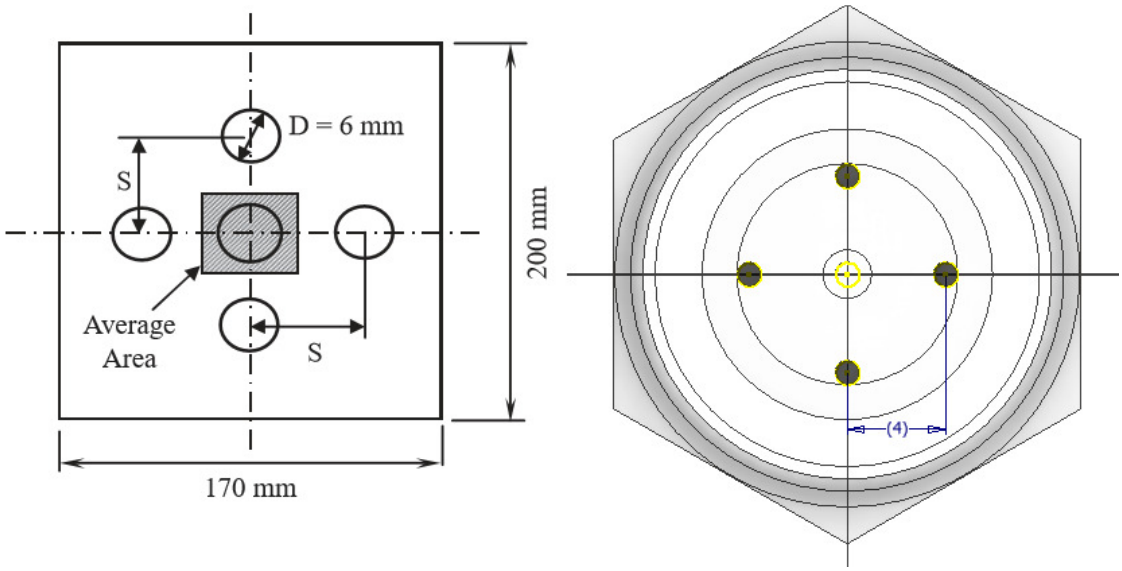

FIGURE 11. Nozzle array and applied dimension for square packed jets. (Attalla, Modified)

4.2.1 Variables

Before using the correlation, we had to determine all the different variables by calculation. At the table (8) below is listed all the measured or known characteristic values of the burning process.

TABLE 8. Values for analytical calculations.

Description	Value	Unit	Sign
Velocity, nozzle exit	107	m/s	V_e
Temperature, nozzle exit	1451	K	T_e
Distance, nozzle to surface	30	mm	H
Nozzle diameter	1	mm	D
Hydraulic diameter	1	mm	D_h
Pitch of nozzle array	4	mm	S
Density of steel	7870	kg/m^3	ρ
Stagnation area	0,012021	m^2	$A_{surface}$
Thermal conductivity, steel	58	W/m·K	k_s
Directly heated mass	24,7	kg	m_{mould}
Specific heat, steel	473	J/kg·K	c_{steel}
Distance, to reference point	75	mm	$d_{reference}$
Cooling mass	11,3	kg	m_{bed}
Machine bed temperature	365	K	T_m

In table (9) we can see the values of the boundary conditions for the calculations.

TABLE 9. Boundary conditions used in calculations.

Description	Value	Unit	Sign
Wanted temperature	473	K	T_w
Delta temperature	987	K	ΔT
Ambient temperature	299	K	T_s
Bed temperature	363	K	T_m
Delta temperature (bed)	383	K	ΔT_c

4.2.2 Calculations for Italian type burner

In order to use the correlations for impinging theory, we had to calculate a couple of variables. Those were the Prandtl number, film temperature, relative nozzle cross-section area and Reynolds number. By using these and all the data collected from the process we were able to figure out the heat transfer coefficient. Prandtl number is calculated by using following definition

$$Pr = \frac{\mu_d \cdot c_p}{k_f}, \tag{22}$$

where μ_d is dynamic viscosity, c_p is specific heat and k_f is thermal conductivity of the fluid. By using pre-collected data about the fluid properties, we could calculate the Prandtl number by using formula (23).

$$Pr = 0{,}7$$

Film temperature is variable used to describe the temperature of convection boundary layer. This temperature variable is calculated by using following formula

$$T_f = \frac{T_s + T_e}{2}, \tag{23}$$

where T_s is temperature of mold surface at beginning stage, T_e is temperature at nozzle exit. By using the data measured from heating process we could calculate the film temperature by using formula (23).

$$T_f = 875\ K$$

By using following correlation put forward in table (2), we calculated the relative nozzle area

$$A_{r.ARN} = \frac{\pi}{4} \cdot \left(\frac{D}{S}\right)^2, \tag{24}$$

where D is diameter of the nozzle and S is the pitch of the nozzle array. When numerical values are substituted in equation (24) we can get the relative nozzle area.

$$A_{r.ARN} = 0{,}049$$

For last we calculated the Reynolds number for the stagnation flow. That was done by using the following equation

$$Re = \frac{v_e \cdot D_h}{\mu_k}, \tag{25}$$

where v_e represents the fluid velocity at nozzle exit, D_h is for hydraulic diameter of nozzle and μ_k is fluid kinematic viscosity. By using data collected from heating and tabular data of flowing fluid we were able to calculate the Reynolds number by using previous formula (25).

$$Re = 6514{,}8$$

The correlation (21) was calculated in separated parts for clearance. First part was the function of F. This can be seen in following equalisation descripted below

$$F = 0{,}5Re^{2/3}, \tag{26}$$

where Re is Reynolds number. When we assign our previously calculated Reynolds number to this equalisation (26), we get value for F.

$$F = 174{,}4$$

After this we calculated function G. This was done by formula descripted forward

$$G = 2A^{0{,}5}\frac{1 - 2{,}2A^{0{,}5}}{1 + 0{,}2(H/D - 6)A^{0{,}5}}, \tag{27}$$

where *A* is for relative nozzle area, *H* is for distance between nozzle exit and stagnation point and *D* is for hydraulic diameter of jet nozzle. By assigning all the previously computed and collected values, we get numerical value for *G*.

$$G = 0{,}11$$

After receiving numerical value for function *G*, we needed to calculate the numerical value for function *K*. This was done by using formula descripted below

$$K = \left[1 + \left(\frac{H/D}{0{,}6/A^{0{,}5}}\right)^{6}\right]^{-0{,}05}, \tag{28}$$

where *H* is distance between nozzle exit and stagnation point, *D* is for hydraulic diameter of nozzle and *A* is for relative jet nozzle area. By assigning all the previously computed and collected values, we get numerical value for function *K*.

$$K = 0{,}486$$

By calculating numerical values for previous functions (27 & 26) we ended up at situation where left side of the correlation had one unknown variable and that was Nusselt number. Multiplying the correlation with Prandtl number to the power of 0,42 gave us the following function

$$Nu = G \cdot F \cdot Pr^{0{,}42}, \tag{29}$$

where every other variable is known besides the Nusselt number. After we substituted the variables with numerical values computed previously, we got a Nusselt number.

$$Nu = 8{,}02$$

Via Nusselt number we got our hands on the heat transfer coefficient. By looking at the definition of Nusselt number from previous section (2.4), we can see that the dimensionless number is a function of convective heat transfer coefficient, characteristic dimension and thermal conductivity. This why we could write it in following form,

$$Nu = \frac{h \cdot D_h}{k_f}, \tag{30}$$

where D_h is hydraulic diameter of nozzle, h is heat transfer coefficient and k_f is thermal conductivity. By doing a little re-organisation we end up getting heat transfer coefficient on the left side of the function. We write the previous equation in following form

$$h = \frac{Nu \cdot k_f}{D_h}, \tag{31}$$

whereupon we could calculate the actual heat transfer coefficient by substituting the variables with measurer and computed values.

$$h = 280{,}7 \ \frac{W}{m^2 \cdot K}$$

We had stagnation area approximated from CAD-model. From the model we were able to calculate the surface area for the power calculations in heat transfer. The calculation for heat flow was done by applying the Newton's law of cooling. Dividing the mass heat flux, shown in equation (1), by surface area we can write the Newton's law of cooling in the following form

$$q = h \cdot A_{surface} \cdot (T_e - T_s), \tag{32}$$

where $A_{surface}$ is stagnation surface area, T_e is for temperature of the fluid at the nozzle exit and T_s is for temperature in the impinging surface. By substituting these with measured and computed values, we got a power of heat transfer process in preheating process via total stagnation area of mould half.

$$q = 3890 \ W$$

For simplicity we ended up for summarization in energy consumption in process. For that we needed to know the outflowing energy in the system. That is why we calculated the required energy to increase the temperature of the mould half. This was done by using following equation

$$Q_n = \Delta T \cdot c_{steel} \cdot m_{mould}\ , \tag{33}$$

where ΔT is the change in temperature, c_{steel} specific heat for steel and m_{mould} is mass for the half mould from stagnation area to the reference depth. Substituting the variables by measured and computed values we were able to calculate the needed heat energy.

$$Q_n = 2034290\ J$$

Because of the measuring arrangement we had a one big mass which was cooling the system down by increasing the mass of the system. This was the bed underneath the mould. We calculated the energy needed for the bed mass to increase from beginning temperature to the value read from the thermal camera picture at the point where the reference temperature reaches the wanted temperature. When the incoming heat flow in the system was known, we needed to compute the outflowing energy from the mould. For this we calculated the energy taken via mould to heat the bed in the machine. This was done by applying the equation (32), where mould mass was replaced by mass of the half bed and delta temperature was formed from bed temperature at beginning and in the end time of the measurements. With this knowledge we ended up to having a value for energy, taken for heating the bed in comparison temperature.

$$Q_{bed} = 452796\ J$$

The theoretical heating time in this ideal system, where energy losses goes only for bed heating. This was calculated just using energy sum principle. Following equalisation gives us the time needed to heat the mould by Italian burner in ideal circumstances

$$t = \frac{Q_n + Q_{bed}}{q}, \tag{34}$$

where Q_n , Q_{bed} are values of energy computed with previous equation and $Q$is total heating power. Substituting these with values calculated previously we got a theoretical time what is needed to increase the temperature of mould in wanted temperature in ideal conditions.

$$t = 10{,}657 \text{ min}$$

Complete calculations for the Italian burner can be found in appendix (7).

4.3 ARN, German burner

Last burner analysed by analytical means is second one used for heating. Its German design. In this burner the discharging of gas is done via nozzles. Although the nozzles should be almost considered as an orifices. This is the biggest difference between this one and the burners in previous calculations and also could bring some error in comparison. The orifice has own correlations suggested by Martin (1977, 22). These correlations are presented in section (2.12) and can be founded in equation (17-20). The illustrative picture (12) of the burner and the nozzle array can be seen below. We computed the values by using the correlations for nozzle.

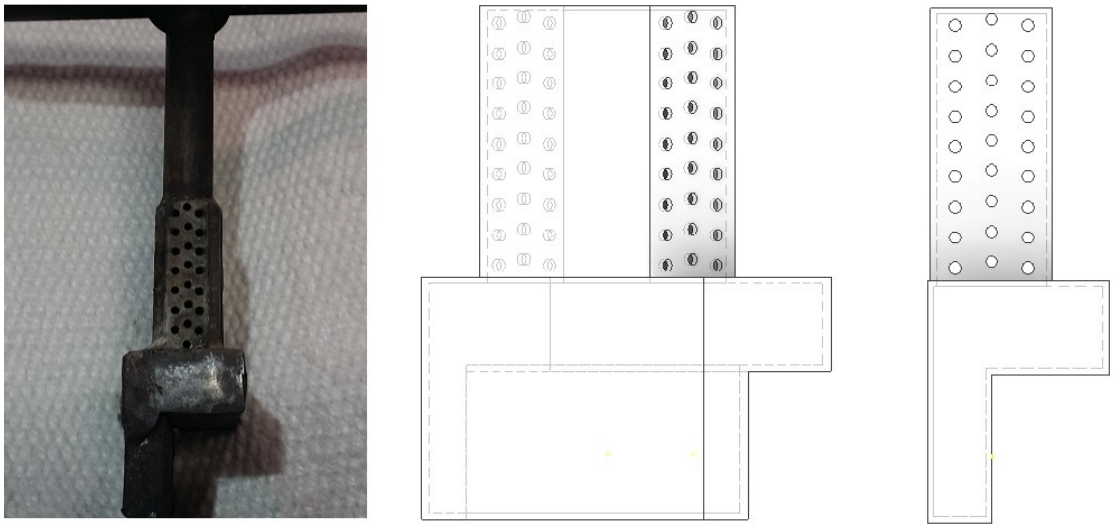

PICTURE 13. Czech burner nozzle head and 3D-model of the jet nozzle head.

4.3.1 Variables

Slight changes are made to the variables for calculations considering the German burner. All the measured values can be seen in the table (11) below.

TABLE (11) Values for analytical calculations.

Description	Value	Unit	Sign
Velocity, nozzle exit	19,1	m/s	V_e
Temperature, nozzle exit	1259	K	T_e
Distance, nozzle to surface	13	mm	H
Nozzle diameter	2	mm	D
Hydraulic diameter	2	mm	D_h
Pitch of nozzle array	3,58	mm	S
Stagnation area	0,009172	m^2	$A_{surface}$

By using similar analytical process what was done in the previous section we ended up to theoretical heating time presented in following.

$$t = 49{,}1 \text{ min}$$

Complete calculations for the German burner can be found in appendices (8).

4.4 ARN, Czech burner

In Czech burner is case we used also an ARN correlations, just like we did on the Italian one. The major difference between these two are in correlation for relative nozzle area and the stagnation area in heating process. The Czech burner has a hexagon staggered array of nozzle jets. This causes the difference between the correlations. It comes via computation of the relative nozzle area. This means that comparing to the earlier, Czech burner have more homogenous flow pattern in across the discharging nozzles. All of the discharging holes can be considered as nozzles, because of their relatively long constant cross-sectional area. This causes the flow to develop more laminar than just discharging the flow through plain orifice. Illustrative picture (12) of the nozzle construction can be seen below.

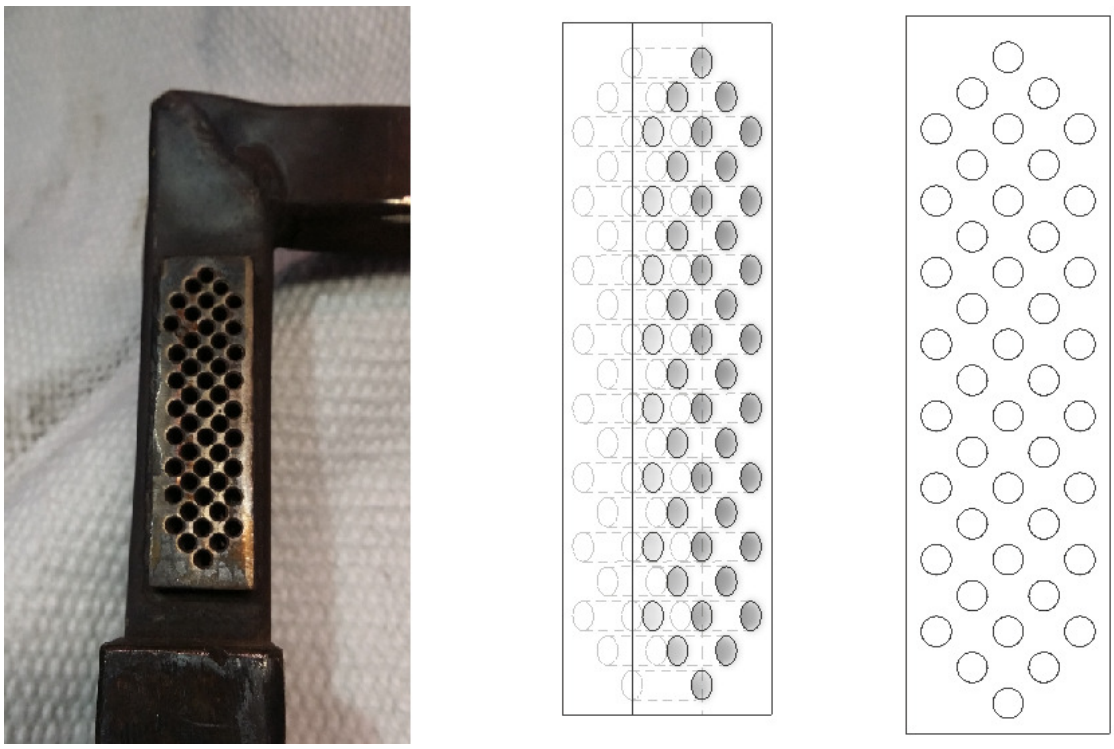

PICTURE 12. Czech burner nozzle and 3D-model of the jet nozzle.

4.4.1 Variables

Because of the differences between burner types, some slight changes needed to be done in calculations. These changes considered values like relative nozzle area, jet nozzle pitch, stagnation area, temperature at the nozzle exit, distance between nozzle and impinging point, nozzle characteristic dimensions and flow velocity at nozzle exit. All these variables are gathered in following table (10)

TABLE (10) Values for analytical calculations.

Description	Value	Unit	Sign
Velocity, nozzle exit	12,3	m/s	V_e
Temperature, nozzle exit	1472	K	T_e
Distance, nozzle to surface	20	mm	H
Nozzle diameter	3	mm	D
Hydraulic diameter	3	mm	D_h
Pitch of nozzle array	4,95	mm	S
Stagnation area	0,012021	m^2	$A_{surface}$

By using similar analytical process what was done in the previous section we ended up to theoretical heating time presented in following.

$$t = 39{,}4 \text{ min}$$

Complete calculations for the Czech burner can be found in appendices (9).

4.5 Results from analytical scrutiny

In following table (12) we have gathered the results of the analytical scrutiny. All the results are described as a function of nozzle exit flow speed. This is done because the exit velocity is really complicated to verify for having some exact values. Therefore the results are presented as a range of flow speed values.

TABLE 12. Theoretical heating times when considered the flow measuring uncertainties.

Type of burner	Italian	German	Czech	Unit
Theoretical heating time.	11,2	35,7	52,9	min
	11,1	35,5	52,8	min
	11	35,3	52,7	min
	10,9	35,1	52,5	min
	10,8	34,9	52,4	min
	10,7	34,6	52,3	min
	10,6	34,4	52,2	min
	10,5	34,2	52	min
	10,4	34	51,9	min
	10,3	33,8	51,8	min
	10,2	33,6	51,7	min

5 OPTIMIZATION BY GEOMETRICAL MEANS

By following the analytical scrutiny results we can write down couple of rules to follow while doing the optimizing the geometry of burner. Optimization by geometrical means follows the route to meet a highest average in heat transfer coefficient in specific application. By these means we try to reach the quickest possible preheating time for the current casting process. Saving time means in this case saving the energy in LNG burning process.

Martin (1977, 45) also considers the optimization process in his paper. Like Martin we noticed that the optimization is possible to proceed by changing the characteristic lengths of the process heater. At least this path can be considered as the easiest option in the case we are studying. These lengths are the nozzle jet hydraulic diameter, nozzle to nozzle spacing called pitch and distance between the nozzle jet exits to the stagnation point. The optimization is done by using the previously calculated information and applying the knowledge of pre- calculated results introduced by Martin, in his paper.

As an example, we are using the Italian burner like we did in the analytical scrutineering section. This we can get a clear picture of the whole process and avoid mixing up the cases for nothing. This was executed because the Italian burner had the best starting level for doing the optimization. Following rules can be applied on any of the burners used in the process.

5.1 Theoretical closure

Based on the previous correlations Martin has also suggested a function for optimal geometrical dimensions. In his paper this is done by setting the distance between nozzle and stagnation surface constant (1977, 46). By these means suggested that the following function leads to the optimal results for heat transfer coefficient

$$\frac{H}{D_h} = \frac{1}{11} \cdot \left(12 + 25 \cdot \frac{22 - 169\varphi}{(11\varphi)^2 - 10\varphi}\right), \tag{34}$$

where φ represents the square root of the relative nozzle cross section area. By using the presented equation, Martin (1977, 48) ends up to suggesting the optimal values for variables presented in table (13).

TABLE 13. Optimal values for presented variables.

Variable	Value
A_{opt}	0,0152
$(H/D)_{opt}$	5,43
G_{opt}	0,385
D_{opt}	0,184H
$S_{opt.hex}$	1,423H
$S_{opt.inl}$	1,324H

5.1.1 Optimal distance between nozzle and surface

As we can imagine, there is a constructional reason for limiting the spacing between the nozzle exit and the stagnation surface. This why in following section we try to find the optimal distance for heat transfer and what is plausible to execute. At the figure (12) we can see the effect of distance between the nozzle jet and stagnation surface as a function of heat transfer coefficient. The function is based on the Italian burner geometry.

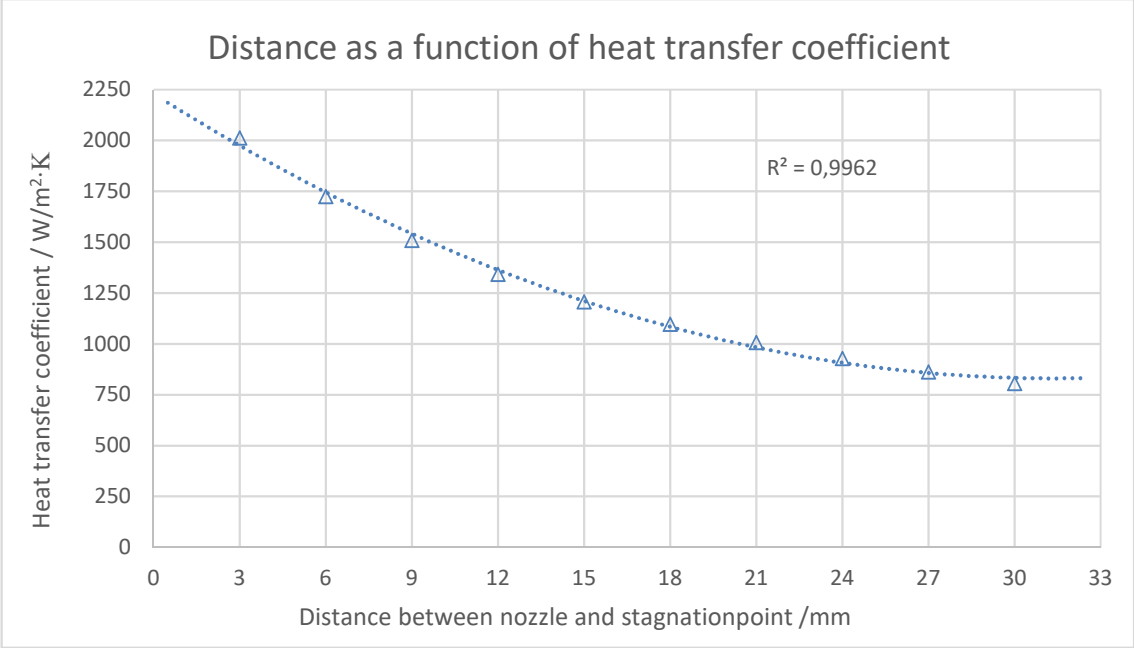

FIGURE 12. Nozzle distance as a function of heat transfer coefficient in Italian burner.

As we can see from the figure (12), the heat transfer coefficient has a second-degree relation for distance, between nozzle exit and stagnation point. According to this correlation we can state that air gap between the nozzle and mould is wasting energy from burning process by following a second-degree dependence. In here we can say that less is more. Because of the complicated correlations, only way to find optimal distance is by using iterative methods. For this kind of tasks, programs like Excel provide some sophisticated tools. Because we know the ultimate limits and the goal, we could use the Excel's own solver tool to find the biggest possible value for heat transfer as a function of distance between the nozzle exit and stagnation point. In the Italian burner -case, it would be a value between the current distance and 10 mm, where minimum distance is limited because of the structure of the jet nozzles body.

As we consider that we are moving in one-millimetre steps and we know that the heat transfer coefficient will increase significantly as a function of distance, we can assume that the optimal distance is 11 mm from the nozzle exit. In this value we have already taken care of the constructional limitations. For Italian type burner there is also limiting factor which comes from the structural design where the nozzles are set in separate housing. This limits the stagnation area by restricting the flow to the area of nozzle body inner diameter. But according to the Martin (1977, 4) Impinging flow reaches its core tip approximately at the distance which equals four times the nozzle diameter. This suggestion

supports our perceptions about the burning temperature measurements. The optimal distance between the impinging point and the nozzle exit increases to the value of 15 mm. The natural gas flame can be seen in the picture (14).

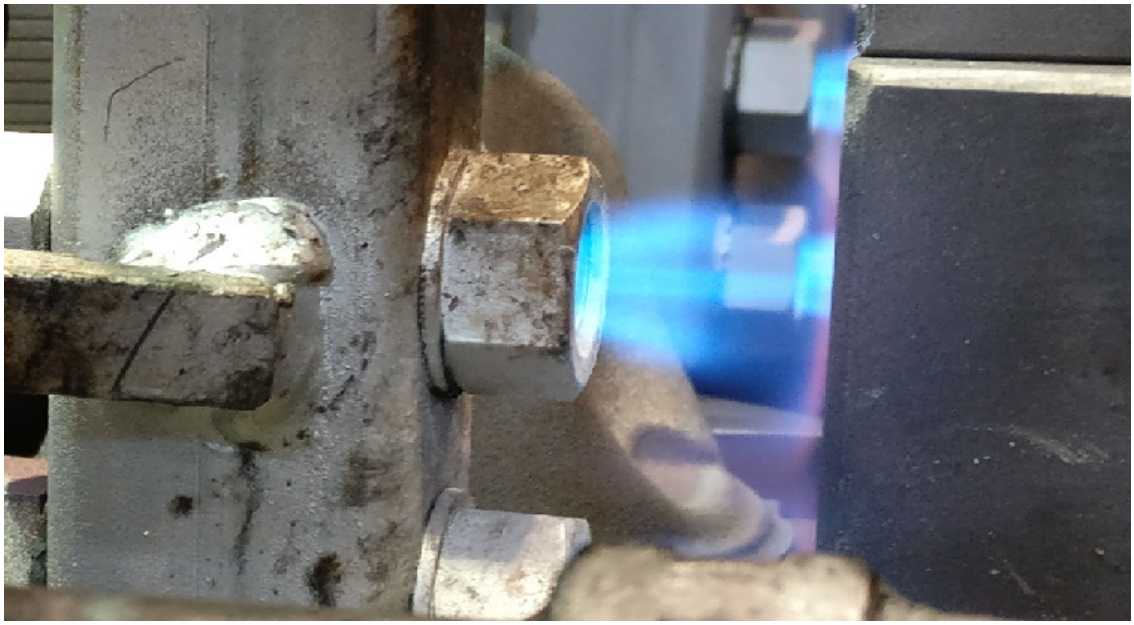

PICTURE 14. Natural gas flame from Italian -model burner.

Taking this into consideration we have to bring the stagnation point a little bit further away from the nozzle jet. First sophisticated guess can be 15 mm which gives us a 2,76 mm for diameter of nozzle. By multiplying this with the approximation of optimal core length we end up pretty close in distance where the core tip and stagnation point meet. The optimal nozzle diameter was calculated by using following ratio

$$D_{opt} = \frac{H}{5{,}43}, \tag{35}$$

where H is desired distance between nozzle exit and impinging surface. By substituting the variable with wanted length, we get optimal diameter of nozzle.

$$\frac{15\ \text{mm}}{5{,}43} = 2{,}76\ \text{mm}$$

By using the settled distance for nozzle exit and mould surface, we can calculate the ideal pitch for the nozzle array by following ratio

$$S_{opt.inl} = 1{,}324 \cdot H\ , \tag{36}$$

by substituting the variable by settled length we get optimal pitch for nozzle array.

$$1{,}324 \cdot 15\ \text{mm} = 19{,}86\ \text{mm}$$

Like we can see from the result, this kind of modification cannot be executed in real life solution with the Italian burner. The dimensions of the ducts not comply with the required nozzle array dimensions. For this reason we study further for the correlation between the distances and heating time. As we mentioned earlier the correlation got a dependency of exponential degree. Leaning on this knowledge, we can assume that one of the biggest effects can be reached by adjusting the primary distance between the impinging surface and nozzle discharge. By using the correlation from the regression from the figure (7), we can assume that the heat transfer can be improved just by adjusting the distance, from original 30 mm to 15 mm. The approximation of heat transfer coefficient can be calculated by using the following correlation

$$h = 1{,}4234 \cdot H^2 - 89{,}27 \cdot H + 2230{,}1\ , \tag{37}$$

where the *H* represents the distance between stagnation point and nozzle exit. By substituting *H* with wanted distance and solving the equation, we get an estimated heat transfer coefficient.

$$h \cong 1200\ \frac{\text{W}}{\text{m}^2 \cdot \text{K}}$$

Like we can see from the previous calculation, by simply adjusting the distance, we can easily triple or even quadruple the heat transfer coefficient when compared to the original situation.

5.1.2 Flow turbulence effect on the heat transfer coefficient.

One big issue in burning process is the form of the flow after discharging from nozzle. In the figure (13) we can see the change of the Reynolds number as a function of heat transfer coefficient.

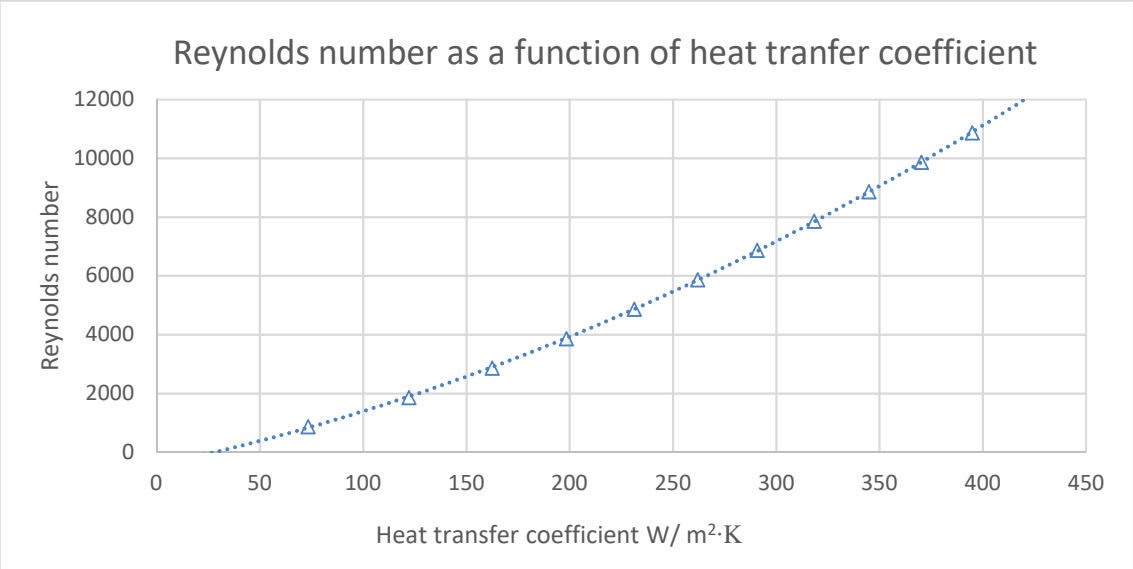

FIGURE 13. Heat transfer coefficient as a function of Reynolds number.

The Reynolds number has basically dependency on two variables, as we assume that the values of fluid remains constant. Those variables are hydraulic dimension of nozzle jet and exit velocity. Because we decided earlier our nozzle dimensions, only remaining option is adjusting the exit velocity. The correlations Martin suggested (1977, 15), where increasing Reynolds number increases the value from function F (14). By increasing the value of function we have a direct effect on Nusselt number, which defines the heat transfer coefficient among with two constant values. By using this conclusion, we can see that the nozzle exit speed is significant factor in the heat transfer process.

When we look the equation of flow speed (Mäkelä, M. et al. 2013, 99)

$$v = \frac{\dot{m}}{A_{nozzle} \cdot \rho_{mix}} \tag{38}$$

$$\Longrightarrow\ v = \frac{\rho_{mix} \cdot \dot{V}}{A_{nozzle} \cdot \rho_{mix}}$$

$$\Longrightarrow v = \frac{\dot{V}}{A_{nozzle}},$$

where $\dot{m}$ is mass flow, $\dot{V}$ represents volume flow and A_{nozzle} is total discharging area. We can clearly see that if our volumetric flow remains constant, only parameter affecting the nozzle exit speed is the total discharge area. This presumption can be made if we treat the flowing gas as an incompressible fluid. When comparing the Reynolds number between the Italian and Czech burners we can see the difference. While flow in the stagnation jet of Czech burner reaches the Reynolds number of 2300 in best case scenario, the Italian reaches the value of 7000. From here we can see the relation between the total cross section and heat transfer coefficient. In following figure (14) we can see how the heat transfer coefficient and the nozzle exit velocity chances the burning process efficiency when we adjust the discharging area of Czech burner.

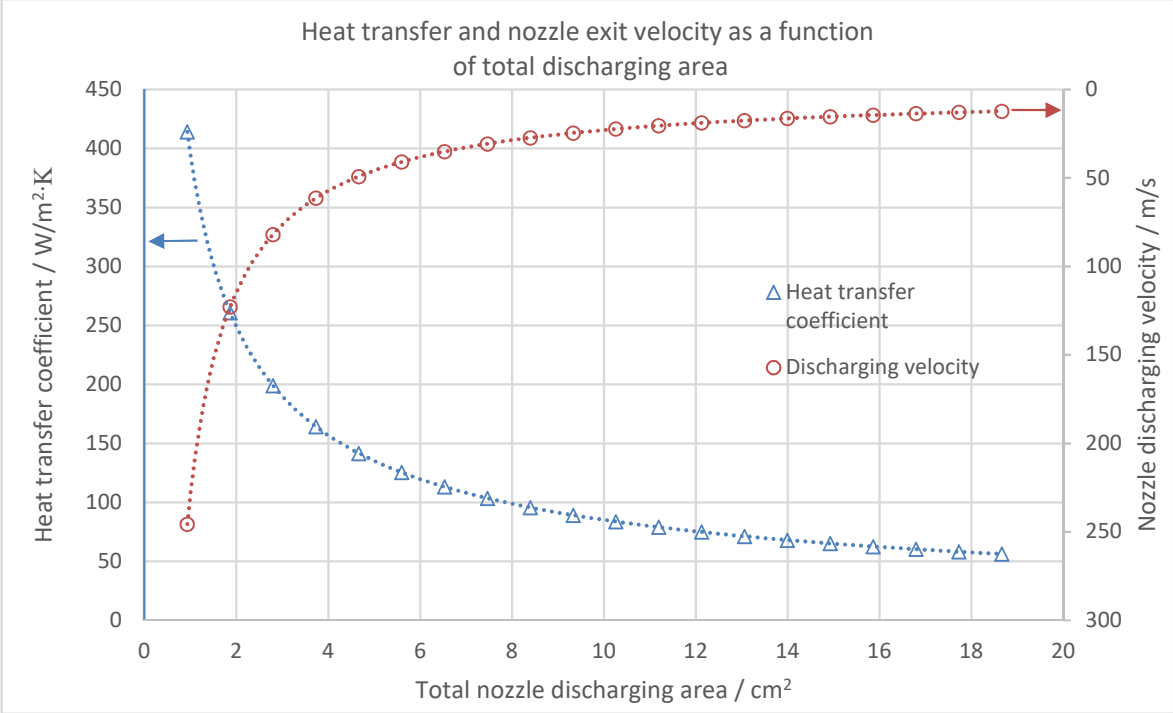

FIGURE 14. Heat transfer coefficient as a function of total discharging area in Czech burner.

Previous correlation is true if mass flow remains constant. The points in figure (14) were plotted by decreasing the total cross-sectional area of jet nozzles by 5 % steps from the original value. Every five percent step roughly means that we prevent the flow from 13 nozzles. This means that if we want to double the heat transfer coefficient, we have to reduce the total area by 65 %. If we want to reach the similar heat transfer coefficient as in Italian burner we have to reduce the total discharging surface area by 90 % from original. In real life this adjusting operation is more trial and error because the nature of the gas flow. Still these correlations give good estimations about the orders of magnitude.

5.2 Czech burner example

For example if we want to double the heat transfer coefficient for Czech burner we need to reduce jet nozzle area by 65 %. In the number of nozzles this means that we have approximately 119 functioning nozzles left in the burner after blocking the majority of them. By these acts we manage to increase the nozzle exit velocity to 35 m/s. If we use this value to calculate the heating time, we end up to roughly 1700 seconds, which means

28 minutes and 20 seconds. After areal reduction we can apply another change in dimensions to improve the heating time. By shortening the distance between stagnation point and nozzle exit from 20 mm to 10 mm we can improve the heating time by 700 seconds. After these improvements the total theoretical heating time would be 945 seconds or 15 minutes and 45 seconds to reach the casting temperature.

5.3 Optimization of Italian burner

We know beforehand that the analytically scrutinised and practically measured heating times did not correspond well in Czech burner case. For this reason we consider that the Italian burner is most efficient base to do the optimization. The reason why we proceed with this type of burner is that it corresponds best for the analytical theory and correlations. As we noticed on previous section the improvements for Italian type burner are quite challenging to execute. This is caused by more complex form of the nozzle housing than in the other burners and limited space in the burner ducts. The only way how it could be optimized is basically based on the distance adjusting between the impinging surface and nozzle exit. In the following section we took a little bit more engineer aspect to optimization of the Italian one. We redeveloped the design and added more complicated modifications than just adjusting the flow jet distance.

First, we decided to remove the distance limiting factor from the burner, which was the nozzle housing. The nozzles can be drilled straight to the burner duct and remove the burr around the drilled hole. Also the edges can be smoothened so the hole will get converged form for naturally low flow resistance. By these acts we get rid of the constructional limits of nozzle housing and the distance can be adjusted more freely. Now we can take a guess for the maximum distance between the impinging surface and nozzle exit and define the optimal hydraulic diameter for the nozzle. The useful range can be from 3 mm to 18 mm. In the following table (14) we have gathered the calculated optimum values for nozzle dimensions as a function of distances.

TABLE 14. Optimal characteristic dimensions of burner based on the wanted distance.

Distance	D_{opt}	$S_{opt.hex}$	$S_{opt.inl}$	Unit
3	0.552	4.269	3.972	mm
4	0.736	5.692	5.296	mm
5	0.92	7.115	6.62	mm
6	1.104	8.538	7.944	mm
7	1.288	9.961	9.268	mm
8	1.472	11.384	10.592	mm
9	1.656	12.807	11.916	mm
10	1.84	14.23	13.24	mm
11	2.024	15.653	14.564	mm
12	2.208	17.076	15.888	mm
13	2.392	18.499	17.212	mm
14	2.576	19.922	18.536	mm
15	2.76	21.345	19.86	mm
16	2.944	22.768	21.184	mm
17	3.128	24.191	22.508	mm
18	3.312	25.614	23.832	mm

From the dimensional values we choose the one that fill the following requirements about the function values in the correlation. These values are listed in the table (14). By choosing wanted diameter from the previous table, we can define all other dimensions for the nozzle arrange.

Let's say we want to choose the gap, between the mould surface and nozzle jet to be 8 mm wide. This require that we must have the nozzle hydraulic diameter of 1,472 mm and 10,592 mm for the pitch of the nozzles. The value of pitch distance comes from the desired form of arrangement of nozzles. While the correlations do not speak out the total discharge area we need to find it by using the values of flowing gas mixture. We can safely assume that the parameters of flow remain constant. By using the knowledge from measured flow parameters, we can do assumption that the Italian burner can- and is wise to be used as basis of the optimisation. Like we saw from the diagram (14), the heat transfer coefficient has a dependency in power to total cross-sectional area of jet nozzles in burner. We can now form similar diagram as we did with Czech burner. In this case

we do it for the optimized Italian burner by using the parameters of flow and set it as a function of total nozzle area. This figure (15) can be seen in following.

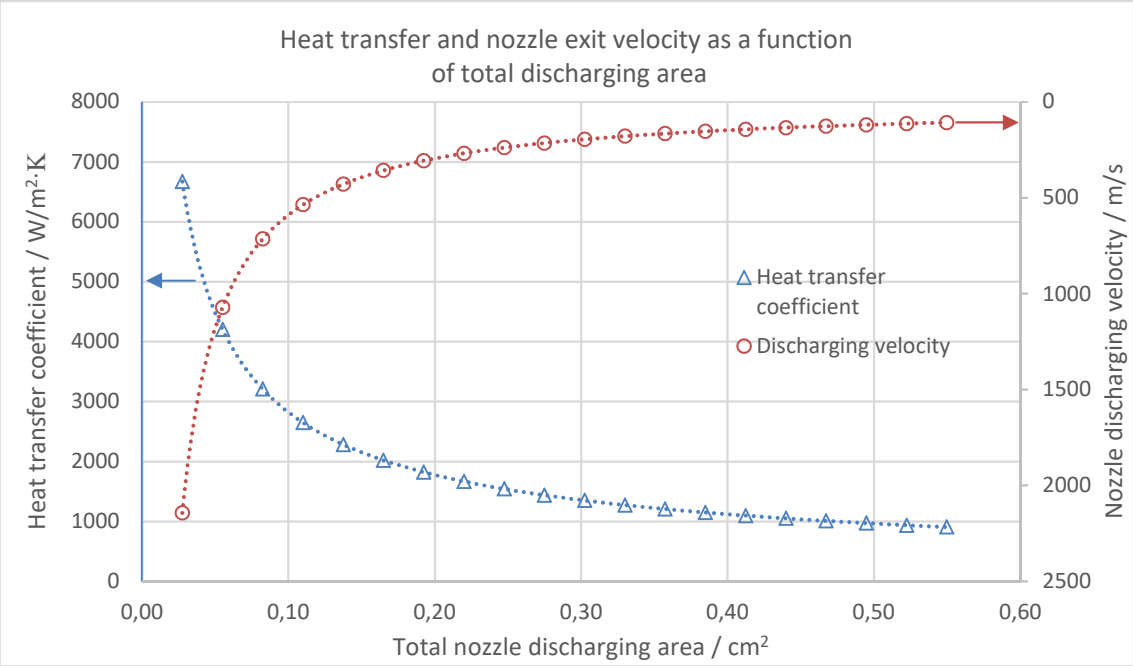

FIGURE 15. Heat transfer coefficient and exit velocity as a function of total nozzle area in Italian burner.

From the figure (15) we can see, like we did in the example case, that the heat transfer coefficient has dependency of total nozzle area in case the flow parameters remains same as it did in the original case. This is caused by the increase of the exit velocity in nozzle. In following table (15) we have calculated total count of nozzles in the burner and what is the theoretical heat transfer coefficient reached by using chosen optimal hydraulic diameter. In the following table, the uppermost row is representing the values measured from the original construction of Italian burner. All the values below first row are calculated by reducing the total discharging area by 5 % step compared to the original one.

TABLE 15. Heat transfer coefficient reached by using the hydraulic diameters, from the figure (10).

Total nozzle area	Quantity of nozzles	Quantity, rounded	Exit speed	Heat transfer
cm^2	$pc.$	$pc.$	m/s	$\bar{h}$
0,55	32.306	32	107.18	906
0,52	30.691	31	112.82	937
0,49	29.075	29	119.08	971
0,47	27.460	27	126.09	1009
0,44	25.845	26	133.97	1051
0,41	24.229	24	142.90	1097
0,38	22.614	23	153.11	1149
0,36	20.999	21	164.88	1207
0,33	19.384	19	178.63	1273
0,30	17.768	18	194.86	1349
0,27	16.153	16	214.35	1438
0,25	14.538	15	238.17	1542
0,22	12.922	13	267.94	1668
0,19	11.307	11	306.21	1823
0,16	9.692	10	357.25	2021
0,14	8.076	8	428.70	2282
0,11	6.461	6	535.88	2648

Because of the processibility we had to reject all the options that include remainder when the wanted total cross-sectional area is divided by the one nozzle area. From the table (15) we chose wanted quantity of nozzles which executes the value of heat transfer coefficient goal and can be divided even to each duct in burner. After this we multiply the wanted quantity of nozzles to the cross-sectional area and use that value in calculations. In this case we decided to make it with 24 nozzles. By these means we could increase the heat transfer coefficient and the number of nozzles is easy to divide to whole burner evenly.

After we had taken care about all the dimensions, we did the analytical calculations for heating time. These calculations were executed by same procedure as we did in the example at the previous section (6.1.2), by substituting all the original values with optimized

ones. All the results can be seen in the table (16), where they are presented alongside with the original ones. Complete calculations can be seen in appendices (10).

TABLE 16. Numerical values of optimized burner and original one.

Variable	Opti-mised	Original	Unit	Improvement
Total area	0,41	0,55	cm^2	26 %
Exit velocity	144,3	107,2	m/s	26 %
Relative area	0,0152	0,049		322 %
Reynolds number	12909	6515		50 %
H / D ratio	5,43	30		82 %
Nusselt number	41	8		510 %
Heat transfer coefficient	971	281	$W/m^2 \cdot K$	346 %
Heat power	13,5	3,9	kW	346 %
Heating time	185	639	s	345 %

By using the relation between the calculated values of original construction and optimized one applied to the measured results, we can find to that the overall gas consumption saving can be nearly 70 %. This claim is based to the straight relation between heating time and gas consumption. Graphic presentation can be seen in following figure (16).

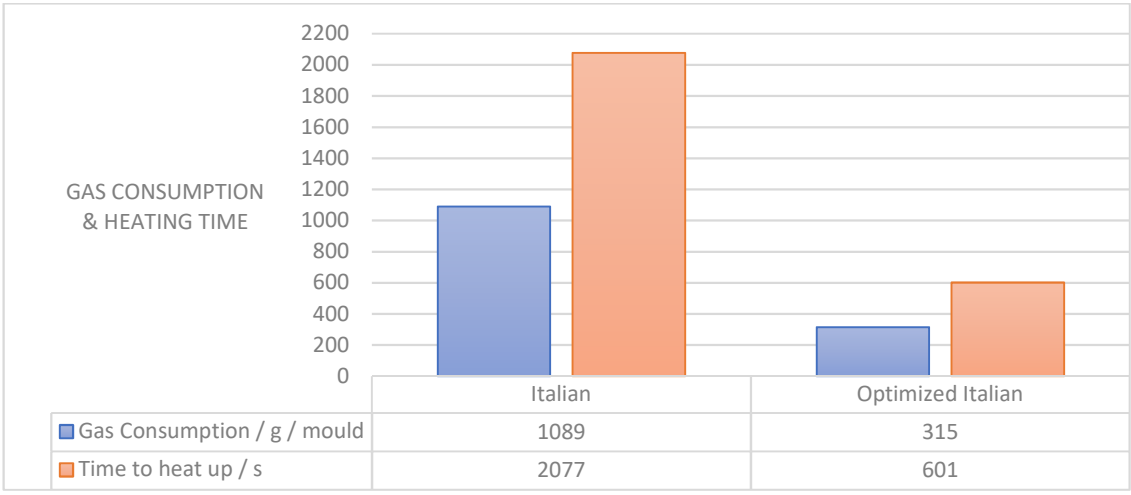

FIGURE 16. Change in gas consumption based on analytical optimisation.

6 COMPUTER AIDED SCRUTINY FOR OPTIMIZED BURNER MODEL

In this section we go through the computer aided scrutiny process for the Italian burner and the optimized version of it. The analysis is done with program called Ansys 18.1. The heat transfer problem is computed by using Fluent solver. The purpose of this act was to double check the order of magnitude from analytical calculations. By using tested correlations and computer aided modelling we can validate the geometrical optimization results. All results can be seen at the end of this section.

6.1 Model geometry

Because the original model of the mould was too large we had turn to more simplified option. We decided to approach the problem by using a uniform block of steel and simulate the heating of the block by using the values of actual burner. For comparison we simulated also the optimized burner geometry. By these means we managed to reduce the calculation time and get the order of magnitude from both burner models. For this purpose we created a model of steel block with a fluid domain over it. The model was created with Ansys Design Modeller and it can be seen in the following picture (15).

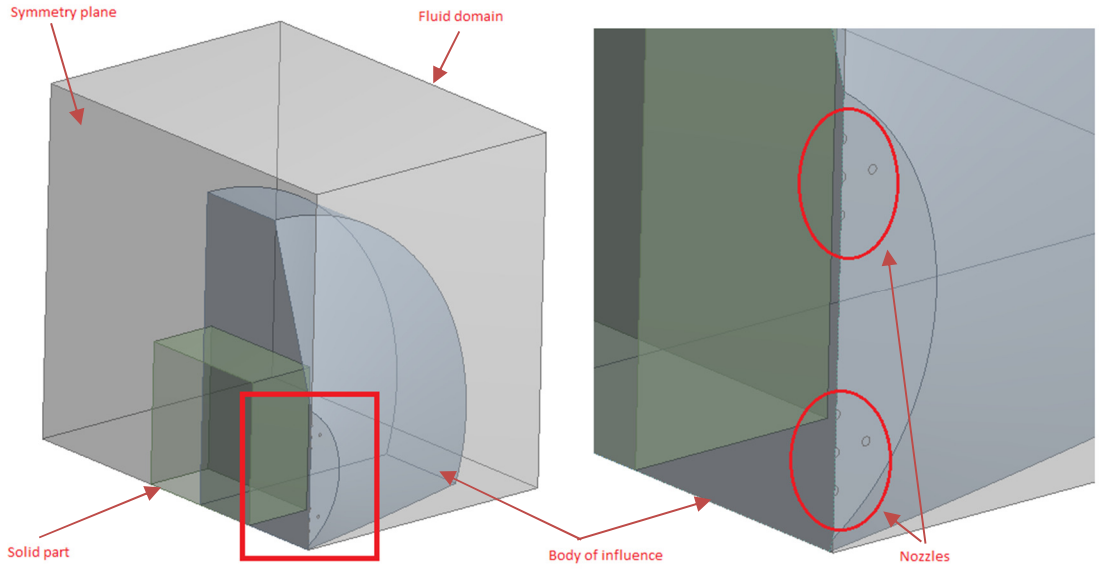

PICTURE 15. Italian burner domain model in Ansys Design Modeller, nozzle area is enlarged.

Differences between used models was the distance between the nozzles and solid domain surface. We also changed the orientation and the diameter of nozzles on the optimized model. The nozzle bodies were not modelled in the domain. Because we didn't use physical bodies for nozzles we made assumption that the flow is fully developed at the nozzle exit. Another reason for this arrangement was that we wanted to keep the model simple as possible. Also, in the optimized model all the nozzles were located near of the solid surface. In this case the space would have been too narrow to fit nozzle bodies in between. In the picture (16) we can see the optimized burner domain.

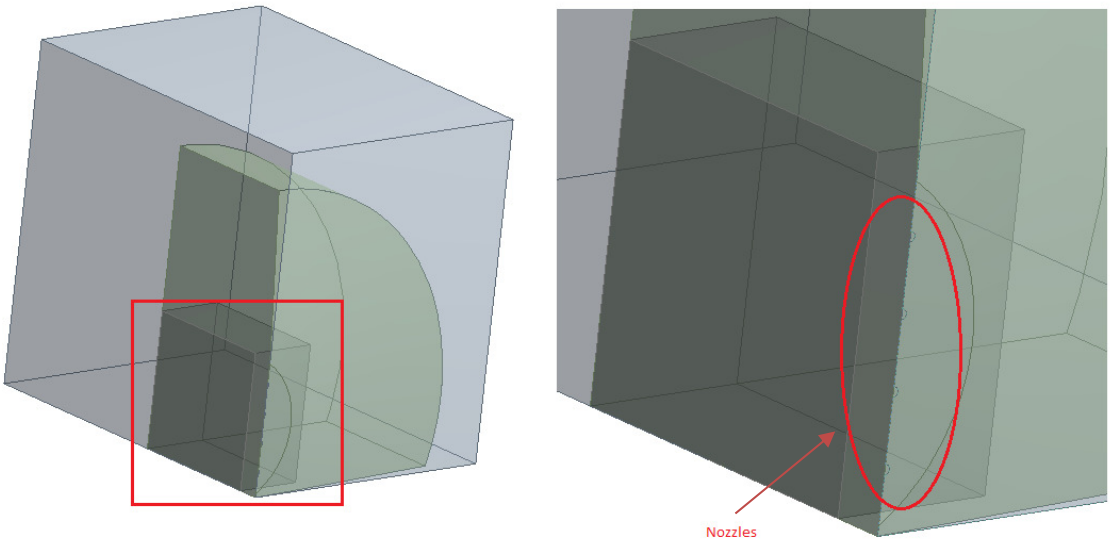

PICTURE 16. Optimized burner domain modelled in Ansys Design Modeller, nozzle area is enlarged.

6.2 Mesh

For generating mesh we used Ansys Workbench meshing platform. For improving the mesh quality we used same platform because it provides also fluent meshing options. Because we had a three-dimensional calculation and highly turbulent model we used the mesh combined the tetra and prism elements in the fluid domain. Tetra elements were in the volume parts and prism elements were used near-wall region. The DM was used to manage the topology of all the parts in domain. When all the bodies are combined in one part the created mesh what is considered as conformal. When using conformal mesh, it gives the freedom to enable contact regions from the model. This how the Fluent finds all the coupled surfaces by using only named selections in domain geometry. In following picture (17) we can see example of the mesh used in the calculations.

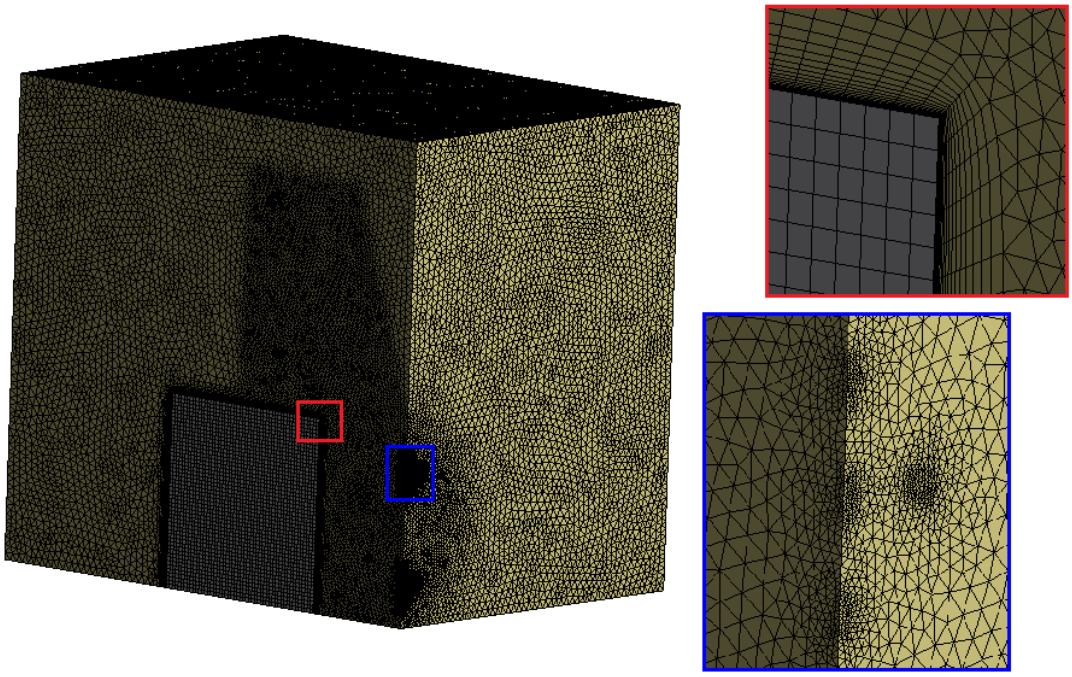

FIGURE 17. Example picture of the mesh used in the calculation, near wall region and nozzle area are enlarged.

The quality of mesh was evaluated by using two indicators. These were the orthogonal quality and skewness of the elements. First mentioned affects directly to the calculation time and how much iterations are needed for completing the computations. Orthogonal quality is defined for each face of each sell element separately. The orthogonality is defined for the cell by using the smallest calculated cosine value between angles of vectors. These vectors are the ones pointing to normal direction from the cell outer surface and ones pointing from the middle point of the cell to the midpoint of the cell side. Illustration of the vectors can be seen in the figure (18) (Ansys User manual).

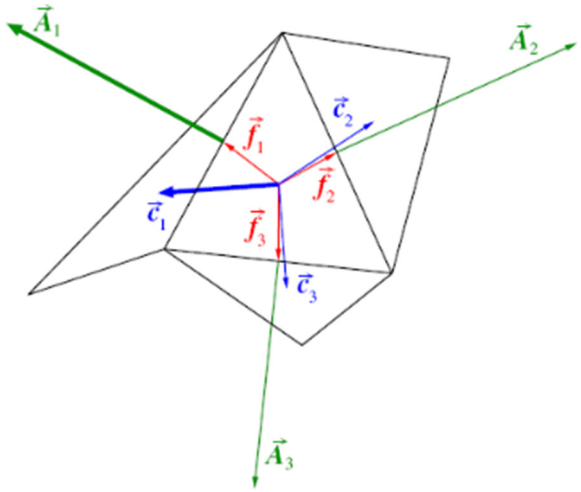

FIGURE 18. Vectors for defining the orthogonal quality of cell element. (Ansys User manual, modified)

Ansys uses a following equation for calculating mesh skewness

$$\text{Skewness} = \frac{\text{optimal cell size} - \text{cell size}}{\text{optimal cell size}}, \tag{40}$$

where the value of quality is evaluated by volume deviation (EDRMedeso Lecture 7 2015, 13). In the following table (17) we can see the scale for evaluating the orthogonal quality.

TABLE 17. Orthogonal value evaluation scale (EDR Medeso).

Unacceptable	Bad	Acceptable	Good	Very good	Excellent
0-0.001	0.001-0.14	0.15-0.20	0.20-0.69	0.70-0.95	0.95-1.00

In the table (18) we can see the scale for evaluating the mesh skewness.

TABLE 18. Skewness value evaluation scale (EDR Medeso).

Excellent	Very good	Good	Acceptable	Bad	Unacceptable
0-0.25	0.25-0.50	0.50-0.80	0.80-0.94	0.95-0.97	0.98-1.00

In the following figure (19) we can see the mesh metrics for the Italian burner model plotted with the workbench meshing platform.

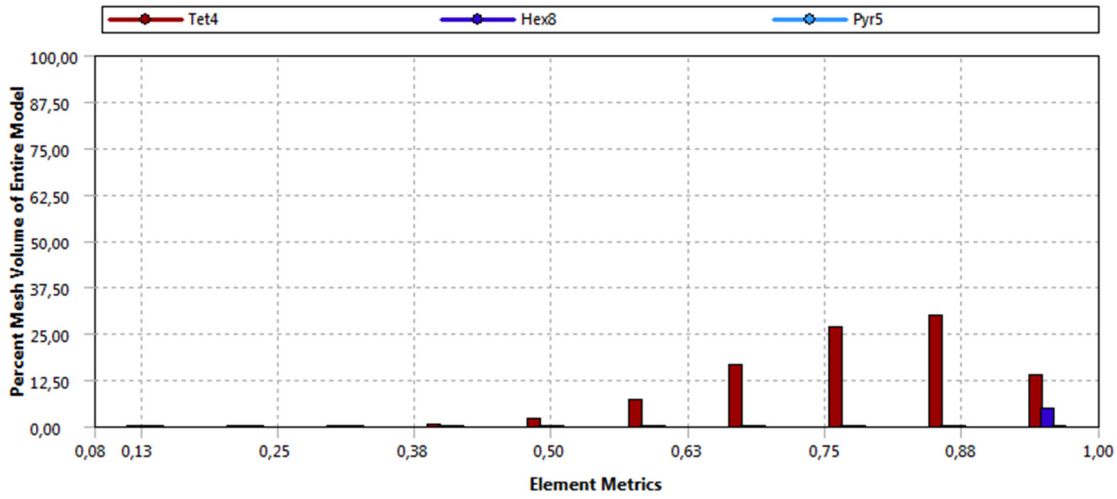

FIGURE 19. Orthogonal quality of mesh used in Italian burner model plotted with workbench tool.

Like we can see from the previous figure (19) the mesh orthogonality is in the acceptable area when compared to the table (17). In the following figure (20) we have evaluated the quality of Italian burner mesh by its skewness.

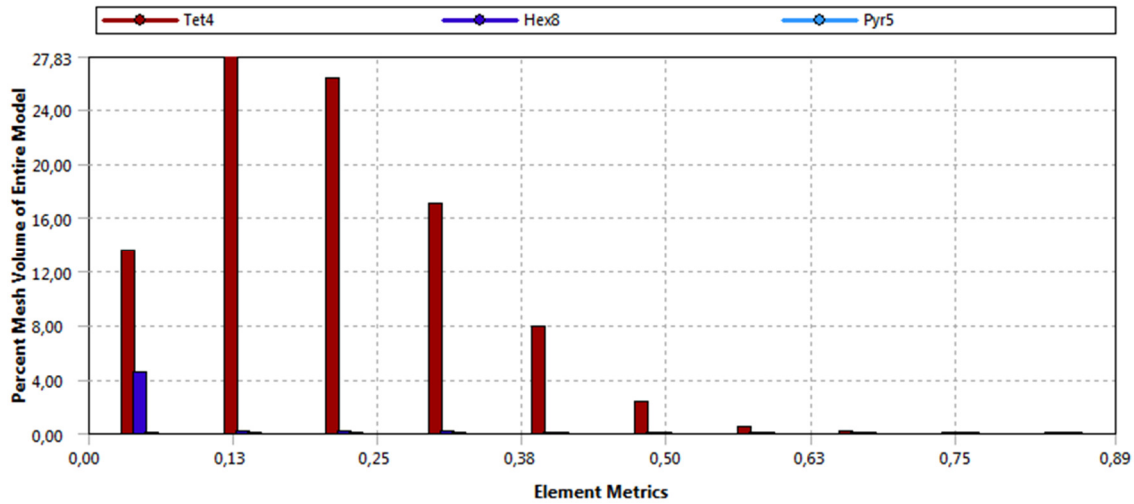

FIGURE 20. Value of skewness for mesh used for Italian burner model plotted with workbench tool.

Like we can see from the previous figure (20) the skewness of the used mesh is in the acceptable area when compared to the table (18). In the figures (21 & 22) we have done same evaluations for the mesh used in the optimized burner model.

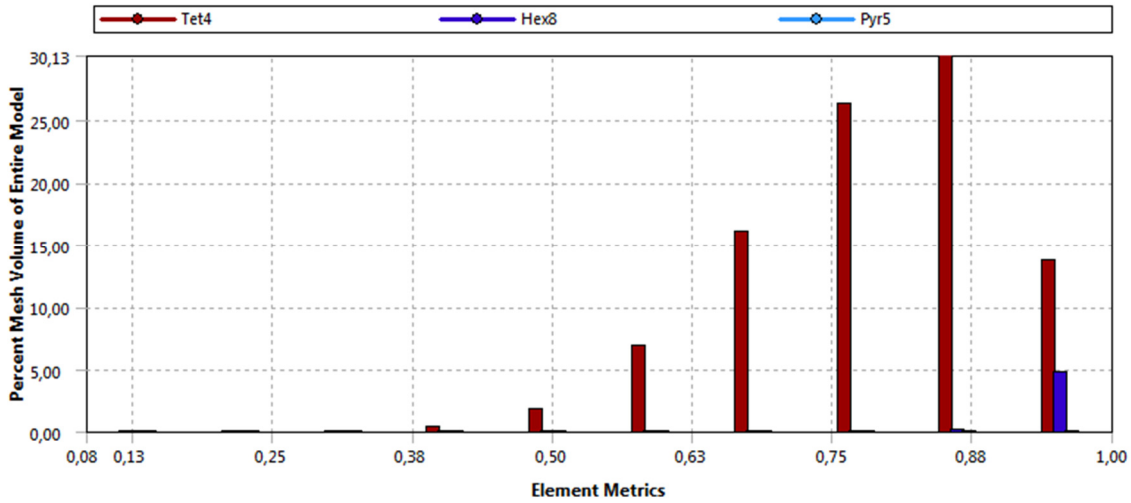

FIGURE 21. Orthogonal quality of mesh used for the optimized burner plotted with work-bench tool.

Like we can see from the previous figure (21) the mesh orthogonality is in the acceptable area when compared to the table (17). In the following figure (22) we have evaluated the quality of Italian burner mesh by its skewness.

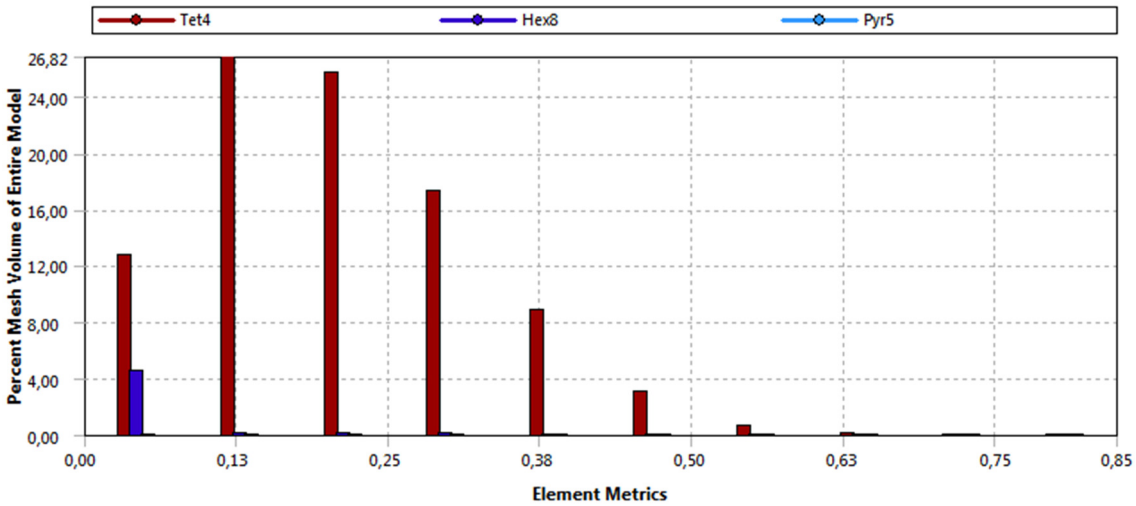

FIGURE 22. Value of skewness for mesh used for optimized burner model plotted with workbench tool.

Like we can see from the previous figure (22) the skewness of the used mesh is in the acceptable area when compared to the table (18). In the table (19) we can see the numerical information about both meshes used in the calculation.

TABLE 19. Quantities of different element types and nodes used in mesh for each domain.

Italian	Nodes	Elements	Tetrahedra	Pyramids	Hexahedra
fluid	754929	3752773	3621523	6250	125000
solid	67626	62500	0	0	62500
All	822555	3815273	3621523	6250	187500
Optimized					
fluid	696236	3403743	3272493	6250	125000
solid	67626	62500	0	0	62500
All	763862	3466243	3272493	6250	187500

6.3 Materials and boundary conditions

For both cases the material properties were same as they were in the analytical scrutiny. These values can be seen in the tables (7 & 8). The outer walls of fluid domain were set at constant pressure and constant temperature of ambient air. All the fluid walls were set to operate as pressure outlets. Interface between solid part and fluid domain was coupled with shared mesh. Bottom of the solid part was set as adiabatic wall. This means that there is no heat transfer through it. Nozzle faces of the domain was fixed as inlets with constant value of velocity and temperature. Values for velocities can be found in table (16) and used burning temperature can be found from table (8). Boundary conditions remained same through the both simulations except the discharge velocity which changed because the total nozzle area changed.

6.4 Turbulence model and solver convergence

Because the impinging jets are more or less vicious to model with CFD we did not expect to reach any accurate results to fit in this industrial application. However, choosing a correct turbulence model we were able to predict the magnitude of values. Because the modelling itself would have required a full-scale study including various models we settled to use knowledge from other studies witch focused on the numerical modelling of impinging jet flows. We ended up using k-ε turbulence model with standard wall functions. According to Bovo and Davidson (2013, 8) the k-ε model performs best for predicting the heat transfer. The k-ε model seems to over predict the heat transfer in stagnation zone, but it performs well in the cases when ratio between nozzle diameter and stagnation area is over two (Bovo & Davidson 2013, 11). Our case fits in this previous definition well. The used turbulence model follows the assumption that the effect of turbulence can be accounted by using scalar property called turbulent viscosity. The value of turbulent viscosity is calculated locally by using the turbulent length and velocity scales. Product is local gradients of the calculated mean flow (Bovo etc. 2013, 7). Big part of the calculation process is to get the model to work so well that the equations convergence in limited quantity of iterations. The used limits for residuals can be seen in the picture (15).

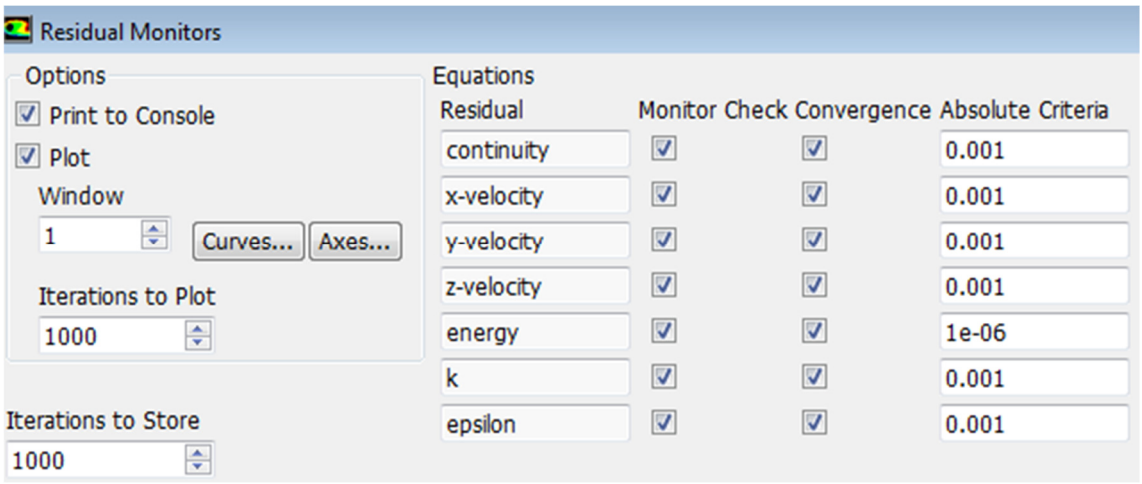

PICTURE 15. Residual criterions used during calculation.

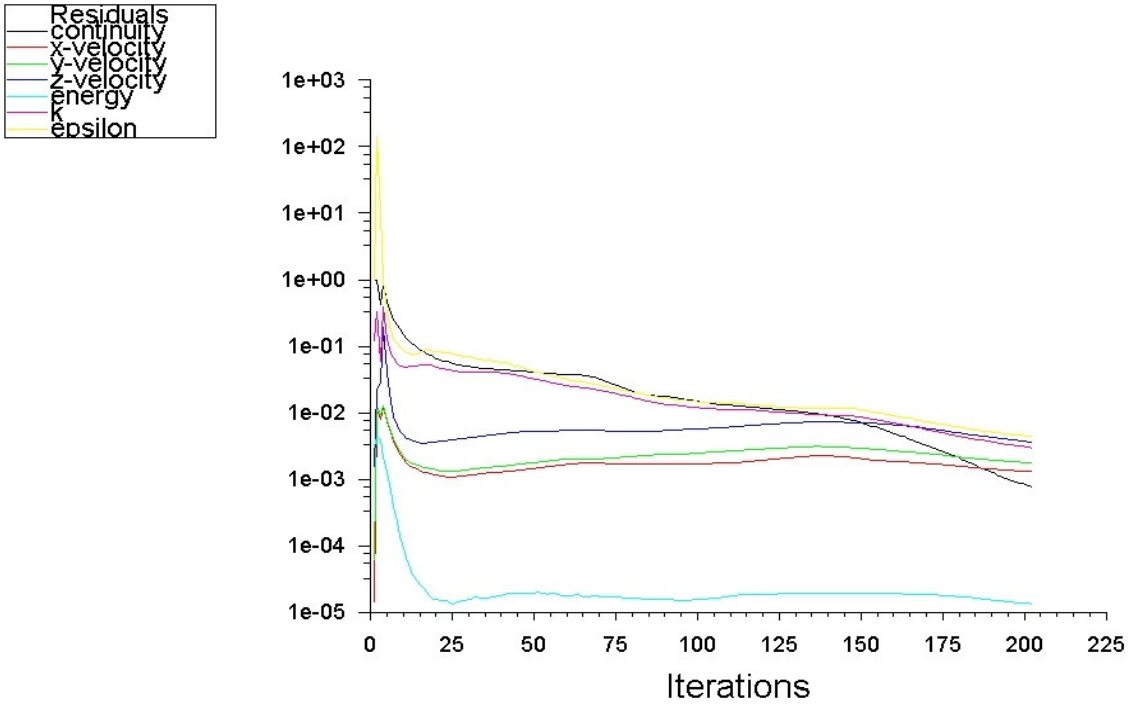

FIGURE 23. Residuals from Italian type burner analysis.

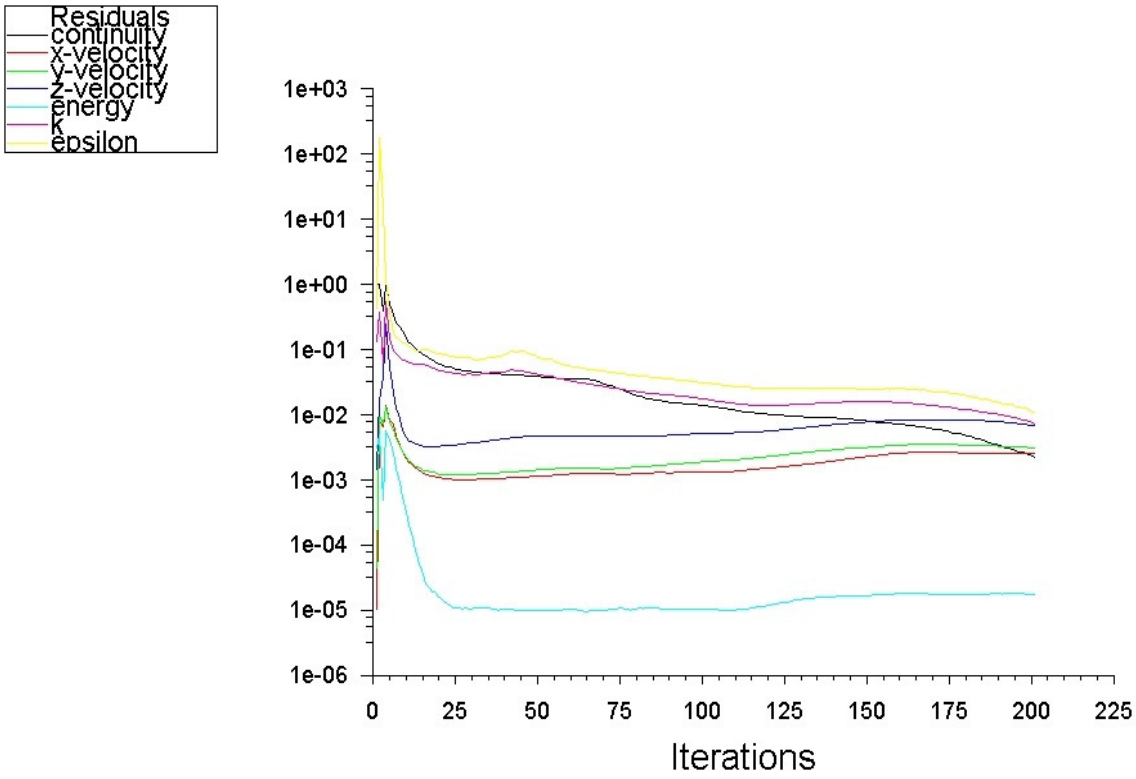

FIGURE 24. Residuals from optimized burner analysis.

As we can see from the Figures (23 & 24) that the solution in both cases can be considered as converged in adequate level. In flame combustion cases lower criteria for convergence may not be reachable.

6.5 Results from computer aided calculations

In figure (25) we can see the calculated heat transfer coefficient for both cases. In the up left we can see the analysis for Italian type burner and up right is results for the optimized burner. In the lowest section we can see the difference between both analyses. The same pattern is used in all the figures presented in this chapter. In the figure (26) we can see the temperature distribution in simulated part. In the figure (27) we can see the Reynolds number in simulated case divided in each cell separately. In the figure (28) we can see the heat flux distribution in solid domain. In the figure (29) we can see the streamline illustration for flow velocity compared to the temperature distribution in simulated part. In the figure (30) we can see the total heat distribution across analysed domain.

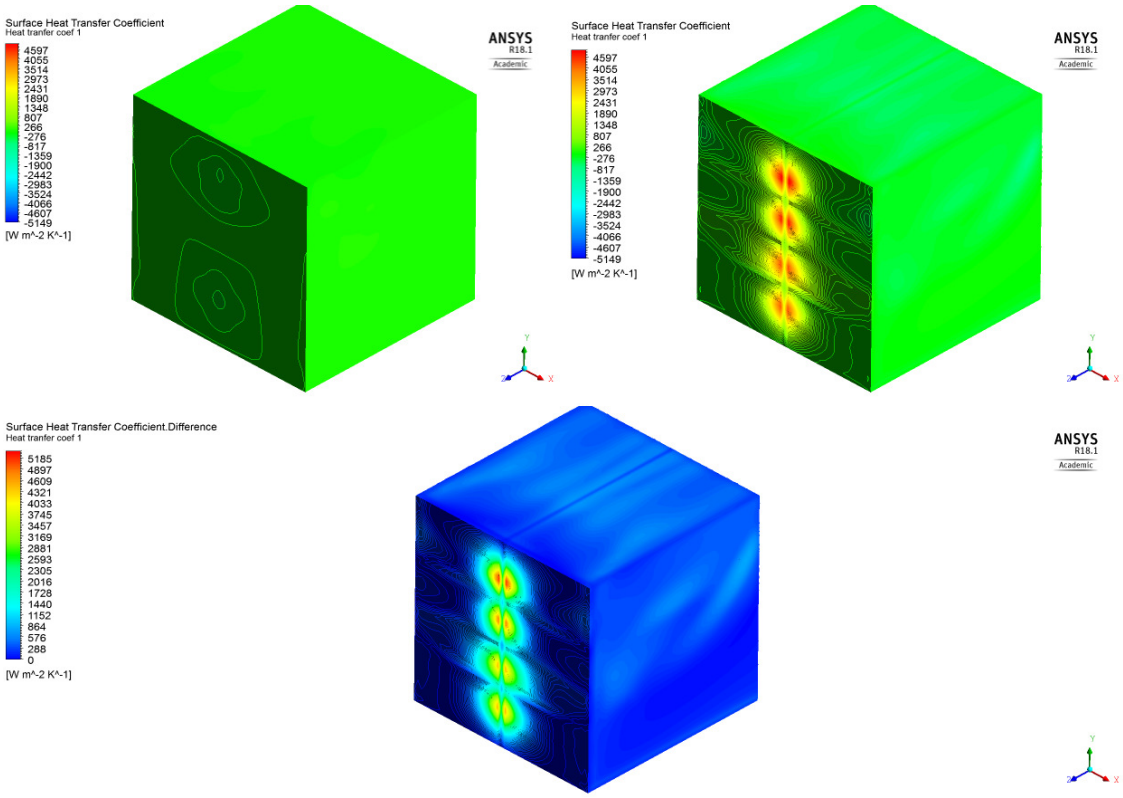

FIGURE 25. Heat transfer coefficient calculated by using Ansys Fluent.

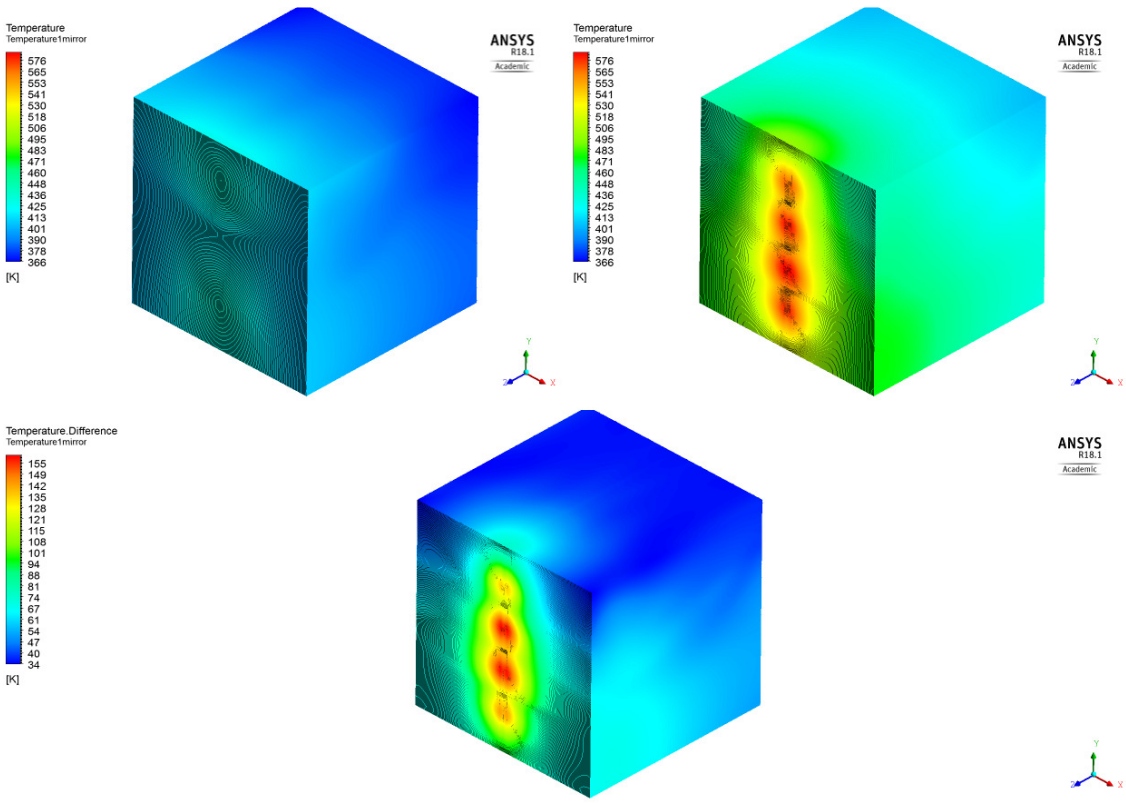

FIGURE 26. Temperature distribution in simulated case.

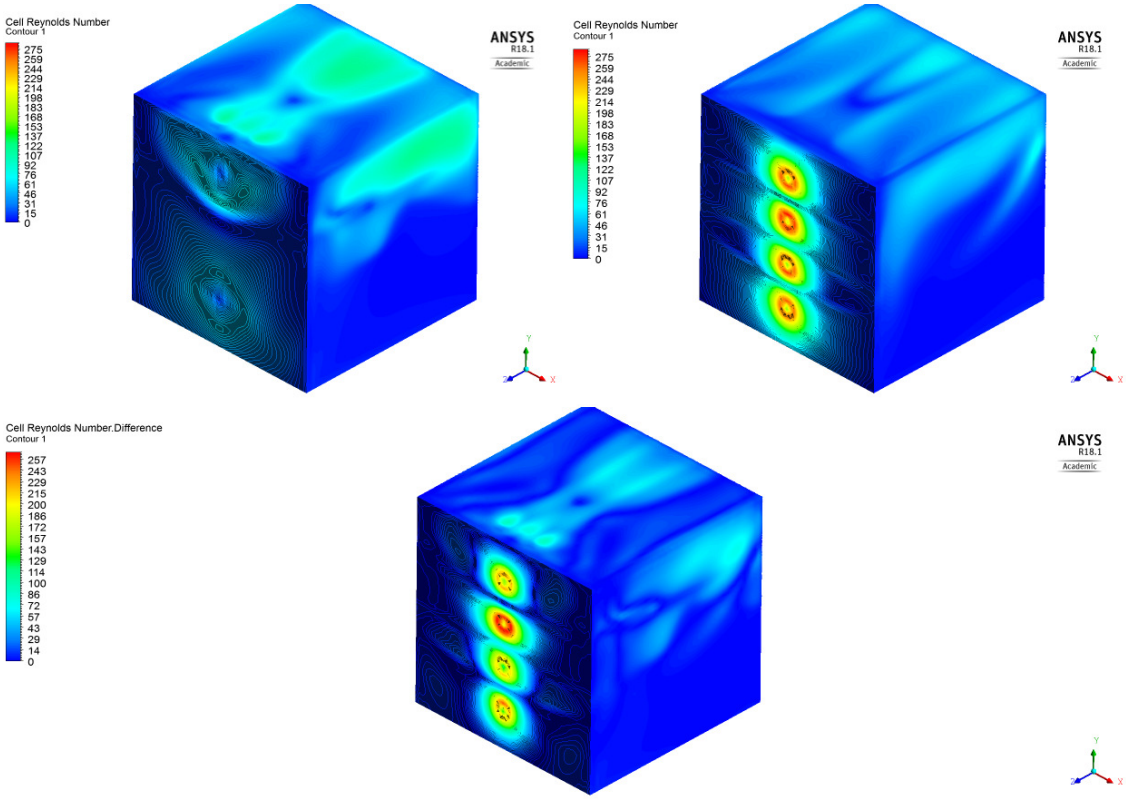

FIGURE 27. Near wall cell Reynolds number in simulated case.

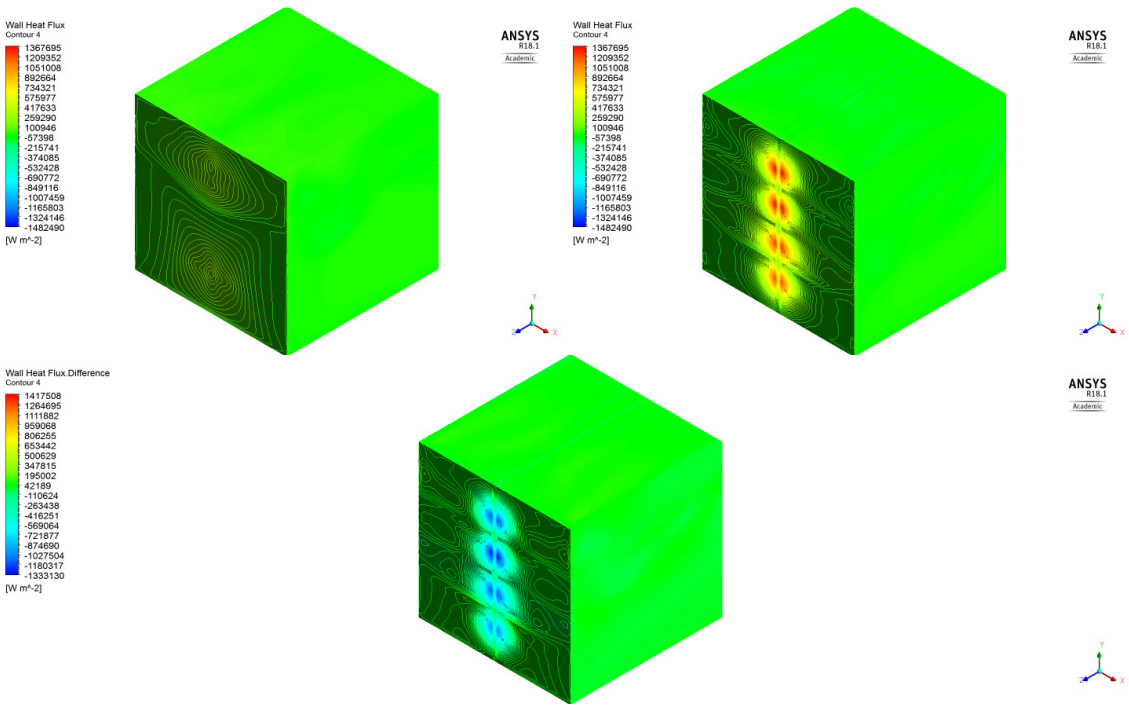

FIGURE 28. Wall heat flux in solid domain

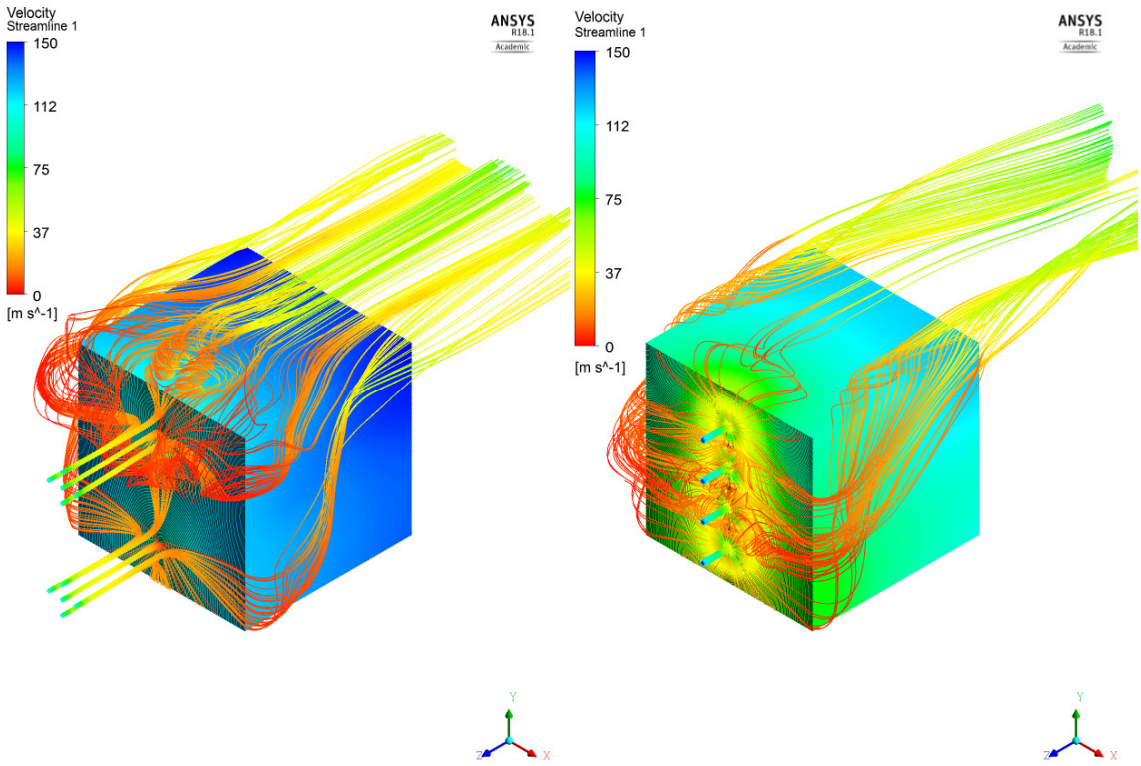

FIGURE 29. Velocity streamlines of flow with inverse scale.

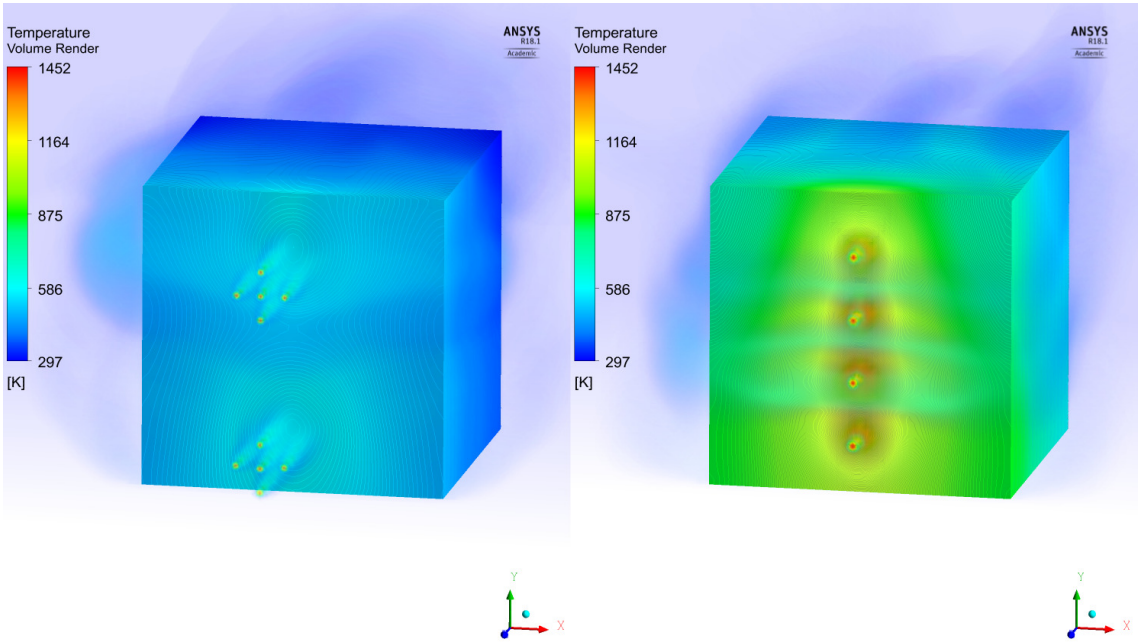

FIGURE 30. Temperature distribution in whole domain.

7 COMPARISON OF RESULTS

In this chapter we have gathered the results from the computer aided calculations and analytical scrutiny. In following table (20) the numerical results are compared with each other. Every average value is printed by using the stagnation face and its cross-sectional area.

TABLE 20. Numerical results from calculations.

Italian	Fluent	Analytical	Unit	Difference %
Average temperature	418	876	K	48
Maximum temperature	438	876	K	50
Minimum temperature	380	300	K	127
Heat transfer coefficient	242	281	$W/m^2 \cdot K$	14
Inlet Reynolds number	15640	6515	-	240
Provided heat power	615	808	W	31
Optimized				
Average temperature	504	876	K	58
Maximum temperature	575	876	K	66
Minimum temperature	387	300	K	29
Heat transfer coefficient	737	971	$W/m^2 \cdot K$	24
Inlet Reynolds number	12520	12909	-	3
Provided heat power	3950	2794	W	41
Difference				
Average temperature	55	-	K	-
Maximum temperature	160	-	K	-
Minimum temperature	33,6	-	K	-
Heat transfer coefficient	495	690	$W/m^2 \cdot K$	28
Inlet Reynolds number	3120	6394	-	49
Provided heat power	3335	1986	W	168

Like with the previously used correlations we can see here that the heat transfer has a significant dependency on the Reynolds number. The simulated Reynolds number is printed by using the inlet cross-section area. This was done because the correlations considered only the nozzle outlet flow turbulence. This how the numbers are comparable to each other. The irrational behaviour of Reynolds number in Fluent simulation can be explained by difference in the number of cells across the inlet boundary.

The heat transfer behaved just like it did with the correlations. Increasing the inlet velocity and decreasing the distance between stagnation surface and jet nozzle affected positively to the heat transfer coefficient. One part of the difference is caused by the increase of the Nusselt number. According to Bovo etc. (2013, 3) the maximum of Nusselt number presents in stagnation point where the layer thickness between boundaries reaches lowest value. In similar point for similar reasons the heat flux maximum occurs. This how the Nusselt number is connected with the flow velocity in the near of boundary layer. By increasing the value of ratio between stagnation area and nozzle diameter the radial flow velocity degreases. This is caused when the flow is spread in wider area and resistance is increased when flow front is penetrating to zero momentum area of ambient.

Straight comparison between analytical results and CFD calculations is not possible because of various reasons. One major reason is that the analytical scrutiny is based on correlations directed from empirical tests and Fluent gives numerical result by using general physics and solving the problem in small control volumes. This why we can assume that the correlations fit in the phenomenon more accurately because it takes various different things under consideration. This is the cause we assumed that the correlations used in analytical scrutiny involved the effect of radiation in some level. In Fluent analysis we did not count the radiation in the model just to keep the problem simple as possible. However we found a paper where the radiation effect is studied in impinging jet application. According to Malikov, G., Lobanov, Malikov, K., Lisienko, Viskanta and Fedorov (2000, 1757) the radiation can carry nearly 40 % of the total heat load in impinging jets combustion. However, this was estimated in super high combustion temperatures (2000 to 2300 K). Still if compared to this thesis case we can safely note that the probability of conservative results in CFD calculations is more than plausible. Complete analytical calculations can be found in appendices (11).

8 DISCUSSION

This thesis took a theoretical aspect and focused mainly studying the heating process by using the heat and mass theories. Furthermore, we wanted also to bring in light some of the more practical means for improving the preheating process. In this chapter we discuss about results of optimization process and some general means for making the process more efficient.

When considering production as it is proceed in the foundry where this thesis work is applied we can easily see the effects of mould preheating. When the total mass of production is huge but it consists a numerous different products the preheating is considered more than a compulsory to proceed. This is caused by the constant casting tool changes in process. By mould preheating the foundry can improve the series lead-time, prevent the wear of moulds, eliminate the need of extra heat treatment and use more complex shapes in final product, says doctoral candidate Kalle Jalava from Aalto University. Not to mention that it saves lots of a material in process. In many cases the preheating is the only way to make the casting process work especially when considering alloys that are hard to cast.

Since this project work begun it was obvious that the total process optimization is a combination of heat transfer problem as well as process control. In this thesis we focused to bring to light the means of taking the most out of the burning process. This was achieved by using the geometrical modifications for burner and adjusting the placement of nozzles. In this study we can say that this aspect is covered quite well. While the phenomenon of impinging jets has been an object of interest for many researchers previously we can still say that many parts in this form of flows is not understood. Particularly the fact that why it is capable of producing one of the highest heat transfer capacities know in single phase flows (Bovo etc. 2013, 1).

In this thesis we managed to reach the goals of improving the preheating process. Although the improvement was done by theoretical means. If the results are scalable for real life situation we can assume that the heating process is definitely more efficient in all indicators. Because of the improved heat transfer coefficient the mould will heat up much

faster and so consume less fuel. If we compare the measured heating time to the theoretical heating time and form a ratio where we assume that the effect has linear dependency we can calculate the effect of optimization to the real heating time. By doing this we should end up close to the 10 minutes limit in total heating time. If the gas mass flow remains same as it was with the Italian burner it would mean, approximately third of the current consumption. These are huge numbers when looking at the bigger picture. This means improved lean-time for the mould and twenty minutes more casting time for the machine in each mould change.

Another mean of improving the process is increasing the level of insulation between the surfaces of mould and casting machine. This insulation could easily be executed by using ceramic insulation panels in the mould construction. This method is already widely used in injection moulding for plastics. In plastic process the insulation is between mould and machine bed. Ceramic panels could hold some superior temperatures and it is made by the same procedure as the insulation of heat treatment ovens. The panels can be modified by milling, but usually it is pressed in final form. Many ceramic materials have extremely low thermal conductivity. Glass ceramics can go as low as 1,5 W/m·K. By these means the preheating process can be sped up when the gas is not used for heating the casting machine frame.

Another solution is also a kind of insulation manner. The heater uses a huge amount of energy to heat up the surrounding air i.e. by emitting heat away. By leaning to the analytical scrutiny we can assume that the wasted energy comes directly by calculating the energy balance. By subtracting the needed energy from the amount of energy provided we can get an approximate value of 1,5 kWh. This value is just for the mould half. According to the measurements the total heating time of mould is over half an hour. When we divide the energy waste by time and multiply it to the both halves of mould, we end up having 1,5 kW of wasted power in each heated mould. Big part of this could be avoided by covering the heating area. By this way we can reduce the mass of heated air and focus the heat flux to the right parts.

The real benefit of this solution can be found only by trial and error. But at least it is a cost-efficient way to try reduce heating time. Because of the steel can be used as cover material the material and production cost are low. There is also a place for danger in this

method. Because the heating is done by using natural gas, the process needs to be monitored continuously. If the burning process comes unstable it could turn the heater a serious safety issue. For avoiding the danger of explosion, the cover needs to be ventilated properly. This could be done just by covering the mould on the top and leave the sides open.

If the process is looked from another point of view and the waste energy reduction is taken as a determinative goal, the mould could be heated separately from the casting machine. By using heat treatment oven for preheating, the amount of used energy could be kept under control in whole different level. The level of insulation in closed heating system is way better than it would be if proceeding the mould isolation from casting machine frame by using glass ceramics. This way the process could be more controllable and it would not require constant supervising. The negative side of separately done preheating is that the mould needs to be installed in casting machine hot. This can cause problems around the internal logistics and the assembling needs to be done by help of machines. This means that the moulds could not be moved by manual labour while hot and requires investments in process.

One idea to improve the heating is change the method from gas burning to use of the water circulation system instead of cooling to heating purposes. By this we mean that instead of running cold water trough channels they could be heated up by using superheated water. So far, this method cannot be considered as an option without significant changes in the whole casting process. By this we mean, material changes in moulds which could resist corrosion, because of the traumatically increased physical properties of water while it is brought near to the critical temperature. Also, the whole circulating system in the mould would have to be pressurized, for maintaining the water in liquid or in semi liquid phase. For the change of the mode from heating to cooling would also be quite challenging. It would have to proceed with automatic means by using two different inlet lines, which another has pressure and another is cool, non-pressurised line. The change between different pressures in lines would need to be done via purge valve and that contains always a risk.

REFERENCES

Attalla, M. 2015. Stagnation Region Heat Transfer for Circular Jets Impinging on a Flat Plate. Experimental Heat Transfer 28, 139-155.

Bergman, L. T., Lavine, A.S., Incropera, F.P. & DeWitt, D.P. 2011. Fundamentals of Heat and Mass Transfer. 7th edition. John Wiley & Sons.

Bovo, M., Davidson, L. 2013. On the Numerical Modelling of Impinging Jets Heat Transfer – A Practical Approach. Numerical Heat Transfer 64 (4), 290-316.

Daintith, J. & Martin, E. 2010. Dictionary of Science. 6th edition. Oxford University Press.

EDR & Medeso Oy 2017. Ansys Fluent. Module 08: Heat Transfer. Introduction to Ansys Fluent. Power Point. course material. Requires access right

EDR & Medeso Oy 2015. Ansys Fluent. Lecture 7: Mesh Quality & Advanced Topics. Introduction to Ansys Meshing. Power Point. course material. Requires access right

Hottel, H. 1994. A Biographical Memoir of Thomas Kilgore Sherwood. National Academy of Science. Washington D.C. Read on 6.1.2018. http://www.nasonline.org/publications/biographical-memoirs/memoir-pdfs/sherwood-thomas.pdf

Incropera, F. P. & DeWitt, D. P. 2002. Introduction to Heat Transfer. 4th edition. John Wiley & Sons.

Jalava, K. Doctoral Candidate. 2018. Interview on 22.2.2018. Interviewer Mastomäki, J. Tampere.

Malikov, G., Lobanov, D., Malikov, K., Lisienko, V., Viskanta, R. & Fedorov, A. 2001. Direct Flame Impingement Heating for Rapid Thermal Materials Processing. International Journal of Heat and Mass Transfer 44, 1751-1758.

Martin, H., Spalding, D. B., Whitaker, S. & Winter, H. H. 1977. Heat and Mass Tranfer between Impinging Gas Jets and Solid Surfaces. Advances in Heat Transfer 13 (1), 1-60.

Massoud, M. 2005. Engineering Thermofluids. Thermodynamics, Fluid Mechanics and Heat Transfer. Springer-Verlag Berlin Heidelberg.

Mäkelä, M., Soininen, L., Tuomola, S. & Öistämö, J. 2013. Technical Formulas. 5th revised edition. Tampere. Amk Publishing Ltd.

Puranen, J. 2015. Lämpö- ja virtausoppi. Talotekniikan koulutus. Tampereen ammattikorkeakoulu. course material. Read on 4.1.2018. Requires access right.

Samaras, C. Measuring the pipe discharge in laboratory. 17.12.2012. blog text. My Engineering World. Read on 4.1.2018. http://www.myengineeringworld.net/2012/12/measuring-pipe-discharge-in-laboratory.html

The Engineering Toolbox. Chemical, Physical and Thermal Properties of Methane – CH_4. website. N/A. Read on 14.01.2018. https://www.engineeringtoolbox.com/methane-d_1420.html

ANSYS Workbench User's Guide. Manual. Version 18.1.0. Read on 15.2.2017. Requires access right.

APPENDICES

Appendix 1. Thermocouple sensor data sheet

Thermocouple sensor data sheet. **1(3)**

Farnell

element14

temperature and process technology

LABFACILITY

TEMPERATURE & PROCESS TECHNOLOGY

IEC Mineral Insulated Thermocouples

Type 'K' & 'N' with threaded pot & tails
310 stainless steel or Inconel® Alloy 600 sheath

- Mineral Insulated Type 'K' Thermocouple
- Choice of 310 stainless steel or Inconel® Alloy 600 sheath
- Highly flexible, sheath can be bent/formed to suit many applications and processes
- Insulated hot junction
- Probe temperature range -40°C to +1100°C
- M8 x 1.0mm fine pitch threaded pot seal (200°C)
- 100mm tails, PFA twin twisted 7/0.2mm, colour coded to IEC 584

Specifications

Sensor type:	Type 'K' (Nickel Chromium/Nickel Aluminium) to IEC 584 Type 'N' (Nicide-chromium-silicon) to IEC 584
Construction:	Flexible mineral insulated probe with 310 stainless steel or Inconel® Alloy 600 sheath with M8 x 1.0mm fine pitch threaded pot seal & tails
Element/hot junction:	Single element, junction insulated from sheath (offers protection against spurious electrical signals)
Termination:	100mm PFA twin twisted 7/0.2mm tails, colour coded in accordance with IEC 584
Probe temperature range:	-40°C to +1100°C >1.0mm diameter -40°C to +750°C – 1.0mm diameter and below (Type 'N' 1200°C)
Pot seal rating:	200°C

About Labfacility

Formed in 1971, Labfacility specialises in the field of Temperature and Process Measurement.

We are the largest UK manufacturer of both temperature sensors and thermocouple connectors.

Quality & Service

Quality and Service are key elements in the continued growth of Labfacility.

Technical support is always freely available from our experienced technical sales teams and the company has ISO9001 accreditation.

Contact Details

Email
sales@labfacility.com

Website
www.labfacility.com

Thermocouple sensor data sheet. **2(3)**

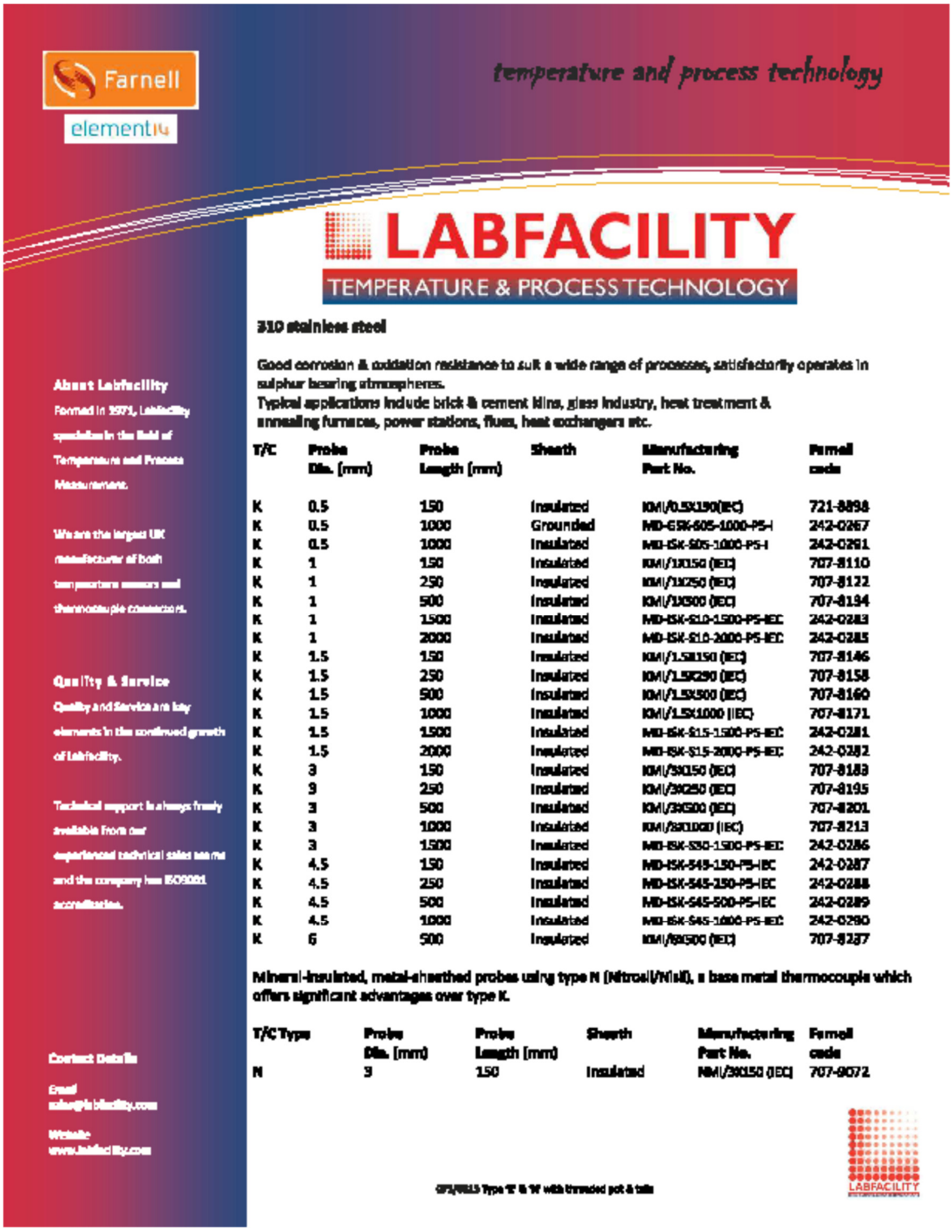

Farnell

element14

temperature and process technology

LABFACILITY

TEMPERATURE & PROCESS TECHNOLOGY

About Labfacility

Formed in 1971, Labfacility specialise in the field of Temperature and Process Measurement.

We are the largest UK manufacturer of both temperature sensors and thermocouple connectors.

Quality & Service

Quality and Service are key elements in the continued growth of Labfacility.

Technical support is always freely available from our experienced technical sales team and the company has ISO9001 accreditation.

Contact Details

Email
sales@labfacility.com

Website
www.labfacility.com

310 stainless steel

Good corrosion & oxidation resistance to suit a wide range of processes, satisfactorily operates in sulphur bearing atmospheres.
Typical applications include brick & cement kins, glass industry, heat treatment & annealing furnaces, power stations, flues, heat exchangers etc.

T/C	Probe Dia. (mm)	Probe Length (mm)	Sheath	Manufacturing Part No.	Farnell code
K	0.5	150	Insulated	KMI/0.5X150(IEC)	721-8898
K	0.5	1000	Grounded	MI-GSK-505-1000-PS-I	242-0267
K	0.5	1000	Insulated	MI-ISK-505-1000-PS-I	242-0261
K	1	150	Insulated	KMI/1X150 (IEC)	707-8110
K	1	250	Insulated	KMI/1X250 (IEC)	707-8122
K	1	500	Insulated	KMI/1X500 (IEC)	707-8134
K	1	1500	Insulated	MI-ISK-510-1500-PS-IEC	242-0283
K	1	2000	Insulated	MI-ISK-510-2000-PS-IEC	242-0285
K	1.5	150	Insulated	KMI/1.5X150 (IEC)	707-8146
K	1.5	250	Insulated	KMI/1.5X250 (IEC)	707-8158
K	1.5	500	Insulated	KMI/1.5X500 (IEC)	707-8160
K	1.5	1000	Insulated	KMI/1.5X1000 (IEC)	707-8171
K	1.5	1500	Insulated	MI-ISK-515-1500-PS-IEC	242-0281
K	1.5	2000	Insulated	MI-ISK-515-2000-PS-IEC	242-0282
K	3	150	Insulated	KMI/3X150 (IEC)	707-8183
K	3	250	Insulated	KMI/3X250 (IEC)	707-8195
K	3	500	Insulated	KMI/3X500 (IEC)	707-8201
K	3	1000	Insulated	KMI/3X1000 (IEC)	707-8213
K	3	1500	Insulated	MI-ISK-530-1500-PS-IEC	242-0286
K	4.5	150	Insulated	MI-ISK-545-150-PS-IEC	242-0287
K	4.5	250	Insulated	MI-ISK-545-250-PS-IEC	242-0288
K	4.5	500	Insulated	MI-ISK-545-500-PS-IEC	242-0289
K	4.5	1000	Insulated	MI-ISK-545-1000-PS-IEC	242-0290
K	6	500	Insulated	KMI/6X500 (IEC)	707-8237

Mineral-insulated, metal-sheathed probes using type N (Nitrosil/Nisil), a base metal thermocouple which offers significant advantages over type K.

T/C Type	Probe Dia. (mm)	Probe Length (mm)	Sheath	Manufacturing Part No.	Farnell code
N	3	150	Insulated	NMI/3X150 (IEC)	707-9072

LABFACILITY

BS1/BS3 Type 'E' & 'K' with threaded pot & tails

Thermocouple sensor data sheet. **3(3)**

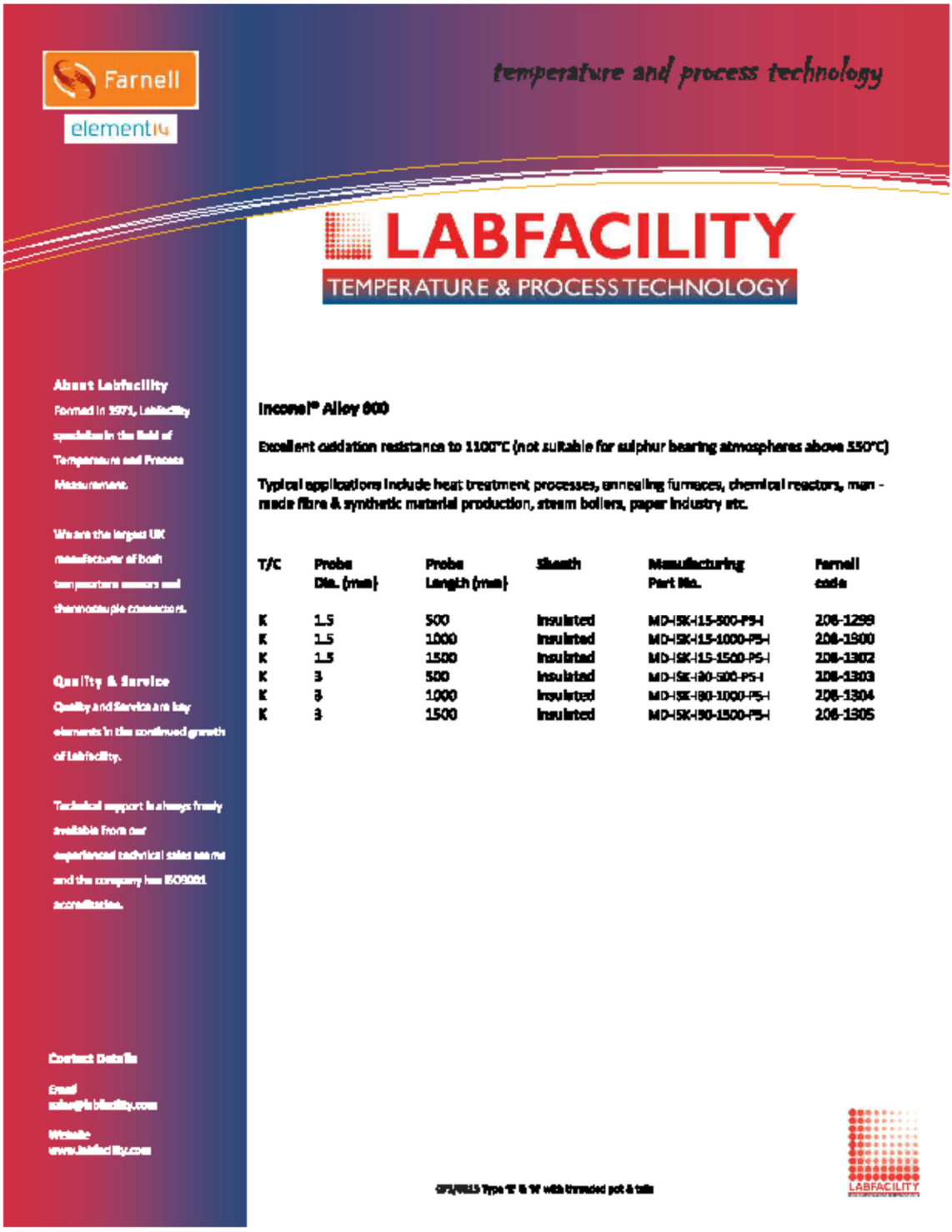

Farnell

element14

temperature and process technology

LABFACILITY

TEMPERATURE & PROCESS TECHNOLOGY

About Labfacility

Formed in 1971, Labfacility specialises in the field of Temperature and Process Measurement.

We are the largest UK manufacturer of both temperature sensors and thermocouple connectors.

Quality & Service

Quality and Service are key elements in the continued growth of Labfacility.

Technical support is always freely available from our experienced technical sales team and the company has ISO9001 accreditation.

Contact Details

Email
sales@labfacility.com

Website
www.labfacility.com

Inconel® Alloy 600

Excellent oxidation resistance to 1100°C (not suitable for sulphur bearing atmospheres above 550°C)

Typical applications include heat treatment processes, annealing furnaces, chemical reactors, man - made fibre & synthetic material production, steam boilers, paper industry etc.

T/C	Probe Dia. (mm)	Probe Length (mm)	Sheath	Manufacturing Part No.	Farnell code
K	1.5	500	Insulated	MD-ISK-I15-500-PS-I	208-1299
K	1.5	1000	Insulated	MD-ISK-I15-1000-PS-I	208-1300
K	1.5	1500	Insulated	MD-ISK-I15-1500-PS-I	208-1302
K	3	500	Insulated	MD-ISK-I30-500-PS-I	208-1303
K	3	1000	Insulated	MD-ISK-I30-1000-PS-I	208-1304
K	3	1500	Insulated	MD-ISK-I30-1500-PS-I	208-1305

LABFACILITY

Appendix 2. Digital Thermometer data sheet.

Corresponding model data sheet for thermometer HH12B. **1(1)**

L

Specifications

Measurement Range:
-200 to 1372°C (-328 to 1999°F)
-199.9 to 199.9°C (-327.8 to 391.8°F)
Accuracy (Type K Chromium-Alum):
± (0.1% rdg +1°C) on -60 to 1372°C
± (0.1% rdg +2°C) on -60 to -200°C
± (0.1% rdg +2°F) on -76 to 1999°F
± (0.1% rdg +4°F) on -76 to -328°F
European Safety Standards:
IEC-1010 and CE - EMC

Temperature Coefficient:
0.1 times the applicable accuracy specification per °C from 0 to 18°C and 28 to 50°C
Display: 3½ digit LCD, maximum reading 1999
Sampling Rate: 2.5/s
Battery: 9V (included)
Battery Life: 200 hours typical
Dimensions: 210 H x 65 W x 33 mm D (8.3 x 2.4 x 1.4")
Weight: 254 g (9 oz)

To Order

Model No.	Description
HH11B	Single-input switchable 0.1 or 1° resolution
HH12B	Dual-input switchable 0.1 or 1° resolution
HH-MAG	Magnet strap hanger that affixes to rubber boot
SC-HH11A	Deluxe carrying case with holster and magnet hanger
CAL-3-HH	NIST-traceable calibration with points

Comes complete with meter, rubber boot, 9V battery, NIST certificate (no points), appropriate number of beaded wire thermocouples and operator's manual.

***Note:** HH11B and HH12B accept the standard SMPW-type connectors only. These units are not compatible with NMP connectors.*

***Ordering Example: HH12B,** dual-input Type K thermocouple meter.*

Appendix 3. Specifications for Benetech GM700 infrared thermometer.

Specifications for Benetech GM700 infrared thermometer. 1(1)

C. Specification

Temperature Range	-50°C~700°C(-58°F~1292°F)
Accuracy	*0°C~700°C(32°F~1292°F): ±1.5°C(±2.7°F) or±1.5% *-50°C~0°C(-58°F~32°F): ±3°C(±5°F) Whichever is greater
Resolution	0.1°C or 0.1°F
Repeatability	1% of reading or 1 °C
Response time	500 mSec, 95% response
Spectral response	8~14 um
Emissivity	0.1 to 1.00 adjustable
Distance to Spot size	12:1
Operating Temperature	0°C~40°C(32°F~104°F)
Operating Humidity	10~95% RH non-condensing up to 30°C(86°F)
Storage Temperature	-20~60°C(-4°F~140°F)
Power	9V battery
Typical battery life	Non-laser mode: 22 hrs; Laser mode: 12 hrs
Weight	222g
Dimension	111x50x172mm

Appendix 4. Heating time measurement proceed.

Italian burner heating time measurements. **1(3)**

Gas consumption	Gas pressure (MPa):	Burner cross section area (mm^2)	Gas density (kg/m^3)	Gas temperature (K)	Starting temperature (K)	Ambient temperature (K)	(K)	Gas Compression factor	Molar mass (kg/kmol)	Molar Density (kmol/m^3)		
	0,106	568,2743	0,717	296,85	298,7	298,95	273,15	0,9981	16,316	0,04303		
Measured:				23,7	25,55	25,8						
Emissivity:	Reference:	Ceramic coating, Pyrotek, Pyromastic										
0,92	0,94	Measure tools: Fluke, thermocamera Ti105,. Infrated Thermometers, Benetech GM700, Fluke 65,. Type-K Thermometers, Testo 925, Omega HH12B,										
Temperatures:	**Time:**											
Burning	0:00:00	3:50:00	6:16:00	8:45:00	11:33:00	15:17:00	19:45:00	23:52:00	28:42:00	34:37:00	***Average:***	Kelvins
Nozzle 1	1154,00	1154,00	1157,00	1157,00	1157,00	1157,00	1192,00	1216,00	1216,00	1223,00	1178,30	1451,45
Seconds	0	230	376	525	693	917	1185	1432	1722	2077		
Mold												
Reference point 1	25,30	40,00	60,00	80,00	100,00	120,00	140,00	160,00	180,00	200,00		
Reference point 2	25,80	51,40	76,00	98,40	120,20	146,80	173,50	194,60	216,00	235,00		
Back point 1		43,00	57,00	73,00	89,00	101,00	122,00	139,00	156,00	173,00		
Back point 2		40,00	50,00	61,00	74,00	93,00	111,00	128,00	144,00	164,00		
Back point 3		43,00	57,00	72,00	88,00	100,00	120,00	139,00	155,00	172,00		
Back point 4		50,00	69,00	83,00	96,00	120,00	148,00	168,00	187,00	203,00		
Back point 5		42,00	53,00	61,00	79,00	101,00	121,00	139,00	159,00	180,00		
Back point 6		49,00	64,00	81,00	93,00	106,00	120,00	145,00	164,00	184,00		

German burner heating time measurements. **2(3)**

Gas consumption	Gas pressure (MPa):	Burner crosssection area (mm^2)	Gas density (kg/m^3)	Gas temperature (K)	Starting temperature (K)	Backround temperature (K)	(K)	Gas Compression factor	Molar mass (kg/kmol)	Molar Density (kmol/m^3)
	0,6	477,522	0,707	296,85	293,45	299,25	273,15	0,9876	16,316	0,28759
Measured:				23,7	20,3	26,1				
Emissivity:	Reference:	Ceramic coating, Pyrotek, Pyromastic								
0,92	0,94	Measure tools: Fluke, thermocamera Ti105,. Infrated Thermometers, Benetech GM700, Fluke 65,. Type-K Thermometers, Testo 925, Omega HH12B,								

Temperatures:	**Time:**											
Burning	0:00:00	4:33:00	6:57:00	9:37:00	12:38:00	15:55:00	19:45:00	23:40:00	28:44:00	34:47:00	***Average:***	Kelvins
Nozzle 1	982,00	991,00	941,00	930,00	1058,00	980,00	982,00	998,00	1015,00	986,33	1279,78	
Seconds	0	273	417	577	758	955	1185	1420	1724	2087		
Mold												
Reference point 1	20,30	40,00	60,00	80,00	100,00	120,00	140,00	160,00	180,00	200,00		
Reference point 2	21,40	44,40	68,30	91,60	118,80	143,30	169,00	192,60	218,00	240,00		
Back point 1		38,00	53,00	68,00	84,00	100,00	116,00	135,00	153,00	172,00		
Back point 2		32,00	43,00	56,00	73,00	88,00	106,00	124,00	146,00	169,00		
Back point 3		31,00	40,00	49,00	60,00	72,00	85,00	98,00	113,00	128,00		
Back point 4		42,00	61,00	79,00	103,00	125,00	147,00	167,00	189,00	208,00		
Back point 5		38,00	52,00	68,00	87,00	105,00	127,00	148,00	173,00	197,00		
Back point 6		37,00	51,00	65,00	83,00	99,00	118,00	135,00	152,00	174,00		

Czech burner heating time measurements. **3(3)**

Gas consumption	Gas pressure (MPa):	Burner crosssection area (mm^2)	Gas density (kg/m^3)	Gas temperature (K)	Starting temperature (K)	Backround temperature (K)	(K)	Gas Compression factor	Molar mass (kg/kmol)	Molar Density (kmol/m^3)
	0,701	1866,106		296,85	306,15	299,25	273,15	0,9876	16,316	0,28759
Measured:				23,7	33	26,1				
Emissivity:	Reference:	Ceramic coating, Pyrotek, Pyromastic								
0,92	0,94	Measure tools: Fluke, thermocamera Ti105,. Infrated Thermometers, Benetech GM700, Fluke 65,. Type-K Thermometers, Testo 925, Omega HH12B,								

Temperatures:	**Time:**												
Burning	0:00:00	0:01:00	4:38:00	7:19:00	11:08:00	14:15:00	17:52:00	22:16:00	28:30:00	36:36:00	***Average:***	Kelvins
Nozzle 1	1261,00	1261,00	1261,00	1261,00	1261,00	1124,00	1124,00	1164,00	1164,00	1180,00	1200,00	1473,15
Seconds	0	1	278	439	668	855	1072	1336	1710	2196		
Mold												
Reference point 1	39,20	40,00	60,00	80,00	106,00	120,00	140,00	160,00	180,00	200,00		
Reference point 2	40,60	41,30	64,40	87,00	115,20	127,60	148,80	166,00	184,20	204,00		
Back point 1		42,00	58,00	75,00	95,00	105,00	120,00	137,00	155,00	170,00		
Back point 2		43,00	62,00	81,00	107,00	108,00	109,00	114,00	126,00	150,00		
Back point 3		43,00	60,00	71,00	88,00	98,00	110,00	126,00	146,00	160,00		
Back point 4		42,00	63,00	83,00	103,00	114,00	132,00	147,00	162,00	179,00		
Back point 5		37,00	64,00	92,00	118,00	123,00	122,00	127,00	140,00	164,00		
Back point 6		42,00	68,00	92,00	110,00	123,00	135,00	148,00	160,00	170,00		

Appendix 5. Flow measurements proceed

Flow measurements proceed (22.1 – 23.1.2018). **1(1)**

Italian	Reading	Flow Testo	Reading	Measurement	Pressure	Pressure	Real flow CH4	Total flow	Volume flow	Mass flow/ total	Gas consumption	Lambda	Gas mixture	Methane density
Source					tabular data	tabular data	Calc. Rotameter	Calc. From CH4 flow	Calc.	Calc.	Calc.	tabular c	calculated	tabular data
	L/min	MAF m^3/h	m/s	nro.	bar	bar	l/min	l/min	m^3/s	kg/hour	kg/heated mould	kg/m^3	kg/m^3	
	20 - 18	7,5	3,12	1	1,613	1,013	30,25370188	318,5714808	0,00530525	23,66348959	1,09	9,53	1,238	0,772
	20 - 18	7,7	3,19	2	1,613	1,013	30,25370188	318,5714808	0,00530525	23,66348959	34:37:00			
	20 - 18	7,5	3,11	10	1,613	1,013	30,25370188	318,5714808	0,00530525	23,66348959				
Mean	19	23,31	3,242			Calc. From MAF	40,7660021	388,5	0,00647 5	28,85778				
				Average				353,5357404	0,00589226 2	26,2606348				

German	Reading	flow speed	Reading	Measurement	Pressure	Pressure	CH4 Flow	Flow l/min	Volume flow	Mass flow/ total	Gas consumption	Lambda	Gas mixture	Methane density
Source					tabular data	tabular data	Calc. From total flow	Calc. Rotameter	Calc.	Calc.	Calc.	tabular c	calculated	tabular data
	l/min	MAF m^3/h	m/s	nro.	bar	bar	l/min	l/min	m^3/s	kg/hour	kg/heated mould	kg/m^3	kg/m^3	
	200 - 205	10,5	11,13	1	6,613	1,013	34,0749815	324,734456	0,00541241	24,12127539	1,54	9,53	1,238	0,772
	200 - 205	10,6	11,61	2	6,613	1,013	34,0749815	324,734456	0,00541241	24,12127539	34:47:00			
	200 - 205	10,8	11,79	10	6,613	1,013	34,0749815	324,734456	0,00541241	24,12127539				
Mean	202,5	32,85	11,955			Calc. From MAF	57,4501574	547,5	0,009125	40,6683				
				Average			45,76256327	436,117228	0,00726862	32,3947869				

Czech	Reading	flow speed	Reading	Measurement	Pressure	Pressure	CH4 Flow	Total flow	Volume flow	Mass flow/ total	Gas consumption	Lambda	Gas mixture	Methane density
Source					tabular data	tabular data	Calc. Rotameter	Calc. From CH4 flow	Calc.	Calc.	Calc.	tabular c	calculated	tabular data
	L/min	MAF m^3/h	m/s	nro.	bar	bar	l/min	l/min	m^3/s	kg/s	kg/heated mould	kg/m^3	kg/m^3	
	20 - 18	4,8	2	1	6,613	1,013	130,5626851	1374,825074	0,02291375 1	102,122006 5	3,69	9,53	1,238	0,717
	20 - 18	4,9	2,05	2	6,613	1,013	130,5626851	1374,825074	0,02291375 1	102,122006 5	36:36:00			
	20 - 18	5	2,09	10	6,613	1,013	130,5626851	1374,825074	0,02291375 1	102,122006 5				
Mean	20	14,88	2,052			Calc. From MAF		248	0,00413333 3	18,42144				
				Average				811,412537	0,01352354 2	60,2717325				

Appendix 6. Calculations for fluid properties and nozzle exit velocity.

Calculations for fluid properties and nozzle discharge velocity. 1(4)

We assume that the measurements have error, what comes from the measuring data uncertainties and bad scale of rotameter.

As we consider the measured value of gas flow in mean value, we insert the data ten points, all given in 5-liter interval, five given on the both side of the scale.

ORIGIN := 1

ITALIAN BURNER

Volume flow, measured; $V := 353.535 \frac{liter}{min}$

Volume flow vector; $V := (329 \ 334 \ 339 \ 344 \ 349 \ 354 \ 359 \ 364 \ 369 \ 374 \ 379)^T \cdot \frac{liter}{min}$

Density of Methane @ 20 Celsius and in 1 atm; $\rho_{methane} := 0.659 \frac{kg}{m^3}$

Density of Air @ 20 Celsius and in 1 atm; $\rho_{air} := 1.20 \frac{kg}{m^3}$

Volume of each component @ ideal air-fuel ratio; $v_{methane} := 1m^3$

$v_{air} := 9.53m^3$

Methane + air density @ 20 degrees of centigrade; $\rho_m := \frac{(\rho_{methane} \cdot v_{methane} + \rho_{air} \cdot v_{air})}{(v_{methane} + v_{air})} = 1.149 \frac{kg}{m^3}$

Mass flow of the gas mixture; $q_m := V \cdot \rho_m =$

	1
1	22.673818
2	23.018405
3	23.362991
4	23.707578
5	24.052165
6	24.396752
7	24.741339
8	25.085926
9	25.430513
10	25.7751
11	26.119687

$\cdot \frac{kg}{hr}$

Calculations for fluid properties and nozzle discharge velocity. 2(4)

Cross section area of all the nozzles in Italian burner;

$$A := 0.785398\,mm^2 \cdot (14 \cdot 5) = 5.497786 \times 10^{-5}\,m^2$$

When;

$$q_m = v \cdot \rho_m \cdot A$$

We can write;

$$v := \frac{q_m}{A \cdot \rho_m} = \begin{array}{|c|r|}\hline & 1 \\ \hline 1 & 99.737 \\ 2 & 101.253 \\ 3 & 102.769 \\ 4 & 104.284 \\ 5 & 105.8 \\ 6 & 107.316 \\ 7 & 108.832 \\ 8 & 110.347 \\ 9 & 111.863 \\ 10 & 113.379 \\ 11 & 114.895 \\ \hline \end{array} \frac{m}{s}$$

Which is the speed of discharged gas compound at burning process.
On the last three points of gas flow speed values, we must take in to account, that the gas cannot be considered as ideal gas, because of compressibility.

GERMAN BURNER

Volume flow, measured;

$$V := 547.5 \frac{liter}{min}$$

Volume flow vector;

$$V := (523\ \ 528\ \ 533\ \ 538\ \ 543\ \ 548\ \ 553\ \ 558\ \ 563\ \ 568\ \ 573)^T \cdot \frac{liter}{min}$$

Mass flow of the gas mixture;

$$q_m := V \cdot \rho_m = \begin{array}{|c|r|}\hline & 1 \\ \hline 1 & 36.043789 \\ 2 & 36.388376 \\ 3 & 36.732963 \\ 4 & 37.07755 \\ 5 & 37.422137 \\ 6 & 37.766724 \\ 7 & 38.111311 \\ 8 & 38.455897 \\ 9 & 38.800484 \\ 10 & 39.145071 \\ 11 & 39.489658 \\ \hline \end{array} \cdot \frac{kg}{hr}$$

Calculations for fluid properties and nozzle discharge velocity. 3(4)

Cross section area of all the nozzles in German burner; $A := 152 \cdot \left[\pi \cdot (1 \cdot mm)^2\right] = 4.7752208 \times 10^{-4}\ m^2$

When; $q_m = v \cdot \rho \cdot A$

We can write; $v := \frac{q_m}{A \cdot \rho_m} =$

	1
1	18.254
2	18.428
3	18.603
4	18.777
5	18.952
6	19.127
7	19.301
8	19.476
9	19.65
10	19.825
11	19.999

$\frac{m}{s}$

Every discharge flow speed is in subsonic level, so we can evaluate the values by using ideal gas theory;

CZECH BURNER

Volume flow, measured; $V := 1374.83 \frac{liter}{min}$

Volume flow vector; $V := (1350\ \ 1355\ \ 1360\ \ 1365\ \ 1370\ \ 1375\ \ 1380\ \ 1385\ \ 1390\ \ 1395\ \ 1400)^T \cdot \frac{liter}{min}$

Mass flow of the gas mixture; $q_m := V \cdot \rho_m =$

	1
1	93.038462
2	93.383048
3	93.727635
4	94.072222
5	94.416809
6	94.761396
7	95.105983
8	95.45057
9	95.795157
10	96.139744
11	96.48433

$\cdot \frac{kg}{hr}$

Calculations for fluid properties and nozzle discharge velocity. **4(4)**

Cross section area of all the nozzles in Czech burner;

$$A := 264\left[\pi \cdot (1.5\text{mm})^2\right] = 1.866 \times 10^{-3}\ \text{m}^2$$

When;

$$q_m = v \cdot \rho \cdot A$$

We can write;

$$v := \frac{q_m}{A \cdot \rho_m} = \begin{array}{|c|r|}\hline & 1 \\ \hline 1 & 12.057 \\ 2 & 12.102 \\ 3 & 12.147 \\ 4 & 12.191 \\ 5 & 12.236 \\ 6 & 12.28 \\ 7 & 12.325 \\ 8 & 12.37 \\ 9 & 12.414 \\ 10 & 12.459 \\ 11 & 12.504 \\ \hline \end{array} \frac{\text{m}}{\text{s}}$$

Appendix 7. Calculations for theoretical heating time, Italian burner.

Theoretical heating time for mould with Italian burner **1(7)**

Known values: ORIGIN := 1

Velocity @ nozzle exit; $v_e := 107.175\frac{m}{s}$ *Calculated from measured mean value; As we call it, a sophisticated guess!*

Velocity @ nozzle exit, from flow speed sheet;

$$v_{ev} := \begin{pmatrix} 99.737 \\ 101.253 \\ 102.769 \\ 104.284 \\ 105.8 \\ 107.316 \\ 108.832 \\ 110.347 \\ 111.863 \\ 113.379 \\ 114.895 \end{pmatrix} \cdot \frac{m}{s}$$

Temperature @ nozzle exit; $T_e := 1451.48K$

Temperature @ atmosphere; $T_s := 298.7K$

Nozzle distance to stagnation surface; $H := 30mm$

Impinging area radius; $r_0 := 7mm$

Nozzle radius; $r := 0.5mm$

Nozzle diameter; $D := r \cdot 2 = 1 \cdot mm$

Hydraulic diameter; $D_h := r \cdot 2 = 1 \cdot mm$

Pitch of nozzle array; $S := 4 \cdot mm$

Theoretical heating time for mould with Italian burner 2(7)

Fluid properties:

Density; $\rho := 1.149\frac{kg}{m^3}$

Dynamic viscosity; $\mu := 10.995 10^{-6}\cdot Pa\cdot s = 1.099\times 10^{-4}\cdot poise$

Kinematic viscosity; $\mu_k := 16.451\cdot 10^{-6}\cdot\frac{m^2}{s} = 0.165\,stokes$

Specific heat; $c_p := 2220\frac{J}{kg\cdot K}$

Thermal conductivity; $k_f := 0.035\frac{W}{m\cdot K}$

Calculated values:

Prandtl number; $Pr := \frac{\mu\cdot c_p}{k_f} = 0.697$

Film temperature; $T_f := \frac{T_s + T_e}{2} = 875.09K$

Relative nozzle cross-section area;

$$A_{r.SRN} := \frac{1}{4}\cdot\left(\frac{D}{r_0}\right)^2 = 0.005$$

$$A_{r.ARN} := \frac{\pi}{2\cdot\sqrt{3}}\cdot\left(\frac{D}{S}\right)^2 = 0.057$$

$$A_{r.ARN.square} := \frac{\pi}{4}\cdot\left(\frac{D}{S}\right)^2 = 0.049$$

Theoretical heating time for mould with Italian burner **3(7)**

Reynolds number;

$$Re := \frac{v_e \cdot D_h}{\mu_k} =$$

	1
1	6062.671
2	6154.823
3	6246.976
4	6339.068
5	6431.22
6	6523.372
7	6615.525
8	6707.617
9	6799.769
10	6891.921
11	6984.074

The ratio between diameters and distance from nozzle exit;

$$HD := \frac{H}{D} = 30$$

Calculations for impinging correlation

Correlation function is calculated part by part;

Function of F;

$$F := 0.5 \cdot Re^{\frac{2}{3}} =$$

	1
1	166.244
2	167.924
3	169.596
4	171.259
5	172.915
6	174.563
7	176.203
8	177.834
9	179.459
10	181.077
11	182.688

Function of G;

$$G := 2 \cdot A_{r.ARN.square}^{\frac{1}{2}} \cdot \frac{1 - 2.2 \cdot A_{r.ARN.square}^{\frac{1}{2}}}{1 + 0.2 \cdot \left(\frac{H}{D} - 6\right) \cdot A_{r.ARN.square}^{\frac{1}{2}}} = 0.11$$

Theoretical heating time for mould with Italian burner **4(7)**

Function of K;

$$K := \left[1 + \left(\frac{HD}{\frac{0.6}{A_{r.ARN.square}^{\frac{1}{2}}}}\right)^{6}\right]^{-0.05} = 0.486$$

When;

$$\frac{Nu}{Pr^{0.42}} = K \cdot G \cdot F$$

We can write;

$Nu := K \cdot G \cdot F \cdot Pr^{0.42} =$

	1
1	7.644
2	7.722
3	7.799
4	7.875
5	7.951
6	8.027
7	8.102
8	8.177
9	8.252
10	8.327
11	8.401

From the Nusselt number;

$$Nu = \frac{h \cdot D_h}{k}$$

we can get the heat transfer coefficient;

$h := \frac{Nu \cdot k_f}{D_h} =$

	1
1	267.555
2	270.259
3	272.95
4	275.626
5	278.291
6	280.943
7	283.583
8	286.209
9	288.824
10	291.428
11	294.02

$\cdot \frac{W}{m^2 \cdot K}$

Theoretical heating time for mould with Italian burner 5(7)

Material values

Thermal conductivity for steel; $k_s := 58 \cdot \frac{W}{m \cdot K}$

Heated mass (DM); $m_{mould} := 34881.424\,g \quad m = 34.881\,kg$

Specific heat for steel; $c_{steel} := 473 \cdot \frac{J}{kg \cdot K}$

Density of steel; $\rho_{steel} := 7870 \frac{kg}{m^3}$

Boundary conditions

Heated surface area (DM); $A_{surface} := 2 \cdot 3156.7\,mm^2 + 5707.2\,mm^2 = 0.012021\,m^2$

Wanted temperature; $T_w := 200°C = 473.15\,K$

Delta temperature; $\Delta T := T_w - T_s = 174.45\,K$

Distance from stagnation point to reference point 1 (DM) ; $d_{reference1} := 75\,mm$

Calculated values

Half mould mass up to first reference point; (DM) $m_{mould.1} := 24653.618\,g \quad m = 24.654\,kg$

Theoretical heating time for mould with Italian burner **6(7)**

Power provided

By using Newton's law of cooling applied for heat transfer;

$$Q := h \cdot A_{surface} \cdot \left(T_e - T_s\right) =$$

	1
1	3707.539
2	3745.014
3	3782.302
4	3819.383
5	3856.31
6	3893.06
7	3929.638
8	3966.022
9	4002.265
10	4038.343
11	4074.261

W

Energy need

Needed heat energy;

$$Q_n := \Delta T \cdot c_{steel} \cdot m_{mould.1} = 2034290\,J$$

Machine bed

Thermal conductivity for steel;

$$k_{sw} := 58 \cdot \frac{W}{m \cdot K}$$

Heated mass (DM);

$$m_{bed} := 11335.5174\,gm = 11.336\,kg$$

Specific heat for steel;

$$c_{steel} := 473 \cdot \frac{J}{kg \cdot K}$$

Density of steel;

$$\rho_{steel} := 7870 \frac{kg}{m^3}$$

Theoretical heating time for mould with Italian burner 7(7)

Boundary conditions

Reference point temperature; $T_w := 200°C = 473.15K$

Mean value for machine bed; $T_m := 110°C = 383.15K$ *Estimated from Flir picture*

Delta temperature; $\Delta T := T_m - T_s = 84.45K$

Energy need

Needed heat energy to rise bed temperature; $Q_{bed} := \Delta T \cdot c_{steel} \cdot m_{bed} = 452796J$

Energy summarization

Theoretical time; $Time := \frac{Q_n + Q_{bed}}{Q} = \cdot s$

	1
1	670.818
2	664.106
3	657.559
4	651.175
5	644.939
6	638.851
7	632.904
8	627.098
9	621.419
10	615.868
11	610.438

Appendix 8. Calculations for theoretical heating time, German burner.

Theoretical heating time for mould with German burner **1(4)**

Known values: ORIGIN := 1

Velocity @ nozzle exit — $v_e := 19.109\frac{m}{s}$ — *Calculated from measured mean value; As we call it, a sophisticated guess!*

Velocity @ nozzle exit, from flow speed sheet;

$$v_{ev} := \begin{pmatrix} 18.254 \\ 18.428 \\ 18.603 \\ 18.777 \\ 18.952 \\ 19.127 \\ 19.301 \\ 19.476 \\ 19.65 \\ 19.825 \\ 19.999 \end{pmatrix} \cdot \frac{m}{s}$$

Temperature @ nozzle exit — $T_e := 1259.48K$

Temperature @ atmosphere — $T_s := 298.7K$

Nozzle distance to stagnation surface — $H := 13mm$

Impinging area radius — $r_0 := 7mm$

Nozzle radius — $r := 1mm$

Nozzle diameter — $D := r \cdot 2 = 2 \cdot mm$

Hydraulic diameter — $D_h := r \cdot 2 = 2 \cdot mm$

Pitch of nozzle array — $S := 3.575mm$

Theoretical heating time for mould with German burner **2(4)**

Calculated values:

Prandtl number

$$Pr := \frac{\mu \cdot c_p}{k_f} = 0.697$$

Film temperature

$$T_f := \frac{T_s + T_e}{2} = 779.09K$$

Relative nozzle cross-section area

$$A_{r.ARN} := \frac{\pi}{2\cdot\sqrt{3}} \cdot \left(\frac{D}{S}\right)^2 = 0.284$$

Reynolds number

$$Re := \frac{v_e \cdot D_h}{\mu_k} =$$

	1
1	2219.196
2	2240.35
3	2261.625
4	2282.779
5	2304.054
6	2325.33
7	2346.483
8	2367.759
9	2388.913
10	2410.188
11	2431.342

The ratio between diameters and distance from nozzle exit

$$HD := \frac{H}{D} = 6.5$$

Calculations for impinging correlation

Correlation function is calculated part by part;

Function of F

$$F := 0.5 \cdot Re^{\frac{2}{3}} =$$

	1
1	85.068
2	85.608
3	86.149
4	86.685
5	87.223
6	87.759
7	88.291
8	88.824
9	89.352
10	89.882
11	90.407

Theoretical heating time for mould with German burner **3(4)**

Function of G

$$G := \left| 2 \cdot A_{r.ARN}^{\frac{1}{2}} \cdot \frac{1 - 2.2 \cdot A_{r.ARN}^{\frac{1}{2}}}{1 + 0.2 \cdot \left(\frac{H}{D} - 6 \right) \cdot A_{r.ARN}^{\frac{1}{2}}} \right| = 0.174$$

Function of K

$$K := \left[1 + \left(\frac{HD}{\frac{0.6}{A_{r.ARN}^{\frac{1}{2}}}} \right)^{6} \right]^{-0.05} = 0.591$$

When;

$$\frac{Nu}{Pr^{0.42}} = K \cdot G \cdot F$$

We can write;

$$Nu := K \cdot G \cdot F \cdot Pr^{0.42} =$$

	1
1	7.523
2	7.571
3	7.618
4	7.666
5	7.713
6	7.761
7	7.808
8	7.855
9	7.902
10	7.949
11	7.995

From the Nusselt number;

$$Nu = \frac{h \cdot D_h}{k}$$

Theoretical heating time for mould with German burner **4(4)**

We can get the heat transfer coefficient;

$$h := \frac{Nu \cdot k_f}{D_h} = \cdot \frac{W}{m^2 \cdot K}$$

	1
1	131.65
2	132.486
3	133.323
4	134.153
5	134.986
6	135.815
7	136.638
8	137.462
9	138.28
10	139.1
11	139.912

Material values

Heated surface area (DM);

$$A_{surface} := 2 \cdot 2048.9719mm^2 + 5073.9803mm^2 = 0.009172m^2$$

Power provided

By using Newton's law of cooling applied for heat transfer;

$$Q := h \cdot A_{surface} \cdot (T_e - T_s) = W$$

	1
1	1160.131
2	1167.491
3	1174.871
4	1182.186
5	1189.519
6	1196.831
7	1204.078
8	1211.345
9	1218.55
10	1225.774
11	1232.935

Energy summarization

Theoretical time;

$$Time := \frac{Q_n + Q_{bed}}{Q} = \cdot s$$

	1
1	2143.798
2	2130.282
3	2116.901
4	2103.803
5	2090.832
6	2078.059
7	2065.551
8	2053.159
9	2041.021
10	2028.992
11	2017.206

Appendix 9. Calculations for theoretical heating time, Czech burner.

Theoretical heating time for mould with Czech burner **1(4)**

Known values: ORIGIN := 1 *Calculated from measured mean value; As we call it, a sophisticated guess!*

Velocity @ nozzle exit $v_e := 12.279\frac{m}{s}$

Velocity vector @ nozzle exit

$$v_{ev} := \begin{pmatrix} 12.057 \\ 12.102 \\ 12.147 \\ 12.191 \\ 12.236 \\ 12.28 \\ 12.325 \\ 12.37 \\ 12.414 \\ 12.459 \\ 12.504 \end{pmatrix} \cdot \frac{m}{s}$$

Temperature @ nozzle exit $T_e := 1472.15K$

Temperature @ atmosphere $T_s := 298.7K$

Nozzle distance to stagnation surface $H := 20mm$

Impinging area radius $r_0 := 7mm$

Nozzle radius $r := 1.5mm$

Nozzle diameter $D := r \cdot 2 = 3 \cdot mm$

Hydraulic diameter $D_h := r \cdot 2 = 3 \cdot mm$

Pitch of nozzle array $S := 5.633\,mm$

Theoretical heating time for mould with Czech burner **2(4)**

Calculated values:

Prandtl number

$$Pr := \frac{\mu \cdot c_p}{k_f} = 0.697$$

Film temperature

$$T_f := \frac{T_s + T_e}{2} = 885.425\text{K}$$

Relative nozzle cross-section area

$$A_{r.ARN} := \frac{\pi}{2\cdot\sqrt{3}} \cdot \left(\frac{D}{S}\right)^2 = 0.257$$

Reynolds number

$$Re := \frac{v_e \cdot D_h}{\mu_k} =$$

	1
1	2198.711
2	2206.918
3	2215.124
4	2223.148
5	2231.354
6	2239.378
7	2247.584
8	2255.79
9	2263.814
10	2272.02
11	2280.226

Calculations for impinging correlation

Correlation function is calculated part by part;

Function of F;

$$F := 0.5 \cdot Re^{\frac{2}{3}} =$$

	1
1	84.544
2	84.754
3	84.964
4	85.169
5	85.379
6	85.583
7	85.792
8	86.001
9	86.205
10	86.413
11	86.621

Theoretical heating time for mould with Czech burner **3(4)**

Function of G;

$$G := \left| 2 \cdot A_{r.ARN}^{\frac{1}{2}} \cdot \frac{1 - 2.2 \cdot A_{r.ARN}^{\frac{1}{2}}}{1 + 0.2 \cdot \left(\frac{H}{D} - 6 \right) \cdot A_{r.ARN}^{\frac{1}{2}}} \right| = 0.11$$

Function of K;

$$K := \left[1 + \left(\frac{HD}{\frac{0.6}{A_{r.ARN}^{\frac{1}{2}}}} \right)^{6} \right]^{-0.05} = 0.595$$

When;

$$\frac{Nu}{Pr^{0.42}} = K \cdot G \cdot F$$

We can write;

$$Nu := K \cdot G \cdot F \cdot Pr^{0.42} =$$

	1
1	4.759
2	4.771
3	4.783
4	4.794
5	4.806
6	4.818
7	4.829
8	4.841
9	4.853
10	4.864
11	4.876

From the Nusselt number;

$$Nu = \frac{h \cdot D_h}{k}$$

We can get the heat transfer coefficient;

$$h := \frac{Nu \cdot k_f}{D_h} =$$

	1
1	55.523
2	55.661
3	55.799
4	55.933
5	56.071
6	56.205
7	56.343
8	56.48
9	56.613
10	56.75
11	56.887

$$\cdot \frac{W}{m^2 \cdot K}$$

Theoretical heating time for mould with Czech burner 4(4)

Material values

Heated surface area (DM);

$$A_{surface} := 2 \cdot 3156.7\,mm^2 + 5707.2\,mm^2 = 0.012021\,m^2$$

Power provided

By using Newton's law of cooling applied for heat transfer;

$$Q := h \cdot A_{surface} \cdot (T_e - T_s) =$$

	1
1	783.181
2	785.128
3	787.073
4	788.973
5	790.913
6	792.808
7	794.744
8	796.677
9	798.565
10	800.494
11	802.42

W

Energy summarization

Theoretical time;

$$Time := \frac{Q_n + Q_{bed}}{Q} =$$

	1
1	3175.621
2	3167.744
3	3159.916
4	3152.308
5	3144.575
6	3137.059
7	3129.418
8	3121.824
9	3114.443
10	3106.939
11	3099.48

·s

Appendix 10. Calculations for optimized Italian burner.

Theoretical heating time calculation for optimized Italian burner **1(4)**

ORIGIN := 1

Comes from structural design;

Nozzle distance to stagnation surface; $H := 8mm$ *Sophisticated guess!*

Value for nozzle diameter comes via distance between nozzle and stagnation point;

Nozzle diameter; $D := 0.184 \cdot H = 1.472 \cdot mm$

*Volume flow, **measured**;* $V := 353.535 \frac{liter}{min}$

Density of Methane @ 20 Celsius and in 1 atm; $\rho_{methane} := 0.659 \frac{kg}{m^3}$

Density of Air @ 20 Celsius and in 1 atm; $\rho_{air} := 1.20 \frac{kg}{m^3}$

Volume of each component @ ideal air-fuel ratio; $v_{methane} := 1m^3$

$v_{air} := 9.53m^3$

Methane + air density @ 20 Celsius; $\rho_m := \frac{(\rho_{methane} \cdot v_{methane} + \rho_{air} \cdot v_{air})}{(v_{methane} + v_{air})} = 1.149 \frac{kg}{m^3}$

Mass flow of the gas mixture; $q_m := V \cdot \rho_m = 24.364706 \frac{kg}{hr}$

Optimized cross-section area Of Italian burner; $A := \pi \cdot \left(\frac{D}{2}\right)^2 \cdot 24 = 4.084 \times 10^{-5} m^2$

When; $q_m = v_e \cdot \rho_m \cdot A$

We can write; $v_e := \frac{q_m}{A \cdot \rho_m} = 144.266 \frac{m}{s}$

Theoretical heating time calculation for optimized Italian burner **2(4)**

Calculated from measured mean value;

Velocity @ nozzle exit, from flow speed sheet; $v_e = 144.266 \frac{m}{s}$

Temperature @ nozzle exit; $T_e := 1451.48K$

Temperature @ atmosphere; $T_s := 298.7K$

Hydraulic diameter; $D_h := D$

Pitch of nozzle array; $S := 1.324 \cdot H = 10.592mm$

Fluid properties:

Density; $\rho_m = 1.149 \frac{kg}{m^3}$

Dynamic viscosity; $\mu := 10.995 \cdot 10^{-6} \cdot Pa \cdot s = 1.099 \times 10^{-4} \cdot poise$

Kinematic viscosity; $\mu_k := 16.451 \cdot 10^{-6} \cdot \frac{m^2}{s} = 0.165 stokes$

Specific heat; $c_p := 2220 \frac{J}{kg \cdot K}$

Thermal conductivity; $k_f := 0.035 \frac{W}{m \cdot K}$

Calculated values:

Prandtl number; $Pr := \frac{\mu \cdot c_p}{k_f} = 0.697$

Film temperature; $T_f := \frac{T_s + T_e}{2} = 875.09K$

Relative nozzle cross-section area; $A_{r.ARN.square} := \frac{\pi}{4} \cdot \left(\frac{D}{S}\right)^2 = 0.015$

Theoretical heating time calculation for optimized Italian burner **2(4)**

Reynolds number;

$$Re := \frac{v_e \cdot D_h}{\mu_k} = 12908.623$$

The ratio between diameter and distance from nozzle exit;

$$HD := \frac{H}{D} = 5.435$$

Calculations for Impinging correlation

Correlation function is calculated part by part;

Function of F;

$$F := 0.5 \cdot Re^{\frac{2}{3}} = 275.142$$

Function of G;

$$G := 2 \cdot A_{r.ARN.square}^{\frac{1}{2}} \cdot \frac{1 - 2.2 \cdot A_{r.ARN.square}^{\frac{1}{2}}}{1 + 0.2 \cdot \left(\frac{H}{D} - 6\right) \cdot A_{r.ARN.square}^{\frac{1}{2}}} = 0.182$$

Function of K;

$$K := \left[1 + \left(\frac{HD}{\frac{0.6}{A_{r.ARN.square}^{\frac{1}{2}}}}\right)^6\right]^{-0.05} = 0.948$$

When;

$$\frac{Nu}{Pr^{0.42}} = K \cdot G \cdot F$$

We can write;

$$Nu := K \cdot G \cdot F \cdot Pr^{0.42} = 40.817$$

From the Nusselt number;

$$Nu = \frac{h \cdot D_h}{k}$$

we can get the heat transfer coefficient;

$$h := \frac{Nu \cdot k_f}{D_h} = 970.511 \frac{W}{m^2 \cdot K}$$

Theoretical heating time calculation for optimized Italian burner 3(4)

Material values

Thermal conductivity for steel; $k_s := 58 \cdot \frac{W}{m \cdot K}$

Heated mass (DM); $m_{mould} := 34881.424g\,m = 34.881\,kg$

Specific heat for steel; $c_{steel} := 473 \cdot \frac{J}{kg \cdot K}$

Density of steel; $\rho_{steel} := 7870 \frac{kg}{m^3}$

Boundary conditions

Heated surface area (DM); $A_{surface} := 2 \cdot 3156.7mm^2 + 5707.2mm^2 = 0.012021\,m^2$

Wanted temperature; $T_w := 200°C = 473.15K$

Delta temperature; $\Delta T := T_w - T_s = 174.45K$

Distance from stagnation point to reference point 1 (DM) ; $d_{reference1} := 75mm$

Calculated values

Half mould mass up to first reference point; (DM) $m_{mould.1} := 24653.618g\,m = 24.654\,kg$

Power provided

By using Newton's law of cooling applied for heat tranfer; $Q := h \cdot A_{surface} \cdot (T_e - T_s) = 13448.472W$

Energy need

Needed heat energy; $Q_n := \Delta T \cdot c_{steel} \cdot m_{mould.1} = 2034290J$

Theoretical heating time calculation for optimized Italian burner 4(4)

Machine bed

Thermal conductivity for steel; $k_{steel} := 58 \cdot \frac{W}{m \cdot K}$

Heated mass (DM); $m_{bed} := 11335.517 g \quad m = 11.336 kg$

Specific heat for steel; $c_{steel} := 473 \cdot \frac{J}{kg \cdot K}$

Density of steel; $\rho_{steel} := 7870 \frac{kg}{m^3}$

Boundary conditions

Reference point temperature; $T_s := 200°C = 473.15K$

Mean value for machine bed; $T_m := 110°C = 383.15K$ *Estimated from Flir picture*

Delta temperature; $\Delta T := T_m - T_s = 84.45K$

Energy need

Needed heat energy to rise bed temperature; $Q_{bed} := \Delta T \cdot c_{steel} \cdot m_{bed} = 452796J$

Energy summarization

Theoretical time; $Time := \frac{Q_n + Q_{bed}}{Q} = 3.082 min$

Appendix 11. Calculations for fluent simulation.

Analytical calculations for Fluent simulation 1(5)

Italian type burner:

Known values:

Velocity @ nozzle exit; $v_e := 107.175\frac{m}{s}$

Temperature @ nozzle exit; $T_e := 1451.48K$

Temperature @ atmosphere; $T_s := 300K$

Nozzle distance to stagnation surface; $H := 30mm$

Nozzle diameter; $D := 1mm$

Hydraulic diameter; $D_h := D$

Pitch of nozzle array; $S := 4 \cdot mm$

Fluid properties:

Density; $\rho := 1.149\frac{kg}{m^3}$

Dynamic viscosity; $\mu := 10.995 10^{-6} \cdot Pa \cdot s = 1.099 \times 10^{-4} \cdot poise$

Kinematic viscosity; $\mu_k := 16.451 \cdot 10^{-6} \cdot \frac{m^2}{s} = 0.165\,stokes$

Specific heat; $c_p := 2220\frac{J}{kg \cdot K}$

Thermal conductivity; $k_f := 0.035\frac{W}{m \cdot K}$

Calculated values:

Prandtl number; $Pr := \frac{\mu \cdot c_p}{k_f} = 0.697$

Film temperature; $T_f := \frac{T_s + T_e}{2} = 875.74K$

Analytical calculations for Fluent simulation **2(5)**

Relative nozzle cross-section area;

$$A_{r.ARN.square} := \frac{\pi}{4}\cdot\left(\frac{D}{S}\right)^2 = 0.049$$

Reynolds number;

$$Re := \frac{v_e \cdot D_h}{\mu_k} = 6514.802$$

The ratio between diameter and distance from nozzle exit;

$$HD := \frac{H}{D} = 30$$

Calculations for impinging correlation

Correlation function is calculated part by part;

Function of F;

$$F := 0.5\cdot Re^{\frac{2}{3}} = 174.41$$

Function of G;

$$G := 2\cdot A_{r.ARN.square}^{\frac{1}{2}}\cdot\frac{1 - 2.2\cdot A_{r.ARN.square}^{\frac{1}{2}}}{1 + 0.2\cdot\left(\frac{H}{D} - 6\right)\cdot A_{r.ARN.square}^{\frac{1}{2}}} = 0.11$$

Function of K;

$$K := \left[1 + \left(\frac{HD}{\frac{0.6}{A_{r.ARN.square}^{\frac{1}{2}}}}\right)^6\right]^{-0.05} = 0.486$$

When;

$$\frac{Nu}{Pr^{0.42}} = K\cdot G\cdot F$$

We can write;

$$Nu := K\cdot G\cdot F\cdot Pr^{0.42} = 8.02$$

From the Nusselt number;

$$Nu = \frac{h\cdot D_h}{k}$$

we can get the heat transfer coefficient;

$$h := \frac{Nu\cdot k_f}{D_h} = 280.697\,\frac{W}{m^2\cdot K}$$

Analytical calculations for Fluent simulation 3(5)

Material values

Thermal conductivity for steel; $k_s := 58 \cdot \frac{W}{m \cdot K}$

Specific heat for steel; $c_{steel} := 473 \cdot \frac{J}{kg \cdot K}$

Density of steel; $\rho_{steel} := 7870 \frac{kg}{m^3}$

Dimensions; $v_{part} := 50mm \cdot 50mm \cdot 50mm = 1.25 \times 10^5 \cdot mm^3$

Heated mass; $m_{part} := v_{part} \cdot \rho_{steel} = 0.984kg$

Boundary conditions

Heated surface area (DM); $A_{surface} := 50mm \cdot 50mm = 0.0025 m^2$

Wanted temperature; $T_w := 200°C = 473.15K$

Delta temperature; $\Delta T := T_w - T_s = 173.15K$

Power provided

By using Newton's law of cooling applied for heat transfer; $q := h \cdot A_{surface} \cdot (T_e - T_s) = 808.043W$

Energy need

Needed heat energy; $Q_n := \Delta T \cdot c_{steel} \cdot m_{part} = 80569J$

The bottom of heated body is adiabatic and is considered as insulated.

Energy summarization

Theoretical time; $Time := \frac{Q_n}{q} = 1.662 min$

Analytical calculations for Fluent simulation 4(5)

With optimized values:

Known values:

Velocity @ nozzle exit; $v_e := 144.266\frac{m}{s}$

Nozzle distance to stagnation surface; $H := 8mm$

Nozzle diameter; $D := 1.472mm$

Hydraulic diameter; $D_h := D$

Pitch of nozzle array; $S := 10.592mm$

Relative nozzle cross-section area; $A_{r.ARN.square} := \frac{\pi}{4}\cdot\left(\frac{D}{S}\right)^2 = 0.015$

Reynolds number; $Re := \frac{v_e \cdot D_h}{\mu_k} = 12908.611$

The ratio between diameter and distance from nozzle exit; $HD := \frac{H}{D} = 5.435$

Calculations for impinging correlation

Correlation function is calculated part by part;

Function of F; $F := 0.5\cdot Re^{\frac{2}{3}} = 275.142$

Function of G; $G := 2\cdot A_{r.ARN.square}^{\frac{1}{2}}\cdot\frac{1 - 2.2\cdot A_{r.ARN.square}^{\frac{1}{2}}}{1 + 0.2\cdot\left(\frac{H}{D} - 6\right)\cdot A_{r.ARN.square}^{\frac{1}{2}}} = 0.182$

Analytical calculations for Fluent simulation **5(5)**

Function of K;

$$K := \left[1 + \left(\frac{HD}{\frac{0.6}{A_{r.ARN.square}^{\frac{1}{2}}}}\right)^{6}\right]^{-0.05} = 0.948$$

When;

$$\frac{Nu}{Pr^{0.42}} = K \cdot G \cdot F$$

We can write;

$$Nu := K \cdot G \cdot F \cdot Pr^{0.42} = 40.817$$

From the Nusselt number;

$$Nu = \frac{h \cdot D_h}{k}$$

we can get the heat transfer coefficient;

$$h := \frac{Nu \cdot k_f}{D_h} = 970.51 \frac{W}{m^2 \cdot K}$$

Power provided

By using Newton's law of cooling applied for heat tranfer;

$$q := h \cdot A_{surface} \cdot (T_e - T_s) = 2793.808 W$$

Energy need

Needed heat energy;

$$Q_n := \Delta T \cdot c_{steel} \cdot m_{part} = 80569 J$$

The bottom of heated body is adiabathic and is considered as insulated.

Energy summarization

Theoretical time;

$$Time := \frac{Q_n}{q} = 0.481 min$$